Studies on the role of actin-binding proteins in platelet production and function in mice

Zur Rolle von Aktin-bindenden Proteinen in der Bildung und der Funktion von Thrombozyten in der Maus

Doctoral thesis for a doctoral degree
at the Graduate School of Life Sciences,
Julius-Maximilians-Universität Würzburg
Section Biomedicine

submitted by

Inga Birkholz
from Stade

Würzburg, 2018

Submitted on: ……

Office Stamp

Members of the *Promotionskomitee*:

Chairperson: Prof. Dr. Manfred Gessler

Primary Supervisor: Prof. Dr. Bernhard Nieswandt

Supervisor (Second): Prof. Dr. Antje Gohla

Supervisor (Third): PD Dr. Heike Hermanns

Date of Public Defence: ……

Date of Receipt of Certificates: ……

„Wenn man es nur versucht, so geht´s,
das heißt mitunter, doch nicht stets.“

-Wilhelm Busch-

SUMMARY

Platelet activation and aggregation at sites of vascular injury involves massive cytoskeletal re-organization, which is required for proper platelet function. Moreover, the cytoskeleton plays central roles in megakaryo- and thrombopoiesis. Thus, cytoskeletal protein aberrations can be the underlying reason for many pathological phenotypes. Although intensive research is carried out to identify the key players involved in cytoskeletal reorganization, the signaling cascades orchestrating these complex processes are still poorly understood. This thesis investigates the role of three actin-binding proteins, *Coactosin-like* (Cotl) 1, *Profilin* (Pfn) 1 and *Thymosin* (T) β4, in platelet formation and function using genetically modified mice.

ADF-H-containing proteins such as Twinfilin or Cofilin are well characterized as regulators of thrombopoesis and cytoskeletal reorganization. Although Cotl1 belongs to the ADF-H protein family, lack of Cotl1 did not affect platelet count or cytoskeletal dynamics. However, Cotl1-deficiency resulted in significant protection from arterial thrombus formation and ischemic stroke *in vivo*. Defective GPIb-vWF interactions and altered second wave mediator release present potential reasons for the beneficial effect of Cotl1-deficiency. These results reveal an unexpected function of Cotl1 as a regulator of thrombosis and hemostasis, establishing it as a potential target for a safe therapeutic therapy to prevent arterial thrombosis or ischemic stroke.

Recent studies showed that the organization of the circumferential actin cytoskeleton modulates calpain-mediated αIIbβ3 integrin closure, thereby also controlling αIIbβ3 integrin localization. The second part of this thesis identified the actin-sequestering protein Pfn1 as a central regulator of platelet integrin function as Pfn1-deficient platelets displayed almost abolished αIIbβ3 integrin signaling. This translated into a profound protection from arterial thrombus formation and prolonged tail bleeding times *in vivo* which was caused by enhanced calpain-dependent integrin closure. These findings further emphasize the importance of a functional actin cytoskeleton for intact platelet function *in vitro* and *in vivo*.

Tβ4 is a moonlighting protein, acting as one of the major actin-sequestering proteins in cells of higher eukaryotes and exerting various paracrine functions including anti-inflammatory, immunomodulatory and pro-angiogenic effects. Although excessively studied, its role for cytoskeletal dynamics, the distinction between endo- and exogenous protein function and its uptake and release mechanisms are still poorly understood. Constitutive Tβ4-deficiency resulted in thrombocytopenia accompanied by a largely diminished G-actin pool in platelets and divergent effects on platelet reactivity. Pre-incubation of platelets with recombinant Tβ4 will help to understand the function of endo- and exogenous protein, which is under current investigation.

ZUSAMMENFASSUNG

Die Aktivierung und Aggregation von Thrombozyten bei Gefäßverletzungen zieht massive Umstrukturierungen des Zytoskeletts nach sich, die eine Voraussetzung für die intakte Funktion der Zellen darstellen. Des Weiteren nimmt das Zytoskelett eine zentrale Rolle in der Megakaryo- und Thrombopoese ein. Daher können Anomalien zytoskeletaler Proteine eine Vielzahl von Krankheitsbildern verursachen. Obwohl intensiv an den beteiligten Proteinen geforscht wird, sind die Signalkaskaden, die den komplexen Vorgang der Umstrukturierung des Zytoskeletts steuern, noch weitgehend unbekannt. In dieser Dissertation wurden drei Aktin-bindende Proteine, *Coactosin-like* (Cotl) 1, *Profilin* (Pfn) 1 und *Thymosin* (T) β4, hinsichtlich ihrer Rolle für die Bildung und Funktion von Thrombozyten mittels genetisch veränderter Mäuse untersucht.

Proteine wie Twinfilin oder Cofilin, die ADF-H-Domänen enthalten, sind oftmals an der Thrombopoese sowie an zytoskeletaler Umstrukturierung beteiligt. Obgleich Cotl1 der ADF-H Proteinfamilie zugehörig ist, konnte in Cotl1-defizienten Mäusen weder eine Veränderung der Thrombozytenzahlen, noch der zytoskeletalen Dynamik festgestellt werden. Unerwarteterweise zog eine Cotl1-Defizienz *in vivo* einen Schutz vor arterieller Thrombose und Schlaganfall nach sich. Defekte GPIb-vWF-Interaktionen sowie eine veränderte Freisetzung von sekundären intrazellulären Mediatoren zeigen mögliche Gründe für den schützenden Effekt einer Cotl1-Defizienz auf. Diese Ergebnisse verdeutlichen, dass Cotl1 ein zentraler Regulator von Thrombose und Hämostase ist und etabliert es damit als potentielle antithrombotische Zielstruktur für eine effektive und sichere Behandlung von kardio- und zerebrovaskulären Erkrankungen.

Studien zeigten, dass die Organisation des kortikalen Aktin-Zytoskeletts die Calpain-vermittelte αIIbβ3-Integrin-Inaktivierung moduliert und dadurch die Lokalisation der Integrine kontrolliert. Der zweite Teil dieser Dissertation identifizierte das Aktin-komplexierende Molekül Pfn1 als zentralen Regulator der Integrinfunktion in Thrombozyten, da Pfn1-defiziente Thrombozyten eine stark verminderte Reaktivität nach αIIbβ3-Integrin Aktivierung zeigten. Dies führte zu einem profunden Schutz vor arterieller Thrombusbildung und verlängerten Blutungszeiten *in vivo*, der durch eine verstärkte Calpain-vermittelte Integrin-Inaktivierung verursacht wurde. Diese Befunde unterstreichen erneut die zentrale Bedeutung eines funktionales Aktin-Zytoskeletts für die Aufrechterhaltung der Thrombozytenfunktion *in vitro* und *in vivo*.

Tβ4 ist ein bivalentes Protein, das einerseits eine Funktion als Aktin-komplexierendes Protein in Zellen höherer Eukaryoten ausübt und andererseits unterschiedliche parakrine Funktionen

hat, zu denen entzündungshemmende, immunmodulierende und pro-angiogene Wirkungen zählen. Obwohl intensiv an Tβ4 geforscht wird, ist seine Bedeutung für die Dynamik des Zytoskeletts sowie die Unterscheidung zwischen endo- und exogener Proteinfunktion und seine Aufnahme- und Freisetzungsmechanismen kaum verstanden. Konstitutive Tβ4-Defizienz zog eine Thrombozytopenie, begleitet von einem stark verminderten G-Aktin-Gehalt in Thrombozyten und gegensätzlichen Effekten auf die Thrombozytenreaktivität, nach sich. Der Effekt von rekombinant exprimiertem Tβ4 auf Thrombozyten, der derzeit untersucht wird, wird zum besseren Verständnis der endo- und exogenen Proteinfunktion, beitragen.

TABLE OF CONTENTS

1. INTRODUCTION

1.1 Platelets

Platelets are small, anucleated, discoid-shaped cell fragments that are released from *bone marrow* (BM) *megakaryocytes* (MKs). Protrusions, reaching into the sinusoidal vessels of the BM, are shed off by shear forces generated by the blood stream and get further fragmented into platelets [1]. This process is permanently active to compensate for the clearing of aged platelets by macrophages in liver and spleen, keeping the platelet concentration at constant levels of 150,000-450,000 μL^{-1} in humans and approximately 1,000,000 μL^{-1} in mice. Whereas human platelets have a lifespan of 7-10 days, murine platelets circulate for approximately 5 days. With a diameter of 3-4 µm (1-2 µm in mice) they are the smallest blood cells. Their main function is to safeguard the integrity of the vascular system. In addition to platelets, efficient hemostasis requires a functional coagulation system with its central product thrombin, which mediates the conversion of fibrinogen into fibrin and further acts as a powerful platelet activator. The coagulation cascade is either initiated by *tissue factor* (TF), which is exposed upon vascular injury, or by negatively charged surfaces via the 'contact-activation' pathway (intrinsic coagulation) initiated by the activation of *coagulation factor* (F) XII.

Although most platelets are cleared without undergoing activation, they are able to respond rapidly to damage of endothelial layers of the vessel wall by forming a plug that prevents excessive blood loss. The exposure of *extracellular matrix* (ECM) proteins, such as collagens and laminins, to the flowing blood leads to initial platelet adhesion and activation. Subsequently, soluble mediators are released and secreted by activated platelets leading to the activation and recruitment of additional platelets to the site of injury, thus facilitating thrombus formation. However, under pathologic conditions, such as the rupture of an atherosclerotic plaque, the exposure of ECM proteins can cause uncontrolled platelet activation. This can lead to thrombotic events resulting in the obstruction of blood flow, loss of oxygen supply and subsequent tissue damage, as seen in myocardial infarction and ischemic stroke [2]. Since these pathologies are the leading causes of death and disability in the developed world, there is a particular demand for the development of effective and safe antithrombotic therapies for the prophylaxis and treatment of ischemic cardio- and cerebrovascular diseases [3, 4].

Maintaining the balance of sealing a wound on the one hand and uncontrolled thrombotic events on the other hand requires a tight regulation of diverse activating and inhibitory platelet receptors and thus a complex network of signaling pathways.

1.2 Platelet activation and thrombus formation

As described above, platelets normally never get in touch with components of the thrombogenic ECM. However, upon injury or pathological alterations of the endothelial barrier, ECM macromolecules are exposed to the flowing blood, activate platelets and allow platelet adhesion. In detail, the complex signaling process, which is involved in platelet activation and thrombus formation can be divided into three major steps. (1) Initial platelet binding occurs via the interaction of platelet receptors with exposed ECM constituents, thereby decelerating the cells. Subsequently, platelets are activated upon initiation of receptor-triggered signaling cascades resulting in integrin activation and granule secretion (2). Ultimately, firm adhesion and platelet aggregation are facilitated through remodeling of the platelet cytoskeleton leading to spreading on the reactive surface and a further recruitment of platelets into the growing thrombus (3) (Fig. 1).

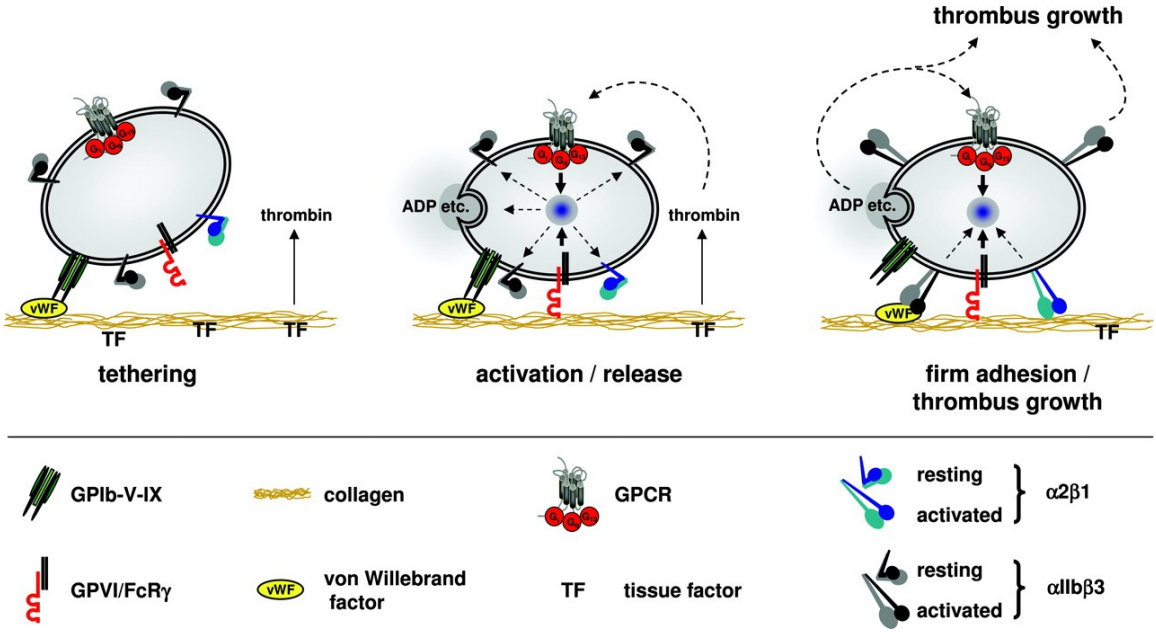

Figure 1. Schematic overview of thrombus formation. Upon endothelial damage, components of the ECM become exposed to the flowing blood allowing platelets to tether upon interaction of GPIb-V-IX with collagen-bound vWF. The interaction of GPVI with collagen leads to integrin activation and the release of second wave mediators such as ADP, TxA_2 and Ca^{2+}. In parallel, locally exposed TF induces thrombin formation enabling additional platelets to become activated and recruited into the growing thrombus. Finally, integrins mediate firm adhesion through binding to ECM components and aggregation of platelets via the interaction with fibrinogen [5]. ECM, *extracellular matrix*; GP, *glycoprotein*; vWF, *von Willebrand factor*; ADP, *adenosine diphosphate*; TxA_2, *thromboxane* A_2; TF: *tissue factor*. Modified from Varga-Szabo *et al*., **ATVB**, 2008 [6].

Tethering of platelets occurs under intermediate or high shear forces (1,000-10,000 s^{-1}), which are predominantly present in arterioles or stenosed arteries. During this process, platelets are decelerated by the transient interaction of platelet *glycoprotein* (GP) *Ib-V-IX* (GPIb) and collagen-bound *von Willebrand factor* (vWF) leading to 'rolling' of the platelets (Fig. 1). The important role of the vWF-GPIb interaction for thrombus formation is reflected by the severe

macrothrombocytopenia and bleeding disorder found in patients suffering from the Bernard-Soulier syndrome, which is caused by absent or dysfunctional GPIb. Activated GPIb can additionally transduce signaling events leading to weak αIIbβ3 integrin activation. Although the underlying mechanisms are not fully understood, proteins such as the actin-binding protein 14-3-3ζ, *phosphoinositide 3-kinase* (PI3K), Src-related tyrosine kinases, GTPase activating proteins and *phospholipase* (PL) D1 have been proposed to be important for GPIb-dependent adhesion processes [7, 8]. Of note, the affinity of GPIb towards vWF is too weak to mediate firm adhesion, thus rather mediating the localization of platelets at the vessel wall. Firm adhesion of platelets to the vessel wall is enabled by the interaction of the platelet GPVI receptor with collagens of the ECM ultimately causing platelet activation. Besides GPVI activation, this initial phase of platelet activation also comprises the activation of the transmembrane-related *C-type lectin-like receptor* (CLEC)-2, the receptor for the snake venom toxin rhodocytin. Signaling induced by these receptors involves tyrosine phosphorylation cascades via the Src family kinases Fyn and Lyn that phosphorylate the noncovalently associated intracellular *immunoreceptor tyrosine-based activation motif* (ITAM)-bearing *Fc receptor* (FcR) γ chain [9]. While the ITAM motif of GPVI harbors two YXXL-motifs through which receptor activation is initiated, CLEC-2 consists of only one YXXL-motif and is therefore called “hemITAM” receptor [10]. Phosphorylation of the YXXL motif leads to subsequent recruitment and activation of the *spleen tyrosine kinase* (Syk), that in turn triggers the activation of other downstream signaling molecules, such as the *linker of activated T-cells* (LAT), the *SH2 domain-containing leukocyte protein of 76 kDa* (SLP-76) or *growth factor receptor-bound protein 2* (Grb2), ultimately culminating in the activation of effector molecules such as PLCγ2 or PI3K [11]. Activated PLCγ2 cleaves the membrane phospholipid *phosphatidylinositol-4,5-bisphosphate* (PIP_2) into *inositol-1,4,5-triphosphate* (IP_3) and *diacylglycerol* (DAG). Binding of IP_3 to the IP_3 receptor present in the membranes of the endoplasmatic reticulum induces the release of intracellular Ca^{2+}. The sarcoplasmic membrane protein *stromal interaction molecule* (STIM) 1 senses the decrease of Ca^{2+} levels in the internal store and in turn induces *store operated calcium entry* (SOCE) through activation of *Ca^{2+} release-activated calcium channel protein 1* (Orai1) [12]. The combined work of Ca^{2+} and PLCγ2-generated DAG activate *protein kinase* (PK)C´s and *Ca^{2+}-dependent DAG-regulated guanine nucleotide exchange factor I* (CalDAG-GEFI). While CalDAG-GEFI and PI3K play important roles in integrin activation, PKCs are involved in platelet spreading, granule release and contribute to the activation of CalDAG-GEFI [13].

The temporally and spatially controlled release of second wave mediators leads to the recruitment of additional platelets into the growing thrombus. Besides a plethora of other molecules platelet α-granules contain the adhesive proteins vWF and fibrinogen, whereas

dense granules secrete the second wave mediators *adenosine diphosphate* (ADP), *adenosine triphosphate* (ATP), Ca^{2+}, histamines and serotonin [14]. Thrombin is locally produced on the surface of activated platelets, linking platelet activation to coagulation. Thrombin catalyzes the conversion of fibrinogen to fibrin and acts as a potent activator of platelets. Its generation can be initiated by two distinct pathways (intrinsic and extrinsic coagulation pathway), both of which culminate in the cleavage and activation of the proenzyme prothrombin (FII) to thrombin. Upon vascular injury, exposed TF interacts with FVII, which circulates in the blood stream, thereby promoting the extrinsic pathway of blood coagulation. In parallel, negatively charged *phosphatidylserine* (PS) is exposed on the platelet surface in response to sustained Ca^{2+} signaling. This allows the assembly and activation of the prothrombinase and tenase complexes accelerating the clotting process [15]. Regarding the intrinsic pathway, negatively charged surfaces, such as polyphosphates or RNA, have been proposed as physiological initiators. This pathway includes the activation of FXII, which in turn triggers sequential activation of FXI, FIX and FX [16]. Among the released second wave mediators, ADP binds to the $P2Y_1$ and $P2Y_{12}$ receptors that activate *G-proteins* $(G)_q$ and G_i, respectively, whereas *thromboxane* A_2 (TxA_2) and thrombin stimulate the TxA_2 (TP) and *protease-activated receptors* (PAR)1/3 or PAR3/4 receptors, which mainly signal through G_q and $G_{12/13}$ (Fig. 2).

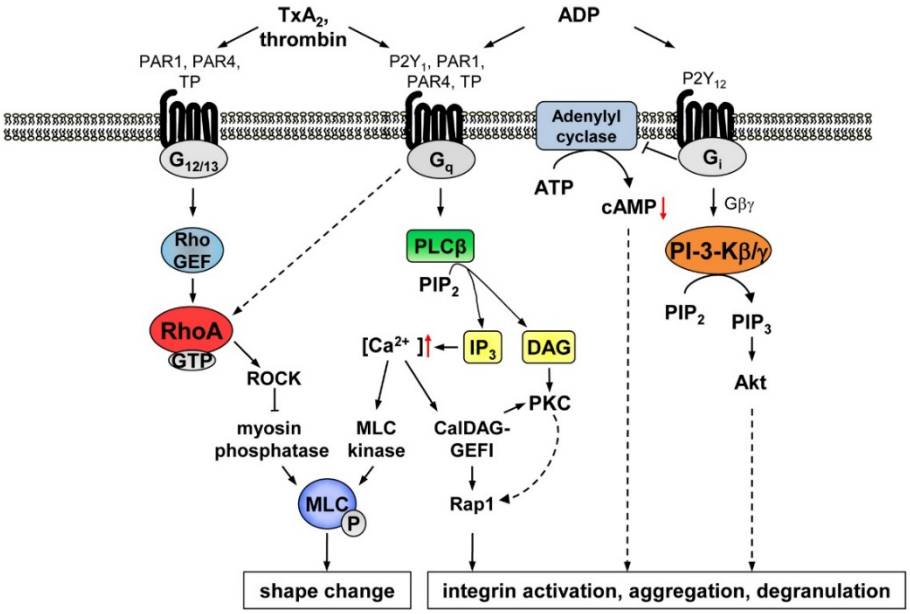

Figure 2. Signaling pathways induced by *G-protein coupled receptor* (GPCR) stimulation in platelets. Platelet agonists such as ADP, TxA_2 and thrombin activate platelets via GPCR. $G_{12/13}$, G_q and G_i, thus linking receptor activation to platelet shape change, integrin activation, aggregation and degranulation. PLC, *phospholipase C*; MLC, *myosin light chain*; DAG, *diacyl glycerol*; CalDAG-GEF, *calcium and diacyl glycerol-regulated guanine nucleotide exchange factor*; PIP_3, *phosphatidylinositol-3,4,5-trisphosphate*; PIP_2, *phosphatidylinositol-4,5-bisphosphate*; PAR, *protease-activated receptor*; TP, *TxA_2 receptor*; RhoGEF, *Rho-specific guanine nucleotide exchange factor*; PI3K, *phosphoinositide-3-kinase*; ROCK, Rho associated coiled-coil containing protein kinase; ATP, *adenosine triphosphate,* cAMP, *cyclic adenosine monophosphate.* Modified from Offermanns *et al.*, **Circ Res**, 2006 [17].

Signaling through *G-protein-coupled receptors* (GPCR) leads to amplification of platelet activation by inducing the generation of TxA_2 and release of ADP and ATP. Signaling through G_q culminates in the activation of PLCβ isoforms, generation of IP_3 and DAG via hydrolysis of PIP_2, which subsequently leads to the increase of the cytoplasmic Ca^{2+} concentration, activation of PKC and consequently to the activation of integrins and granule release (Fig. 3) [17, 18].

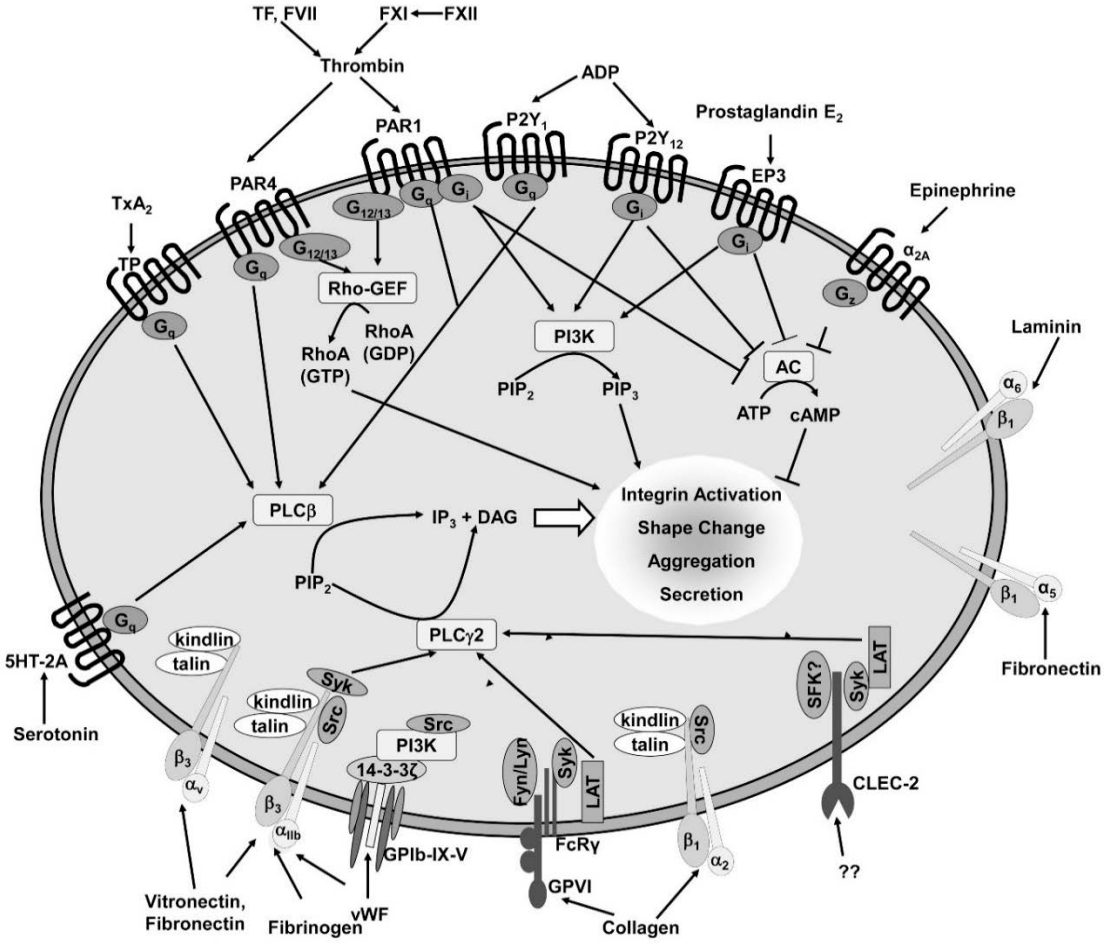

Figure 3. Signaling mechanisms during platelet activation. Different signaling pathways are induced upon platelet receptor stimulation. GPCRs transduce signals through different G-proteins. $G_{12/13}$ activation triggers Rho kinase-dependent pathways and G_q activates PLCβ, while $G_{i/z}$ inhibits AC. (hem)ITAM signaling initiates a complex tyrosine phosphorylation cascade resulting in the activation of PLCγ2. Active PLCs generate IP_3 and DAG, increasing the cytosolic Ca^{2+} concentration and activating PKCs. Altogether these events lead to the activation of integrins resulting in platelet aggregation, secretion and shape change. PIP_2, *phosphatidylinositol-4,5-bisphosphate*; PAR *protease-activated receptor*; TxA_2*, thromboxane A2;* TP*, TxA2 receptor*; Rho-GEF, *Rho-specific guanine nucleotide exchange factor*; PI3K, *phosphoinositide-3-kinase*; IP_3, *inositol-1,4,5-triphosphate*; DAG, *diacyl glycerol*; PIP_3, *phosphatidylinositol-3,4,5-trisphosphate*. Taken from Stegner *et al*., **J Mol Med**, 2011 [19].

Very recently, G_q signaling was shown to be critical for the proper phosphorylation of *protein kinase B* (Akt) downstream of G_i signaling [20]. In contrast, activation of $G_{12/13}$ family members

leads to the activation of *Rho specific guanine nucleotide exchange factor* (Rho-GEFs) that activate RhoA, which culminates in increased phosphorylation of *myosin light chain* (MLC) through *Rho associated coiled-coil containing protein kinase* (ROCK)-mediated inhibition of the myosin phosphatase. Activated MLC in turn induces the reorganization of the platelet cytoskeleton, known as shape change [21]. Moreover, stimulation of the G_i-coupled $P2Y_{12}$ receptor inhibits *adenylyl cyclase* (AC) activity and activates PI3K, which in turn generates *phosphatidylinositol-3,4,5-triphosphate* (PIP_3) that activates multiple downstream effectors such as Akt and ultimately leads to integrin activation (Fig. 3) [22, 23]. Finally, GPVI and PAR signaling act synergistically to fully activate platelets and mediate firm adhesion mainly through binding of $\alpha_2\beta1$ integrins to collagen and αIIbβ3 integrins to fibrinogen and collagen-bound vWF. Platelet aggregation is mainly mediated through binding and cross-linking of activated αIIbβ3 integrins to fibrinogen. The activation of platelets in general is characterized by a marked rearrangement of the actin and tubulin cytoskeleton, resulting in the formation of membrane protrusions, so-called filopodia and lamellipodia [24].

1.3 The platelet cytoskeleton

The cytoskeleton consists of a highly interconnected structure of filamentous polymers and associated proteins that enables a eukaryotic cell to cope with deforming forces, allows active transport of intracellular cargos and facilitates the shape change of the cell, which is required for movement. This is achieved by the combined functions of a plethora of cytoplasmic proteins and organelles. Although the name cytoskeleton indicates a stable and rigid structure, it is a highly adaptive and dynamic network and the components are in a constant equilibrium of assembly and disassembly. Three major types of filaments can be distinguished: micro-tubules, intermediate and actin filaments.

1.3.1 Tubulin cytoskeleton

The tubulin cytoskeleton consists of different α- and β-tubulin isoforms which in their GTP-bound state, form heterodimers and can be further assembled into long and polarized plus- (β-subunit is exposed) and minus-end (α-subunit is exposed) protofilaments. Thirteen of these protofilaments can further associate laterally and thereby build microtubules, which are hollow cylinders with an average diameter of 24 nm that can have a length of up to 50 µm [25, 26]. Microtubules exist in a steady state of assembly and disassembly termed dynamic instability. In general, assembly can occur at both, the plus- and minus-end, even though it occurs much faster at the plus-end [27]. Hydrolysis of GTP bound to the β-subunit of the polymerized heterodimer decreases filament stability and leads to microtubule depolymerization. Once the microtubule tip (plus-end) contains GDP-tubulin, a rapid depolymerization occurs, which is

termed ‘catastrophe’. This process can be rescued by the addition of new GTP-tubulin heterodimers [28]. Microtubule stability strongly depends on posttranslational modifications such as acetylation, detyrosination, polyglutamylation or polyglycylation [29]. Thus, an acetyl-residue added to lysine 40 of the α-tubulin subunit indicates stable microtubules. Acetylation is mostly mediated via the *α-tubulin N-acetyltransferase 1* (α-TAT1), while deacetylation is mainly accomplished by *histone-deacetylases* (HDAC) 5/6 and *the nicotinamide adenine dinucleotide* (NAD)-*dependent deacetylase sirtuin-2* (SIRT2) [30-33]. Similarly, removal of the C-terminal tyrosine from the α-tubulin subunit leading to the exposure of the preceding C-terminal glutamate is another indicator for stable microtubules. The enzyme mediating the detyrosination, however, still needs to be identified [29, 34]. Polyglutamylation and polyglycylation can occur on both the α- and β-tubulin subunits and are mediated via *tubulin-tyrosine ligase* (TTL)-*like family member enzymes* (TTLLs), that add a γ-linked glutamine or glycine to one or more of the five C-terminal glutamates [29]. The temporal and spatial coordination of microtubule dynamics is essential as microtubules do not only maintain the structure of the cell, but are also of critical importance for cell migration, mitosis, meiosis, developmental processes and for the transportation of intracellular cargos. In platelets, microtubules are organized into the characteristic marginal band that consists of 8-12 microtubule coils in the platelet periphery that maintains the discoid shape of resting platelets. Consequently, microtubule disassembly induced at temperatures below 16°C or upon treatment with microtubule destabilizing toxins, such as colchicine or nocodazole, leads to a spherical platelet shape [35]. The critical role of microtubules for maintaining a discoid platelet shape was further confirmed by a *knockout* (KO) mouse model lacking the hematopoietic lineage-specific β1-tubulin that displayed a macrothrombocytopenia with spherical platelets with a markedly reduced number of discontinuous microtubule coils within the marginal band [36].

1.3.2 Actin cytoskeleton

The intracellular actin cytoskeleton participates in a large variety of cellular processes such as cytokinesis, cell motility and polarization, phago- and exocytosis. These processes critically depend on its dynamic behavior to depolymerize existing *filamentous* (F-) actin filaments to replenish the *globular* (G-) actin pool and on the contrary to build new actin filaments. F-actin is composed of monomeric G-actin molecules, of which in mammals, three isoforms have been identified: the mainly muscle specific α-actin and the ubiquitously expressed β- and γ-actin isoforms [37]. The typical helix structure is achieved by a 166° rotation of two parallel F-actin strands, which yields an F-actin microfilament with an average diameter of 7 nm. Platelets contain over two million actin molecules, which are present in a dynamic monomer-polymer

equilibrium [38, 39]. Approximately 40-50% of the total actin monomers are present in the filamentous form in a resting platelet and constitute 2,000-5,000 actin filaments [40].

The remaining 50-60% of monomeric actin is stored in stoichiometric 1:1 complexes with *thymosin* (T) β4, *profilin* (Pfn) 1, *Twinfilin* (Twf) 1/2a and other actin sequestering proteins and becomes incorporated into filaments upon platelet activation. Within 20 seconds after platelet stimulation with thrombin the total amount of F-actin increases up to 70% [41, 42]. The actin filaments of resting platelets are highly cross-linked and form a stiff network through numerous actin crosslinking molecules such as *filamin* (Fln) A, spectrins or α-actinin. FlnA recruits and positions numerous proteins including *Ras homologue gene family member* (Rho) A, *Ras-related C3 botulinum toxin substrate* (Rac) 1, *p21/ Cdc42/ Rac1-activated kinase* (PAK1) and many others [43, 44]. The dynamics of the well-organized cytoskeletal architecture need to be tightly regulated, which is achieved by the combined action of actin-binding proteins.

1.4 Regulation of actin dynamics

Actin polymerization is a two-step process that comprises nucleation and elongation. The formation of polymerization-competent nuclei is the rate-limiting step, since it is energetically unfavorable, whereas the elongation process proceeds rapidly. During association to one end of a growing filament, ATP bound to G-actin is hydrolyzed into ADP and phosphate. Since ATP-hydrolysis associated with polymerization occurs with a delay after subunit association, two different filament ends can be distinguished: The fast growing plus (+) - or barbed end with ATP-actin subunits and the slow-growing minus (-) - or pointed end with ADP-actin subunits. Both differ in their rates of monomer association and dissociation. Elongation of growing actin filaments occurs until the free monomer concentration has fallen to the *critical concentration* (c_c) of polymerization that is closer to the *dissociation constant* (K_D) of the barbed end. At c_c, the number of actin subunits that associate to the barbed end, equals the number of monomers dissociating from the pointed, the so-called actin treadmilling [45]. In resting cells, G-actin levels are maintained far above c_c for polymerization, as found in lamellipodia, where levels of G-actin and F-actin are estimated to 150 and 500 µM, respectively. Therefore, the barbed ends are blocked by so-called *capping proteins* (CP) to prevent nonproductive polymerization [46]. As shown in Figure 5, the availability of the G-actin pool is tightly regulated by the actin-sequestering proteins, Tβ4, Pfn1 and Twf1/2a.

β-thymosins are short peptides that can completely sequester G-actin, whereas Pfn1 can both sequester G-actin in isolation as well as actively participate in barbed end elongation in the presence of actin nucleation and elongation machineries. Twf was shown to inhibit actin filament growth by two modes: (1) inhibition of barbed end growth by capping of barbed ends

and (2) inhibition of pointed end growth by sequestration of G-actin monomers, resulting in a decreased availability of G-actin [47, 48].

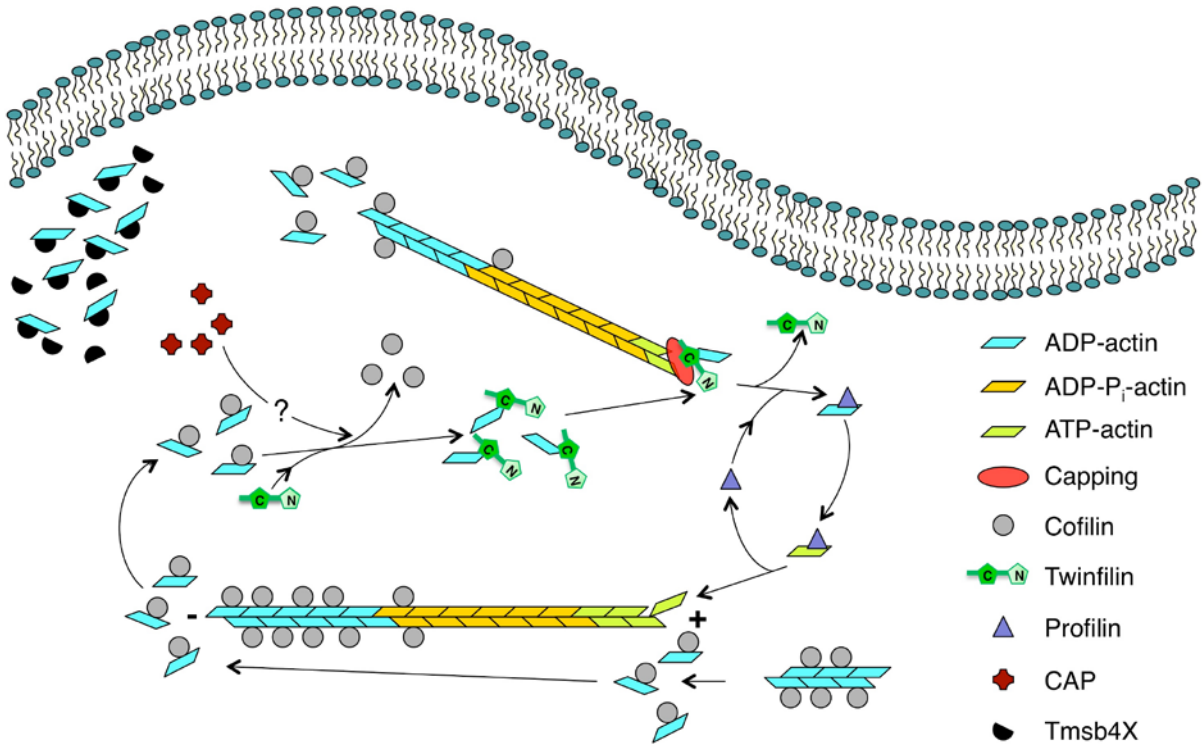

Figure 5. Proposed model of actin dynamics (not all involved proteins are depicted). Actin filaments consist of G-actin monomers, which can be divided into three energetic states: ATP-G-actin (bright green), ADP-P_i-G-actin (orange) and ADP-G-actin (light blue). Cofilin (grey) severs and depolymerizes ADP-G-actin from actin filaments. Severing results in free barbed ends (+), thus providing a new target available for polymerization and for disassembly at the newly provided pointed end (-). Twinfilins (green) compete with cofilin in binding to ADP-G-actin monomers. Since twinfilin has a higher affinity for ADP-G-actin, this interaction is preferred. Moreover, twinfilin was shown to interact with heterodimeric capping protein (red). Profilin (dark blue) acts as a nucleotide exchange factor for G-actin monomers replenishing the pool of high-energy ATP-G-actin for the assembly of actin filaments. Furthermore, twinfilin, profilin and cofilin were shown to interact with PIP_2, which results in a down-regulation of the sequestering function of twinfilin and profilin on G-actin monomers and the severing activity of cofilin. CAP, *cyclase-associated protein*; Tmsb4x, *Thymosin β4* [38, 40, 49-51]. Figure was kindly provided by Dr. Simon Stritt.

Actively elongating filaments are created through controlled uncapping, severing or nucleation mechanisms. Spontaneous actin nucleation can either occur by activation of formin family members such as the *mammalian diaphanous 1 protein* (mDia1, DIAPH1) by small GTPases or binding of *adenomatous polyposis coli* (APC), which both can overcome the inhibitory effects of CPs. On the other hand, nucleation can be induced by the action of the Arp2/3 complex, which in turn can be activated by binding of *Wiskott-Aldrich syndrome protein* (WASp) family members via their *verprolin, central, acidic* (VCA) domain. Actin turnover and the creation of new barbed ends is achieved by the action of severing proteins such as *cofilamentous structures with actin* (Cofilin/Cof) or *cyclase-associated proteins* (CAP). Cof has the unique

property to induce a twist in the actin filament of about 5° rotation per subunit, thereby weakening the lateral binding. Following this, actin turnover is enhanced by dissociation of actin monomers from the pointed end and by filament severing [52-54]. CAPs are highly conserved actin monomer binding proteins present in all eukaryotes [55], which were first identified in budding yeast (here called Srv2) as a suppressor of the activated ras allele [56] and as factor associated with AC [57]. In yeast cells, CAP/Srv2 localizes to cortical actin patches through an interaction with the *actin filament binding protein* (Abp1) [58] [59]. The loss of CAP was accompanied by cytoskeletal defects in budding yeast, *Dictyostelium* and *Drosophila* [55]. Interestingly, depletion of the isoform CAP1 leads to an accumulation of Cof into abnormal cytoplasmic aggregates and to similar cytoskeletal defects observed in Cof knockdown cells, demonstrating that CAP1 is required for recycling of *actin-depolymerizing factor/destrin* (ADF)/cofilin for new rounds of filament depolymerization and actin monomers to replenish the assembly-competent pool of actin [42] [59] [60]. Another study identified an interaction between CAP and Twf, which accelerated depolymerization of actin filaments at their barbed and pointed ends. This interaction could explain the observed discrepancy between very rapid *in vivo* actin filament turnover and the slow depolymerization of purified actin filaments *in vitro*. [61].

Cytoskeletal protein aberrations are the underlying reason for many pathological phenotypes. Several studies showed that a deregulated actin cytoskeleton, e.g. defects in proteins controlling actin dynamics, have been associated with platelet disorders in humans and mice. For instance, patients suffering from the *Wiskott-Aldrich-syndrome* (WAS), an X-linked inherited disorder, display microthrombocytopenia, immunodeficiency, eczema and an increased risk of autoimmune disorders and cancer (Online Mendelian Inheritance in Man; Accession number #301000) [62]. WAS is caused by mutations within the WAS gene encoding the *WAS protein* (WASp), which was reported to be involved in the signal transduction from membrane receptors to the actin cytoskeleton. WASp was shown to regulate the activity of the Arp2/3 complex, thereby enabling the nucleation of new actin filaments [63]. Consequently, WASp is an important regulator of actin assembly and is constitutively associated with *WASp-interacting protein* (WIP) in resting and activated platelets to prevent its degradation [64-66]. The severe phenotype found in these patients underscores the important role of the actin cytoskeleton for the proper function of platelets.

Interestingly, cytoskeletal abnormalities were not only shown to be of importance in platelet disorders, but further influence the outcome of a variety of other diseases including cardiovascular disease syndromes, neuro-degeneration, cancer (invasion), liver cirrhosis, pulmonary fibrosis and blistering skin diseases. Attempts to modulate the cytoskeleton by

peptides or other specific drugs have already yielded interesting results, thus rendering the cytoskeleton a possible new therapeutic target. Two convincing examples: anti-cytoskeletal (microtubule targeted) drugs are already used to inhibit cell division in certain cancer types and antibodies against the cytoskeleton are widely used for diagnostic purposes [67].

1.4.1 The ADF-H protein family

The *ADF homology domain* (ADF-H) is one of the best-characterized actin-binding motifs. It is present in at least three distinct groups of actin-binding proteins: ADF/cofilins, twinfilins, and Abp1/debrins [68]. Each group of ADF-H family members shows unique actin-binding properties and biological activities. Whereas ADF/cofilins contain only one ADF-H domain and can bind both G- and F-actin [69], Twfs consist of two ADF-H domains separated by a short linker region and are only able to bind monomeric actin [38, 66]. Abp1/debrins on the other hand are relatively large proteins consisting of an N-terminal ADF-H domain, a variable region and a C-terminal SH3 domain. These proteins only bind F-actin [58, 59, 70]. As a fourth class of ADF-H-containing proteins, Coactosins have been identified. However, due to low sequence homology to other ADF-H proteins it has long been unclear whether *coactosin like F-actin binding protein 1* (Cotl1) is indeed an ADF-H family member.

1.4.1.1 Cofilin

In the early 1980s, the first members of the ADF/cofilin family were identified. ADF and cofilin are actin-binding proteins of a molecular mass of about 15-21 kDa, which share a sequence identity of about 70%. Both proteins contain a single ADF-H domain; the actin binding site as well as a phosphorylation site at serine 3 are the most conserved regions of ADF/cofilin between different species [51, 71]. In mammals, three isoforms of the ADF/cofilin family exist on different chromosomes, ADF, cofilin-1 (*non-muscle* (n)-cofilin) and cofilin-2 (*muscle* (m)-cofilin). ADF and n-cofilin are expressed in most tissues, whereas m-cofilin is only found in muscle cells [72, 73]. ADF was first observed to rapidly reduce the viscosity of F-actin in solution, whereas cofilin was primarily found to bind to F-actin. After dephosphorylation, ADF and n-cofilin preferentially bind in a cooperative manner to ADP-bound F-actin, which acts as a turnover marker for older filaments [71, 74]. Upon binding to actin, ADF and n-cofilin have the unique property to induce a twist in the actin filament (5° rotation per subunit) thereby weakening the lateral binding. Following this, actin turnover is enhanced by (1) dissociation of actin monomers from the pointed end, which are transferred to the barbed end and (2) by filament severing, which provides new barbed ends for the addition of actin monomers [52-54, 69, 75]. Although the activity of ADF/n-cofilin is regulated by several mechanisms, including the isoform expression pattern, competitive binding with other proteins like tropomyosin or PIP_2 binding [51], the main and best studied regulatory mechanism is (de)phosphorylation of ADF/n-

cofilin at the highly conserved amino acid serine 3 [76]. *LIM kinase* (LIMK) and *testicular protein kinase* (TESK) phosphorylate and inactivate ADF/n-cofilin activity, whereas dephosphorylation and thereby activation of ADF/n-cofilin is mediated by phosphatases such as the serine phosphatases PP1 and PP2A, slingshot and chronophin [77-81]. Activation of phosphorylated ADF/n-cofilin is a rapid process in response to different stimuli in many cell types [77]. In platelets, approximately 90% of n-cofilin is phosphorylated at position serine 3 in the resting state, suggesting a slow actin turnover. After stimulation with thrombin, maximal n-cofilin dephosphorylation of about 75% occurs within 10 minutes [82].

Studies on different model organisms have revealed an essential role for ADF/cofilin during development. Deficiency for either ADF or cofilin in yeast or *Drosophila (D.) melanogaster* resulted in lethality [83, 84]. The same was found in *Caenorhabditis (C.) elegans* when both isoforms UNC-60A and UNC-60B were affected [85, 86]. In mice, n-cofilin deficiency led to embryonic lethality due to defects in neural crest cell migration and neural tube closure [87]. Furthermore, conditional gene targeting in mice revealed an association of n-cofilin with cell cycle control in the cerebral cortex and disorders in neuronal migration. In contrast, mice constitutively lacking ADF are viable and display no obvious defects in brain development [88]. However, mice with a combined deficiency for ADF and n-cofilin in MKs and platelets displayed a severe macrothrombocytopenia combined with an abnormal ultrastructure of the platelets, which was the result of almost abolished proplatelet formation. Analysis of BM MKs revealed a hypermegakaryoplasia with an abnormal ultrastructure. Moreover, agonist-induced F-actin polymerization was almost eliminated in platelets of these mice. This study clearly demonstrates that dynamic changes of the actin cytoskeleton play a critical role for platelet production from MKs *in vivo* [82].

1.4.1.2 Twinfilin

Human Twf was first identified in 1994 and initially thought to represent the catalytic domain of PKC [89-91]. Twf homologues have been identified in human, mouse, and *C. elegans*, but not in plants [47]. Although the sequence homology of Twfs two ADF-H domains and ADF/cofilin is rather low, their crystal structures are almost superimposable [47, 92]. While unicellular organisms and lower animals, such as *Saccharomyces (S.) cervesiae* or *D. melanogaster*, respectively, only have one Twf isoform, the ubiquitously expressed Twf1 and Twf2a, as well as the muscle-specific Twf2b have been identified in mammals [93, 94]. Although both Twf ADF-H domains can bind G-actin, they interact in a molar ratio of 1:1, with the affinity towards ADP-G-actin being approximately 10-fold higher compared to ATP-G-actin [47, 69, 94, 95]. Twf was shown to inhibit actin filament growth by two distinct mechanisms: on the one hand, Twf prevents barbed end growth by capping of actin filaments (Fig. 5). On the other hand, it

inhibits pointed end growth by sequestering G-actin monomers, thus reducing the pool of free monomers [47, 48]. Moreover, Twfs interact with heterodimeric CPs and, at least in yeast, this interaction was reported to be important for its proper function in actin dynamics [96]. Of note, binding of CPs to actin filament barbed ends inhibits both depolymerization as well as the addition of new monomers. However, the Twf-CP interaction is thought to localize ADP-G-actin monomers close to places of rapid actin turnover, thus providing new monomers for actin filament growth [52, 94, 96]. Upon ADF/cofilin-mediated dissociation of G-actin monomers from actin filaments, Twf is thought to compete with ADF/cofilin in binding to these monomers [93, 95, 97]. In addition, Twf also interacts with PIP_2, which inhibits its actin monomer sequestering function [50].

In vivo, Twf-deficiency in yeast resulted in mild alterations in the cortical actin patches and a defective budding pattern. However, the combination of a Cof or Pfn1 functional mutant with a Twf-deficiency in yeast resulted in synthetic lethality [47]. In contrast, *D. melanogaster* mutants lacking Twf displayed a reduced body size, were less active, exhibited a retarded development, a rough eye phenotype and an aberrant, often bend and rough bristle morphology, which was due to an uncontrolled polymerization of actin [98]. In 2011, Nevalainen *et al.* generated a constitutive Twf2a-deficient mouse line (*Twf2a*$^{-/-}$) and studied the morphology and histology of different organs. However, they could not detect a striking phenotype, which led to the conclusion that Twf2a is dispensable in mouse development [94]. Nevertheless, Nevalainen *et al.* hypothesized that the functionally redundant Twf1 isoform might compensate for the lack of Twf2a [94]. In 2017, Stritt *et al.* performed additional studies on the *Twf2a*$^{-/-}$ mouse line, and found a mild macrothrombocytopenia resulting from a markedly accelerated, macrophage-independent platelet clearance in the spleen. *Twf2a*$^{-/-}$ platelets showed enhanced integrin activation and α-granule release in response to stimulation of (hem)ITAM receptors and GPCRs, increased adhesion and aggregate formation on collagen under flow, accelerated clot retraction and enhanced spreading on fibrinogen. *In vivo*, Twf2a-deficiency resulted in shortened tail bleeding times and faster occlusive arterial thrombus formation. The hyperreactivity of *Twf2a*$^{-/-}$ platelets was attributed to enhanced actin dynamics, characterized by an increased activity of n-cofilin and Pfn1, leading to a thickened cortical cytoskeleton and hence sustained integrin activation due to limited calpain-mediated integrin inactivation. Thus, Twf2a-controlled actin rearrangements dampen platelet activation responses in a Cof- and Pfn1-dependent manner, thereby indirectly regulating platelet reactivity and lifespan in mice. However, an MK- and platelet-specific Twf1-deficient mouse did not reveal any defects in MK maturation, thrombopoiesis, platelet function, or actin assembly, thus further suggesting that the two Twf isoforms at least in part functionally overlap [99].

1.4.1.3 Cotl1

Cotl1 was originally identified in *Dyctyostelium (D.) discoideum* as a 17 kDa protein copurifying with actomyosin complexes [100]. To date, coactosin homologues have been identified in *D. melanogaster*, *Xenopus (X.) laevis* and mammals [101]. Like ADF/cofilins, Cotl1 contains one ADF-H domain. As shown in Figure 6, the amino acid sequences of coactosins from different species share less than 25% sequence identity to other ADF-H family members. Nevertheless, their 3D structures are almost identical [100, 101]. Especially, the regions important for actin filament interactions are structurally highly conserved between ADF/cofilin and Cotl1 suggesting a similar binding mode. Indeed, Coactosins were shown to bind F-actin, although with relatively weak affinity and they do not interact with actin monomers [100, 101]. Site-directed mutagenesis has determined that lysine 75, located in the ADF-H domain, plays a critical role in F-actin binding.

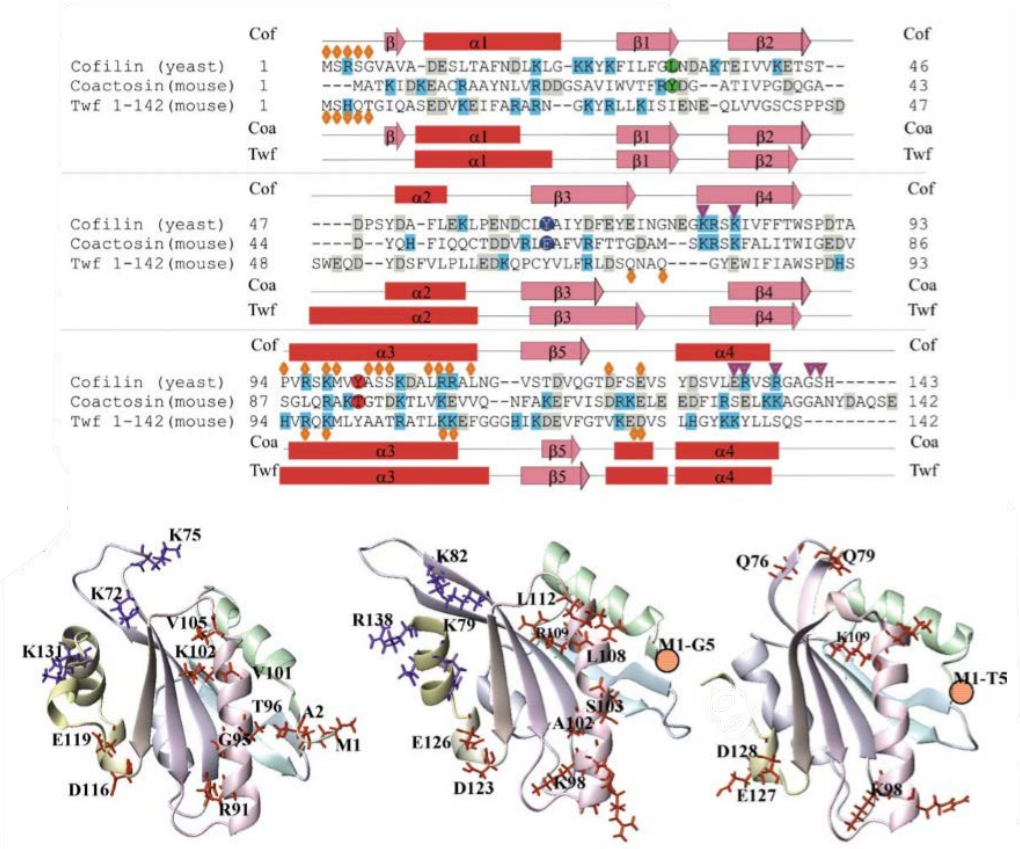

Figure 6. Structural comparison of Cotl1, yeast cofilin and N-twinfilin. Structural sequence alignment. The secondary structure elements and sequences of cofilin, coactosin and N-twinfilin are indicated. Acidic and basic amino acids are color-coded with light blue and grey rectangles, respectively. The residues that have been shown to be important for actin monomer and filament interactions in ADF/cofilins and N-twinfilin are marked with orange diamonds and violet triangles. Ribbon diagrams of coactosin (left), cofilin (middle; residues 6-138 shown, crystal structure) and N-twinfilin (right; residues 7-139 shown, crystal structure). The side chains of the residues important for F-actin and G-actin binding in cofilin are color-coded as in the sequence alignment. The residues conserved in coactosin are indicated with the same color scheme and the corresponding residues are labelled to cofilin and N-twinfilin. Orange-colored circles schematically indicate positions of N-terminal residues of cofilin and N-twinfilin involved in G-actin binding. Aligned secondary structure elements of the three proteins are equally colored. Taken from Hellman *et al.*, **FEBS Letters**, 2004 [102].

Biochemical analyses have demonstrated that Cotl1 has a different role in actin dynamics from the ones of ADF/cofilin, Twf or Abp1/debrin, since it does not affect actin polymerization. Instead, in *D. discoideum,* coactosin was shown to counteract the activity of capping proteins [103]. Moreover, Cotl1 was identified as a regulator of T cell activation. Mechanistically, Cotl1 was shown to prevent cofilin-mediated depolymerization of actin filaments, thereby promoting lamellipodia formation at the immune synapse [104].

Besides its interaction with F-actin, Cotl1 was shown to bind *5-lipoxygenase* (5-LO) in a yeast-two-hybrid assay [105]. 5-LO is a key enzyme in *leukotriene* (LT) biosynthesis, since it catalyzes two of the initial steps, which is the oxygenation of *arachidonic acid* (AA) to *5(S)-hydroperoxy-6-trans-8,11,14-cis-eicosatetraenoic acid* (5-HPETE) and the subsequent dehydration into the epoxide LTA_4 (Fig. 7). LTs are inflammatory lipid mediators, which cause leukocyte chemotaxis and increased vascular permeability. The effects of LTs are well established in the pathogenesis of asthma, and accumulating data indicated a role for LTs in atherosclerosis.

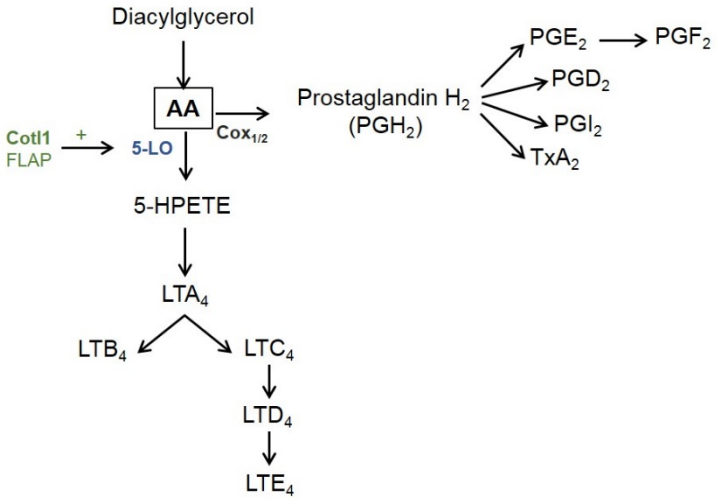

Figure 7. The 5-LO pathway. Different enzymes metabolize AA: (1) 5-LO catalyzes the oxygenation of AA to 5-HPETE, which results in the production of LTs. (2) Cox metabolizes AA to Prostaglandins and TxA_2. AA, *arachidonic acid*; 5-HPETE, *5(S)hydroperoxy-6-trans-8,11,14-cis-eicosatetraenoic acid;* LT, *leukotriene*; TxA_2, *thromboxane* A_2, 5-LO, *5-lipoxygenase,* Cox, *Cyclooxy-genase*.

In addition, 5-LO products are implicated in cancer cell survival, as recently shown in leukemia stem cells [106-109]. Cotl1 and another accessory protein, *5-lipoxygenase-activating protein* (FLAP), can upregulate and modulate 5-LO activity [110] . Additional results showed that Cotl1 functions as a chaperone for 5-LO, stabilizing 5-LO in resting cells and serving as a scaffold protein during Ca^{2+}-induced 5-LO activity [111]. However, its defined cell biological role as well as the mechanisms by which Cotl1 contributes to cytoskeletal dynamics in general remain enigmatic.

1.4.2 Actin-sequestering proteins

The availability of G-actin is tightly regulated by the two main monomer-binding proteins Pfn1 and Tβ4. β-thymosins are short peptides that can completely sequester G-actin, whereas

profilins can both sequester G-actin in isolation as well as actively participate in barbed end elongation in the presence of actin nucleation and elongation machineries [47, 48].

1.4.2.1 Profilin1

Pfn1 is a 14 kDa protein initially isolated from platelets in 1977 [112]. In mammals, four different Pfn isoforms are described: the well-characterized ubiquitously expressed Pfn1, the brain-specific Pfn2 (with two sub-isoforms Pfn2a and 2b), and the mainly testis-specific Pfn3 and 4 [112-116]. Pfn harbors, besides its actin-binding domain, a phosphatidyl-inositide binding site, with a strong preference towards PIP_2 and a *poly-L-proline* (PLP) binding domain, which is required for its interaction with other ligands (Fig. 8) [49, 117].

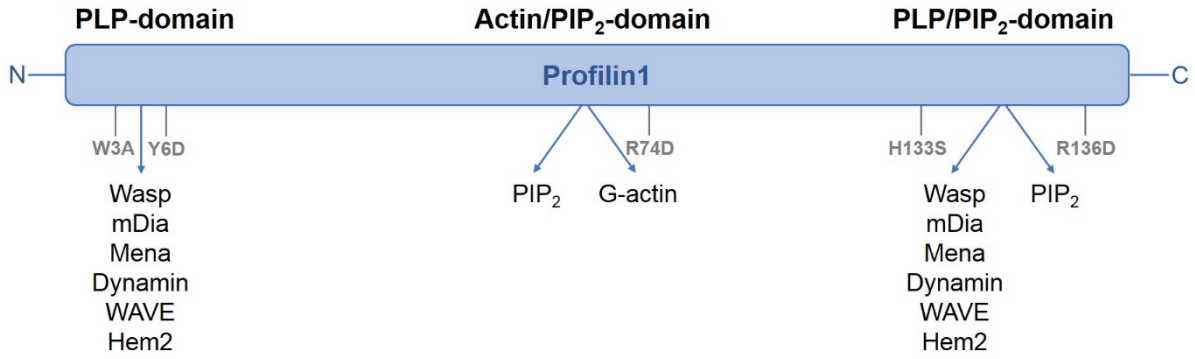

Figure 8. Domain architecture and interacting proteins of Pfn1 (not all interaction partners are depicted). Pfn1 consists of an N- and C-terminal PLP binding domain, a central actin binding site with an overlapping binding site for phosphatidylinositides, exhibiting a strong preference for PIP_2 and another PIP_2-binding site that overlaps with the PLP-binding domain in the C-terminus. The N- and C-terminal PLP-binding sites allow the association with numerous interaction partners, such as WASp, mDia, Mena, dynamin, WAVE or Hem2 [118]. Binding of Pfn to PIP_2 on the one hand prevents phospholipase-mediated hydrolysis to IP_3 and DAG and on the other hand inhibits the association with actin monomers. W3A, Y6D, R74D, H133S, and R136D highlight point mutants of profilin that specifically disrupt the function of single domains [119, 120]. Hem2, *hematopoietic protein 2;* Mena, *mammalian Enabled;* PLP, *poly-L-proline;* WAVE*, WASp family verprolin-homologous protein*. Adapted from [121].

Pfn was first identified as a small actin-binding protein (molar ratio of 1:1) and was initially thought to function as an ATP-G-actin sequestering protein, thus interfering with F-actin assembly. However, this hypothesis was questioned over time, since Pfn1 concentrations of around 0.5 µM in platelets are too low to account for all the sequestered G-actin molecules. In fact, Pfn1 acts as an ATP exchange factor for actin, recharging ADP- bound G-actin monomers to ATP-G-actin [122]. Moreover, Pfns were shown to regulate the addition of new monomers to growing actin filaments [123, 124]. Additionally, Pfn interacts with a huge number other PLP-stretch-containing proteins, among these are proteins involved in membrane trafficking like synapsin, clathrin, and dynamin, or proteins present in focal contacts, such as *mammalian enabled orthologue* (Mena) or *vasodilator-stimulated phosphoprotein* (VASP) [118, 125, 126].

Furthermore, Pfn is involved in the regulation of small Rho-GTPases, e.g. by the interaction with the WIP complex, downstream of Cdc42 or mDia1, a known effector of RhoA [119].

Pfn plays an essential role for development. In *Drosophila*, constitutive deletion of Pfn1 resulted in late, in mice in early embryonic lethality, indicating an essential biological function in mitosis and signaling [127, 128]. In 2014, Bender, Stritt *et al.*, studied a conditional MK- and platelet-specific Pfn1 KO mouse (*Pfn1*$^{fl/fl\text{-}Pf4Cre}$). Surprisingly, these mice fully reproduced key features of WAS patients (see section 1.4). They displayed a microthrombocytopenia due to accelerated turnover of platelets and premature platelet release into the bone marrow. *Pfn1*$^{fl/fl\text{-}Pf4Cre}$ MKs produced less and smaller-sized platelets into the circulation, which had a thicker marginal band and a partially disrupted actin cytoskeleton. These severely misarranged and hyperstable microtubules were also found in platelets isolated from WAS patients, which established Pfn1 as a new regulator of microtubule stability and reorganization [129].

1.4.2.2 Thymosin β4

β-thymosins are a family of 5 kDa peptides. Tβ4 was first isolated from calf thymus and therefore thought to exert hormone-like activities [130, 131]. Indeed, until now, various paracrine effects have been reported, including cardiac protection, angiogenesis, wound healing and immunomodulatory effects [129]. Besides its paracrine effects, Tβ4 is, together with Pfn1, the major G-actin sequestering protein within cells of higher eukaryotes. Of the 15 existing, highly homologous β-thymosins, Tβ4 is the most abundant form [129]. *Nuclear magnetic resonance* (NMR) studies on Tβ4 in aqueous solution revealed that it is highly unstructured. This lack of defined secondary structure element is also referred to as *intrinsically unstructured proteins* (IUPs). Mostly, IUPs obtain a defined tertiary structure only upon binding to their interaction partners. IUPs are often involved in various cellular activities and therefore interact with many different proteins, which is enabled by their ability to attain different conformations, thus adapting to their target interactions partners. Since it exerts intra- and extracellular functions, Tβ4 is a so-called moonlighting protein [132].

1.4.2.2.1 Intracellular function of thymosin β4

Tβ4 can be found in the cytoplasm of many different cell types in concentrations ranging from 100 to 500 µM. Its intracellular concentration is particularly high, in the range of 300–600 µM, in cells that rapidly respond to external signals by increased motility like polymorphonuclear leukocytes (neutrophils) and macrophages or by profound shape changes like platelets [133]. Its main intracellular function is to bind G-actin in a 1:1 stoichiometry (K_D = 0.4-0.7 µM), thereby inhibiting actin polymerization. In resting cells, Tβ4 complexes about half of the total actin amount. Due to a lack of any regulatory site on Tβ4, it has been speculated that actin release from Tβ4 after cellular activation is enabled by a drop in the c_c of actin polymerization below

the K_D of Tβ4 to G-actin. This is possibly due to a stimulus-dependent increase in barbed end concentrations, e.g. by removal of capping proteins from or severing of existing filaments or the action of actin polymerization nucleating proteins, suggesting that the affinity of Tβ4 towards actin does not change [132].

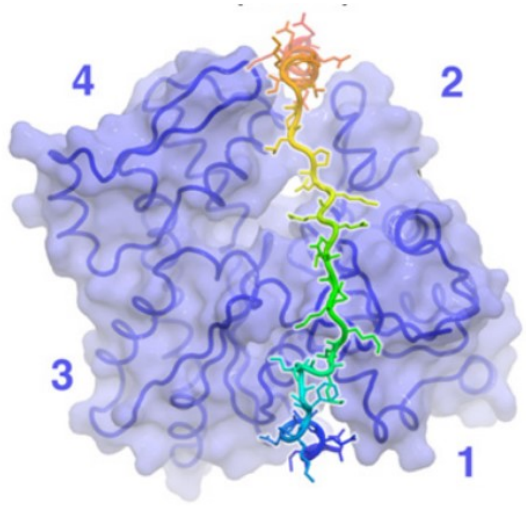

Figure 9. Structure of the Tβ4-actin complex. The protein complex was purified from *Pichia (P.) pastoris*. Actin is shown as a surface, with the subdomains indicated by numbers, and Tβ4 as a rainbow-colored cartoon with sticks. Tβ4 makes extensive contact with actin, spanning the nucleotide binding cleft from the barbed to the pointed face of the actin monomer. Taken from Xue *et al.,* **PNAS**, 2014 [134].

Tβ4 makes extensive contacts with actin, its N-terminal helix elongates into the cleft between subdomain 1 and 3 and its C-terminus stretches between subdomains 2 and 4, resulting in 3 contact regions (Fig. 9), the N- and C-terminal part and the extended region in between containing a widely spread actin binding consensus sequence (^{17}LKLTET^{22}) [134]. The extended region with its actin-binding consensus sequence is essential for actin binding, the structural topology is termed the *β-thymosin* (βT) domain or, more frequently, the WASP-homology (WH2)-domain [135].

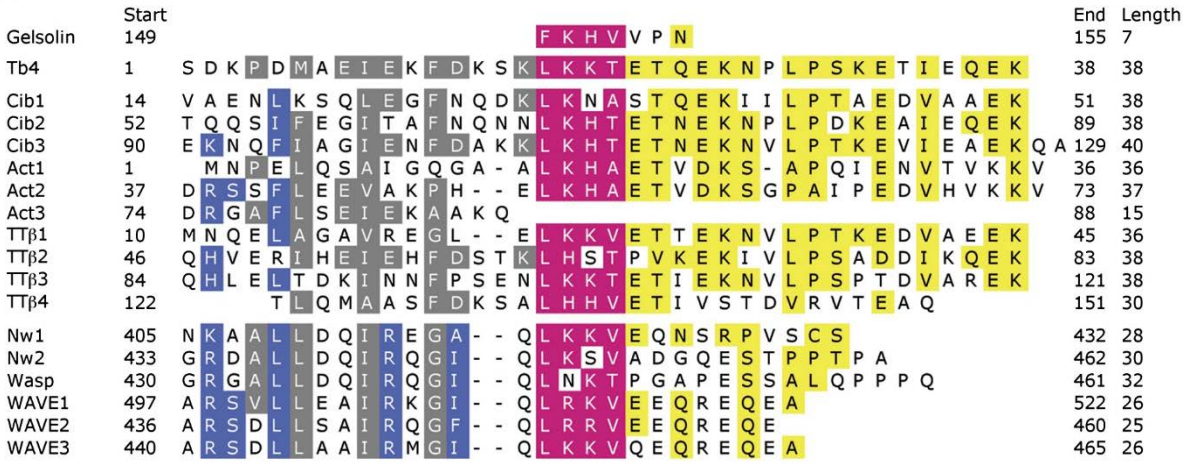

Figure 10. Structural-based sequence alignment of WH2/Tβ domains. Tβ4-like residues within the C-terminal half are depicted in yellow. Functionally analogous residues in both gelsolin and WH2/Tβ domain families are shown in pink. Tβ4-like residues within the N-terminal half are marked in gray. Blue highlights conserved residues throughout the WH2 family, except for Tβ4. Accession numbers are: gelsolin (X04412), Tβ4 (NM_021109), ciboulot (Cib, NM_167001), TTβ (NM_077029), actobindin (Act, A36614), N-WASP (NM_003941), WASP (U12707), WAVE1 (BC044591), WAVE2 (AB026542), and WAVE3 (AB026543). Taken from Aguda *et al.*, **Structure**, 2006 [136].

The common feature of WH2-containing proteins is their ability to bind to the barbed end of actin, although WH2-domains from different proteins share only 15% sequence identity (Fig. 10) [136]. In contrast to Tβ4, most of the depicted proteins support actin polymerization. This is due to a differential binding affinity of Tβ4, which is promoted by single residues. Therefore, some point mutations are sufficient for the switch from actin sequestration to nucleation [137].

Since a considerable amount of Tβ4 has been detected intranuclearly, it has been speculated to act as transcription factor, however, its function in the nucleus has not been further elucidated so far [138].

1.4.2.2.2 Extracellular function of thymosin β4

Tβ4 is present in extracellular body fluids. For example, plasma concentrations of Tβ4 are 0.03-0.4 µg mL^{-1} [139]. A recent study by Huff *et al.* showed that platelets release Tβ4 upon activation. The released Tβ4 is partially crosslinked to fibrin by FXIIIa, a transglutaminase, which might represent a mechanism to maintain Tβ4 at sites of injury (Fig. 11) [133]. However, possible secretion pathways remain elusive so far. Interestingly, Tβ4 is synthesized without a signal peptide, thus excluding a secretory pathway.

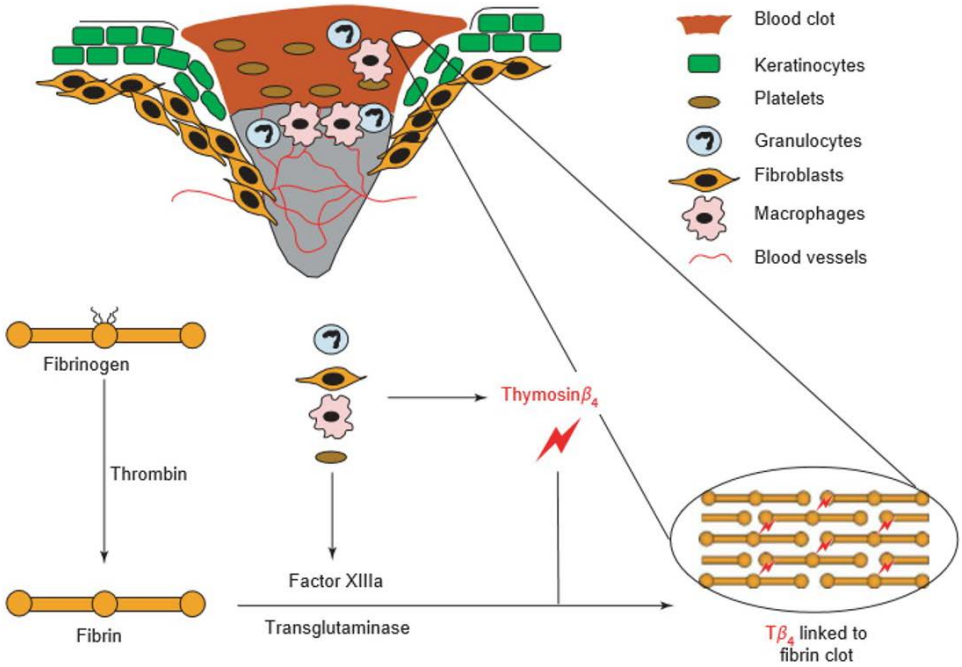

Figure 11. Integration of Tβ4 into blood coagulation and wound repair. As blood enters a wound, clotting proteins and enzymes such as fibrinogen, thrombin and complement are activated. Fibrinogen is converted to fibrin and a clot is formed. Cells such as granulocytes, macrophages, platelets and lymphocytes enter the wound. At the same time, platelets co-release other proteins including FXIIIa which crosslinks Tβ4 with the aC domains of fibrin. Granulocytes, macrophages and other cells at the wound site also release significant amounts of Tβ4. Tβ4, which is bound covalently to the clot matrix, is a chemoattractant for *endothelial cells* (ECs) and keratinocytes. These cells migrate rapidly into the wound site and the healing process begins. Taken from Goldstein *et al.*, **Trends Mol Med**, 2005 [129].

Besides blood, Tβ4 has been found in wound, lacrimal and oral human fluids [140-142]. Tβ4 concentrations are highest in platelets and *polymorphonuclear monocytes* (PMNs), which are among the first cells to enter a site of injury and recruit additional cells to the wound site. Tβ4 concentrations in wound fluids are around 13 µg mL^{-1}, most likely released from platelets.

Extracellular Tβ4 has multiple biological functions. It was identified as an angiogenic factor in a screen of early genes induced during *endothelial cell* (EC) differentiation. Accordingly, it promotes EC migration, tubule formation and angiogenesis *in vitro* [143]. Moreover, it was shown to promote angiogenesis and wound repair *in vivo* [144, 145]. It has been reported that monocytes produce an oxidized form of Tβ4 (Tβ4 sulfoxide) that blocks neutrophil chemotaxis *in vitro* and has anti-inflammatory properties *in vivo* [146]. Additionally, in the eye, topical application of Tβ4 promotes corneal wound repair through increase of the cell-cell and cell-matrix contacts and promoting of conjunctival epithelial cell migration [147]. In septic shock models, e.g. upon treatment of mice with lethal doses of endotoxins, Tβ4 significantly increased the survival of mice in a dose- and time-dependent manner [148]. Direct administration of Tβ4 following a myocardial infarction in mice protected heart tissue from cell death and enabled heart myocytes to survive after hypoxia by upregulating PINCH-ILK-Akt survival pathway [144]. After coronary artery ligation in mice, Tβ4 treatment resulted in upregulation of ILK and Akt activity, which enhanced early myocyte survival and improved cardiac function [143]. Figure 12 summarizes the moonlighting properties of Tβ4.

All these observations make Tβ4 a potential therapeutic agent, although its mode of action remains largely unknown [129].

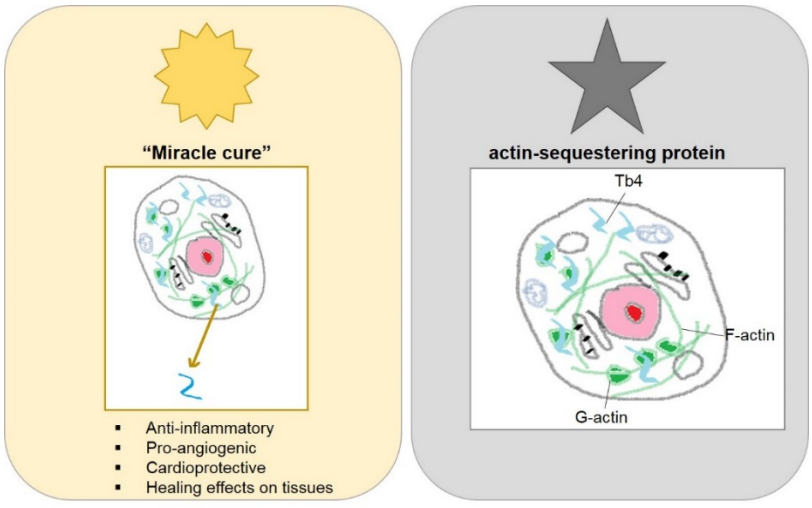

Figure 12. Moonlighting properties of Tβ4. Tβ4 has many functions in addition to its role as major actin sequestering molecule. It stimulates the migration of endothelial cells and has anti-inflammatory and anti-microbial properties. Moreover, it protects the heart from damage following myocardial infarction and accelerates the process of healing and remodeling of tissues such as dermis or cornea [129].

2. AIM OF THE STUDY

Rearrangements of the actin cytoskeleton play a crucial role for platelet formation and reactivity and several actin-binding proteins have already been reported to be importantly involved in these processes, such as the ADF-H family members Cofilin and Twf2a. Therefore, we were interested to investigate the role of two additional actin-binding proteins, the ADF-H family protein Cotl1 and the actin-sequestering protein Tβ4, in platelet formation and function by analyzing a conditional (Cre-loxP system) *Cotl1*$^{fl/lf\text{-}Pf4Cre}$ and a constitutive *Tβ4*$^{-/-}$ knock-out mouse line. Moreover, although the role of the second major actin-sequestering protein Pfn1 for platelet formation has already been described, we aimed to further investigate the loss of Pfn1 for platelet function and reactivity using a conditional *Pfn1*$^{fl/f\text{-}Pf4Cre}$ mouse.

Given the fact that platelets exert key roles in hemostasis under physiological conditions as well as during thrombotic events under pathological conditions, progress in elucidating platelet signaling pathways is essential to identify new potential targets for antithrombotic therapy. Exogenous Tβ4 has been shown to protect heart tissue from cell death after myocardial infarction. It is thought to exert its various beneficial effects by upregulation of the survival kinase Akt. However, the distinction between endo- and exogenous protein function, its release mechanisms, its uptake and its mode of action is mostly unknown. Therefore, with the analysis of a constitutive knockout of Tβ4, we aimed to investigate its effect on platelet physiology, hemostasis, thrombosis and ischemia and to shed light on the underlying signaling network by analyzing the effect of recombinant Tβ4.

3. MATERIALS AND METHODS

3.1 Materials

3.1.1 Chemicals and Reagents

A23187	AppliChem (Darmstadt, Germany)
Acetic acid	Roth (Karlsruhe, Germany)
Adenosine diphosphate (ADP)	Sigma-Aldrich (Steinheim, Germany)
Adenosine triphosphate (ATP)	NEB (Frankfurt am Main, Germany)
Agarose	Roth (Karlsruhe, Germany)
Alexa F488	Molecular Probes (Eugene, USA)
Alexa F647	Molecular Probes (Eugene, USA)
Ammonium persulfate (APS)	Roth (Karlsruhe, Germany)
Apyrase (grade III)	Sigma-Aldrich (Steinheim, Germany)
Aspirin	Bayer (Wuppertal, Germany)
β-mercaptoethanol	Roth (Karlsruhe, Germany)
Botrocetin	Pentapharm Ltd. (Basel, CH)
Bovine serum albumin (BSA)	Sigma-Aldrich (Steinheim, Germany)
Bromophenol blue (3',3",5',5"-tetrabromophenol-sulfonphthalein)	Sigma-Aldrich (Steinheim, Germany)
Cacodylate	AppliChem (Darmstadt, Germany)
Calcium chloride ($CaCl_2$)	Roth (Karlsruhe, Germany)
Chloroform	AppliChem (Darmstadt, Germany)
Collagen Horm® suspension + SKF sol.	Takeda (Linz, Austria)
Coomassie Brilliant Blue G-250	Roth (Karlsruhe, Germany)
Complete protease inhibitors (#11836153001)	Roche Diagnostics (Mannheim, Germany)
Convulxin (CVX)	Enzo Life Sciences (New York, USA)
Cryo-Gel	Leica Microsystems (Wetzlar, Germany)
Cytochalasin D	AppliChem (Darmstadt, Germany) & Abcam (Cambridge, UK)
4',6-diamidino-2-phenylindole (DAPI)	Invitrogen (Karlsruhe, Germany)
Dade® Innovin (tissue factor)	Siemens Healthcare Diagnostics (Deerfield, IL, USA)
Dimethyl sulfoxide (DMSO)	Sigma-Aldrich (Steinheim, Germany)
Disodiumhydrogenphosphate ($Na_2HPO_4 \times 2H_2O$)	Roth (Karlsruhe, Germany)
Dithiothreitol (DTT)	Roth (Karlsruhe, Germany)
DreamTaq DNA Polymerase (5 U L^{-1})	Life Technologies (Darmstadt, Germany)
DreamTaq Green PCR Master Mix, 2x	Life Technologies (Darmstadt, Germany
Dry milk, fat-free	AppliChem (Darmstadt, Germany)
Deoxynucleotide triphosphates (dNTP) mix	Life Technologies, Darmstadt, Germany
DNAse I	NEB (Frankfurt am Main, Germany)
DyLight-488	Pierce (Rockford, USA)
DyLight-649	Pierce (Rockford, USA)
Epinephrine	Sigma-Aldrich (Steinheim, Germany)
Ethylenediaminetetraacetic acid (EDTA)	AppliChem (Darmstadt, Germany)
Ethylene glycol tetraacetic acid (EGTA)	Sigma-Aldrich (Steinheim, Germany)
Eukitt® quick-hardening mounting medium	Sigma-Aldrich (Steinheim, Germany)

Enhanced chemiluminescence (ECL) detection substrate	MoBiTec (Göttingen, Germany)
Eosin	Roth (Karlsruhe, Germany)
Ethanol	Roth (Karlsruhe, Germany)
Fentanyl	Janssen-Cilag GmbH (Neuss, Germany)
Fetal calf serum (FCS)	Gibco (Karlsruhe, Germany)
Fibrinogen from human plasma (F3879+ F4883)	Sigma-Aldrich (Steinheim, Germany)
Fluorescein-isothiocyanate (FITC)	Molecular Probes (Oregon, USA)
Fluoroshield™	Sigma-Aldrich (Steinheim, Germany)
Fluorshield™ with DAPI	Sigma-Aldrich (Steinheim, Germany)
Fura2/*acetoxymethyl ester* (AM)	Invitrogen (Karlsruhe, Germany)
GeneRuler DNA Ladder Mix	NEB (Frankfurt am Main, Germany)
Glucose	Roth (Karlsruhe, Germany)
Glutaraldehyde	EMS (Hatfield, USA)
Glycerol	Roth (Karlsruhe, Germany)
Glycine	AppliChem (Darmstadt, Germany)
Hematoxylin	Sigma-Aldrich (Steinheim, Germany)
High molecular weight heparin	Ratiopharm (Ulm, Germany)
Hydrochloric acid (HCl)	Roth (Karlsruhe, Germany)
N-2-Hydroxyethylpiperazine-N'-2-ethane sulfonic acid (HEPES)	Roth (Karlsruhe, Germany)
Igepal® CA-630	Sigma-Aldrich (Steinheim, Germany)
Immobilon® PVDF transfer membrane	Merck Millipore (Darmstadt Germany)
Indomethacin	Alfa Aesar (Karlsruhe, Germany)
Integrilin® (Eptifibatide)	Millennium Pharmaceuticals Inc. (Cambridge, USA)
Ionomycin	Invitrogen (Karlsruhe, Germany)
Isopropyl-β-D-thiogalactopyranoside (IPTG)	Roth (Karlsruhe, Germany)
Iron-III-chloride hexahydrate ($FeCl_3$ x 6 H_2O)	Roth (Karlsruhe, Germany)
Isofluran CP®	cp-pharma (Burgdorf, Germany)
Isopropanol	Roth (Karlsruhe, Germany)
Kanamycin sulfate	Roth (Karlsruhe, Germany)
Latrunculin A	AppliChem (Darmstadt, Germany) & Abcam (Cambridge, UK)
Lysozym	Roth (Karlsruhe, Germany)
Magnesium chloride ($MgCl_2$)	Roth (Karlsruhe, Germany)
Magnesium sulfate	Roth (Karlsruhe, Germany)
Manganase chloride	Roth (Karlsruhe, Germany)
MDL-28170	Sigma-Aldrich (Steinheim, Germany)
Medetomidine (Dormitor)	Pfizer (Karlsruhe, Germany)
Methanol	Roth (Karlsruhe, Germany)
Midazolam (Dormicum)	Roche (Grenzach-Wyhlen, Germany)
Midori Green™	Biozym Scientific (Oldenburg, Germany)
3-(N-morpholino) propanesulfonic acid (MOPS)	AppliChem (Darmstadt, Germany)
NuPAGE® LDS Sample Buffer (4x)	Life Technologies (Darmstadt, Germany)
Osmium tetroxide	Merck Millipore (Darmstadt, Germany)
PageRuler® Prestained Protein Ladder	Fermentas (St. Leon-Rot, Germany)

Paraformaldehyde (PFA)	Roth (Karlsruhe, Germany)
Phalloidin	AppliChem (Darmstadt, Germany)
Phalloidin-Atto647N	Sigma-Aldrich (Steinheim, Germany)
Phalloidin-FITC	Enzo Life Sciences (New York, USA)
Phenol/chloroform/isoamyl alcohol	AppliChem (Darmstadt, Germany)
Phenylmethylsulfonyl fluoride (PMSF)	Life Technologies, Darmstadt, Germany
Piperazine-N,N'-bis(2-ethanesulfonic acid) (PIPES)	Roth (Karlsruhe, Germany)
Poly-L-lysine	Sigma-Aldrich (Steinheim, Germany)
Potassium acetate	Roth (Karlsruhe, Germany)
Potassium chloride (KCl)	Roth (Karlsruhe, Germany)
Pluronic F-127	Invitrogen (Karlsruhe, Germany)
Propidium iodide (PI)	Invitrogen (Karlsruhe, Germany)
Prostacyclin (PGI_2)	Calbiochem (Bad Soden, Germany)
Proteinase K	NEB GmbH, Frankfurt am Main, Germany
RNase A (# R4875)	Sigma-Aldrich (Steinheim, Germany)
R-phycoerythrin (PE)	EUROPA (Cambridge, UK)
Rotiphorese Gel 30% (PAA)	Roth (Karlsruhe, Germany)
SeeBlue® Plus2 pre-stained standard	Life Technologies (Darmstadt, Germany)
Sodium azide (NaN_3)	Sigma-Aldrich (Steinheim, Germany)
Sodium bicarbonate ($NaHCO_3$)	Roth (Karlsruhe, Germany)
Sodium chloride (NaCl)	AppliChem (Darmstadt, Germany)
Sodium citrate	AppliChem (Darmstadt, Germany)
Sodiumdihydrogenphosphate (NaH_2PO_4)	Roth (Karlsruhe, Germany)
Sodium dodecyl sulfate (SDS)	Sigma-Aldrich (Steinheim, Germany)
Sodium hydroxide (NaOH)	AppliChem (Darmstadt, Germany)
Sodium orthovanadate (Na_3VO_4)	Sigma-Aldrich (Steinheim, Germany)
Sucrose	Sigma-Aldrich (Steinheim, Germany)
Spectra™ Multicolor Low Range Protein Ladder	Thermo Scientific (Rockford, IL, USA)
Sulfuric acid (H_2SO_4)	Roth (Karlsruhe, Germany)
10x Taq Buffer (+KCl, -$MgCl_2$)	NEB (Frankfurt am Main, Germany)
Taq-Polymerase	NEB (Frankfurt am Main, Germany)
Taxol	AppliChem (Darmstadt, Germany)
Tetramethylethylenediamine (TEMED)	Roth (Karlsruhe, Germany)
3,3,5,5-tetramethylbenzidine (TMB)	EUROPA (Cambridge, UK)
Thrombin from human plasma	Roche Diagnostics (Mannheim, Germany) Sigma-Aldrich (Steinheim, Germany)
Thymosin β4 (recombinant)	Peprotech (Rocky Hill, USA)
Tris(hydroxymethyl)aminomethane (Tris)	Roth (Karlsruhe, Germany)
Triton X-100	Sigma-Aldrich (Steinheim, Germany)
TRIzol®	Invitrogen (Karlsruhe, Germany)
Tryptone	Roth (Karlsruhe, Germany)
Tween 20®	Roth (Karlsruhe, Germany)
U46619	Alexis Biochemicals (San Diego, USA)
Uranyl acetate	EMS (Hatfield, USA)
Vectashield hardset mounting medium	Vector Labs, Inc. (Burlingame, USA)
Water, nuclease-free	Roth (Karlsruhe, Germany)

Yeast extract	AppliChem (Darmstadt, Germany)

Rhodocytin (Rhd) was kindly provided by J. Eble (University Hospital Frankfurt, Germany). *Collagen-related peptid*e (CRP) was a generous gift from Paul Bray (Baylor College, USA). *Annexin V* (Anxa5) was generously provided by Jonathan F. Tait (Medical Center Washington, USA) and conjugated in our lab.

3.1.2 Consumables, Kits

NucleoSpin® Gel and PCR Clean-up kit	Macherey-Nagel (Düren, Germany)
NucleoSpin® Plasmid	Macherey-Nagel (Düren, Germany)
SuperScript® First-Strand Synthesis System	Invitrogen (Karlsruhe, Germany)
NuPAGE® Novex® 4-12% Bis-Tris Gels, 1mm, 15 well	Life Technologies (Darmstadt, Germany)
NuPAGE® Novex® 16% Tricine Gels, 1mm, 15 well	Life Technologies (Darmstadt, Germany)
TxB_2 ELISA Kit	DRG (Marburg, Germany)
Total LT ELISA Kit (MSB747931)	My Biosource (San Diego, USA)
Nunc® 96 DeepWell™ plate, MediSorb	Nunc (Roskilde Denmark)
CHRONO-LUME #395 Luciferin-Luciferase	CHRONO-LOG (Havertown, USA)

3.1.3. Molecular cloning

Fast-Alkine Phosphatase	NEB (Frankfurt am Main, Germany)
Quick Ligation™ Kit	NEB (Frankfurt am Main, Germany)
FastDigest® Restriction Enzymes	NEB (Frankfurt am Main, Germany)
5x Phusion® buffer HF	NEB (Frankfurt am Main, Germany)
Phusion® High-Fidelity DNA polymerase	NEB (Frankfurt am Main, Germany)

3.1.4. Plasmids

pETM-52: *E. coli* expression vector providing N-terminal DsbA, hexahistidine (6x His)-tobacco etch virus (TEV) protease recognition site and a C-terminal 6x His sequence; resistance: Kanamycin. European Molecular Biology Laboratory (Heidelberg, Germany) [149].

3.1.5. *Escherichia (E.) coli* strains

Competent TOP10 *E. coli*	Iba Lifesciences (Göttingen, Germany)

(*E. coli* F^- *mcrA* (mrr^- $hsdRMS^-$ mcrBC) 80lacZ M15 lacX74 *recA1 ara139* (*ara-leu*)7697 galU galK rpsL (StrR) endA1 nupG)

BL21-CodonPlus R (DE3)	Stratagene (San Diego, USA)

(*E. coli* B F^- *ompT hsdS*(r_B^- m_B^-) dcm^+ Tet^r *gal* λ (DE3) *end*A Hte[*argU ileY leuW* **Cam^r**]*)

*Concentration of antibiotic used for selection: chloramphenicol 34 µg mL^{-1}

3.1.6 Antibodies

3.1.6.1 Commercial antibodies

Antibody	Origin	Manufacturer
anti-α-tubulin (B-5-1-2)	mouse	Sigma-Aldrich (Steinheim, Germany)
anti-β-actin	rabbit	Sigma-Aldrich (Steinheim, Germany)
anti-β-tubulin	mouse	Sigma-Aldrich (Steinheim, Germany)
anti-CD105	rat	BioLegend (San Diego, USA)
anti-Cofilin	rabbit	Cell Signaling (Denver, USA)
anti-Cotl1 (10781-1-AP)	rabbit	Proteintech (Manchester, UK)
anti-Cdc42 (# ACD03-S)	mouse	Cytoskeleton (Denver, USA)
anti-FlnA (EP2405Y)	rabbit	Epitomics (Burlingame, USA)
anti-GAPDH (G5262)	rabbit	Sigma-Aldrich (Steinheim, Germany)
anti-Itgb3 (β3 integrin) Ab762 und AbΔ747	rabbit	*
anti-LAT (#5347)	rabbit	Cell Signaling (Denver, USA)
anti-phospho-Cofilin Ser 3	rabbit	Cell Signaling (Denver, USA)
anti-phospho-LAT (Y132) ab4476	rabbit	Abcam (Cambridge, UK)
anti-phospho-tyrosine (clone 4G10)	mouse	Merck Millipore (Darmstadt, Germany)
anti-phospho-PLCγ2 (Y759) (#3874)	rabbit	Cell Signaling (Danvers, MA; USA)
anti-total-PLCγ2 (Q-20) (#sc-407)	rabbit	Santa Cruz (Heidelberg, Germany)
anti-Profilin1 (#sc-137235)	mouse	Santa Cruz (Heidelberg, Germany)
anti-phospho-Syk (Y525/526) (clone C87C1) (#2710)	rabbit	Cell Signaling (Danvers, MA; USA)
anti-total-Syk (clone D1I5Q) (#12358)	rabbit	Cell Signaling (Danvers, MA; USA)
anti-Thymosin β4 (A 9522.1)	rabbit	Immundiagnostik (Bensheim, Germany)
anti-Tln1 (C-20, #sc-7534) & (A-11, #sc-365460)	goat	Santa Cruz (Dallas, USA)
anti-Twf1	rabbit	**
anti-Twf1/2	rabbit	**
anti-vWF	mouse	DAKO (Hamburg, Germany)
platelet depletion antibody	rat	Emfret Analytics (Eibelstadt, Germany)

*Anti-Itgb3 Ab762 und AbΔ747 were kindly provided by Xiaoping Du (University of Illinois, Chicago IL 60612, USA)

**Anti-Twf1 and anti-Twf1/2 antibodies were generously provided by Pekka Lappalainen (Helsinki, Finland).

Antibody conjugate	Origin	Manufacturer
anti-α-tubulin-Alexa F488	mouse	Invitrogen (Karlsruhe, Germany)
anti-CD29-FITC (HMβ1-1)	hamster	BioLegend (San Diego, USA)
anti-mouse IgG-Cy3	donkey	Jackson Immuno (Suffolk, UK)
anti-mouse IgG-Alexa F405	donkey	Jackson Immuno (Suffolk, UK)
anti-mouse IgG-Alexa F488	goat	Invitrogen (Karlsruhe, Germany)
anti-mouse IgG-HRP	rat	DAKO (Hamburg, Germany)
anti-goat IgG-Cy3	donkey	BioLegend (San Diego, USA)
anti-rabbit IgG-Cy3	goat	Jackson Immuno (Suffolk, UK)
anti-rabbit IgG-Alexa F647	goat	Invitrogen (Karlsruhe, Germany)
anti-rabbit IgG-Alexa F488	donkey	Invitrogen (Karlsruhe, Germany)
anti-rabbit IgG-HRP	goat	Cell Signaling (Denver, USA)
anti-rabbit IgG-HRP	donkey	Jackson Immuno (Suffolk, UK)
anti-rat IgG-Cy3	goat	BioLegend (San Diego, USA)
anti-rat IgG-Cy3	donkey	Jackson Immuno (Suffolk, UK)
anti-rat IgG-Alexa F405	donkey	Jackson Immuno (Suffolk, UK)
anti-rat IgG-Alexa F488	goat	Invitrogen (Karlsruhe, Germany)
anti-rat IgG-HRP	goat	Dianova

3.1.6.2 Home-made antibodies

The monoclonal antibodies listed below were generated in our laboratory and labeled with either *fluorescein isothiocyanate* (FITC) or with *phycoerythrin* (PE) using commercial kits following manufacturer's instructions. Annexin-A5 was purified in our laboratory and coupled to DyLight488.

Antibody	Clone	Isotype	Antigen	Described in
p0p3	7A9	IgG2a	GPIbα	[150]
p0p4	15E2	IgG2b	GPIbα	[151]
p0p5	13G12	IgG1	GPIbα	[152]
p0p/B	57E12	IgG2b	GPIbα	[153]
p0p1	3G6	IgG1	GPIbβ	[150]
DOM2	89H11	IgG2a	GPV	[151]
p0p6	56F8	IgG2b	GPIX	[151]
JAQ1	98A3	IgG2a	GPVI	[154]
INU1	11E9	IgG1	CLEC-2	[155]

ULF1	97H10	IgG2a	CD9	[151]
JER1	10B6	IgG1	CD84	[156]
LEN1	12C6	IgG2b	α2	[157]
MWReg30	5D7	IgG1	αIIb	[150]
BAR-1	25B11	IgG1	α5	[157]
EDL-1	57B10	IgG2a	β3	[151, 157]
JON/A	4H5	IgG2b	αIIbβ3	[152, 157]
JON6	14A3	IgG2b	αIIbβ3	unpublished
WUG 1.9	5C8	IgG1	P-selectin	unpublished
HB.197™	2.4G2	IgG2b	FcgR	[158]

3.1.7. Buffers and Media

All buffers were prepared using deionized water obtained from a MilliQ Water Purification System (Millipore, Schwalbach, Germany). pH was adjusted using HCl or NaOH.

***Acid-Citrate-Dextrose* (ACD) Buffer, pH 4.5**

Trisodium citrate dehydrate	85 mM
Anhydrous citric acid	65 mM
Anhydrous glucose	110 mM

Blocking Buffer (Western Blot)

Washing Buffer (1x)	—
BSA or fat-free dry milk	5%

Blocking Buffer (Immunohistochemistry)

PBS (1x)	—
Tween 20®	0.1%
BSA	3%
Rat serum	0.3%

Coating Buffer, pH 9.6

Na_2CO_3	15 mM
$NaHCO_3$	85 mM

Coomassie Staining Solution

Acetic acid	10%
Methanol	40%
Coomassie Brilliant blue	0.01%

Coomassie Destaining Solution

Acetic acid	10%
Methanol	40%
H_2O	50%

Cytoskeleton Extraction Buffer

1x PHEM	—
Triton X-100	0.75%
Phalloidin	1 µM
Taxol	1 µM

Decalcification Buffer, pH 7.4

PBS (1x)	—
EDTA	10%

Fixation Buffer I (Electron microscopy)

Cacodylate, pH 7.2	0.1 M
Glutaraldehyde	2.5%
Formaldehyde	2%

Fixation Buffer II (Electron microscopy)

Sodium cacodylate, pH 7.2	50 mM
Osmium tetroxid	2%

Fluorescent Thrombin Substrate

Z-GGR-AMC	2.5 mM
HEPES	20 mM
NaCl	140 mM
$CaCl_2$	200 mM
BSA	6%

Gel Filtration Buffer

Tris base, pH 8.0	50 mM
NaCl	150 mM
DTT	5 mM

IP Buffer (Phosphorylation studies)

Tris base, pH 8.0	15 mM
NaCl	155 mM
EDTA	1 mM
NaN_3	0.005%
Na_3VO_4	4 mM
Protease Inhibitor Mix	1x

Igepal®CA-630	1%

Karnovsky Fixation Buffer, pH 7.2

Paraformaldehyde	2%
Glutaraldehyde	2.5%
Cacodylate	0.1 M

Laemmli Buffer (SDS-PAGE)

Tris base	40 mM
Glycine	0.95 M
SDS	0.5%

LB Medium

Peptone (pancreatic digested)	10 g L^{-1}
Yeast extract	5 g L^{-1}
NaCl	171 mM

LB Plates

LB-Medium	—
Agar	15 g L^{-1}

Lysis Buffer (DNA Lysis)

Tris base	100 mM
EDTA	5 mM
NaCl	200 mM
SDS	0.2%
Freshly added Proteinase K (20 mg mL^{-1})	100 µg mL^{-1}

Lysis Buffer (Protein Purification)

Tris base, pH 8.0	50 mM
NaCl	150 mM
Lysozym	100 mg
DNAse I	1 U mL^{-1}
DTT	1 mM

PBS/EDTA (Platelet Lysates)

PBS (1x)	—
EDTA	5 mM

PBS Fixation Buffer

PBS (1x)	—
PFA	4%

PHEM Buffer, pH 6.8

PIPES	100 mM
HEPES	5.25 mM
EGTA	10 mM
$MgCl_2$	20 mM

PHEM Complete Buffer

PHEM Fixation Buffer	—
Igepal®CA-630	0.1%

PHEM Fixation Buffer

PHEM (1x)	—
PFA	4%

Phosphate-Buffered Saline (PBS), pH 7.14

NaCl	137 mM
KCl	2.7 mM
KH_2PO_4	1.5 mM
Na_2HPO_4 x $2H_2O$	8 mM

PRP Reagent (Thrombin generation assay)

HEPES	20 mM
NaCl	140 mM
BSA	0.5%
Tissue Factor	3 pM

Sample Buffer (Agarose Gels), 6x

Tris base (150 mM)	33%
Glycerol	60%
Bromophenol blue	0.04%

SDS Sample Buffer, 4x

Tris base (1 M), pH 6.8	20%
Glycerol	40%
SDS	4%
β-mercaptoethanol (reducing conditions)	20%
Bromophenol blue	0.04%

Separating Gel Buffer (Western Blot), pH 8.8

Tris base	1.5 M

Stacking Gel Buffer (Western Blot), pH 6.8

Tris base	0.5 M

Stripping Buffer (Western Blot), pH 2.0

PBS (1x)	—
Glycine	25 mM
SDS	1%

Sodium-Citrate-Buffer, pH 7.0

Sodium Citrate	0.129 M

TAE, 50x, pH 8.0

Tris base	0.2 M
Acetic acid	5.7%
EDTA	50 mM

TE-Buffer, pH 8.0

Tris base	10 mM
EDTA	1 mM

Transfer-Buffer (Western Blot)

Tris Ultra	50 mM
Glycine	40 mM
Methanol	20%

Tris-Buffered Saline (TBS), pH 7.3

NaCl	137 mM
Tris base	20 mM

Tyrode’s Buffer, pH 7.3

NaCl	137 mM
KCl	2.7 mM
$NaHCO_3$	12 mM
NaH_2PO_4	0.43 mM
HEPES	5 mM
$CaCl_2$	2 mM
$MgCl_2$	1 mM
BSA	0.35%
Glucose	0.1%

Washing Buffer PBS-T (ELISA)

PBS (1x)	—
Tween 20®	0.1%

Washing Buffer TBS-T (Western Blot)

TBS (1x)	—
Tween 20®	0.1%

3.1.8 Chromatography columns and media

Superdex Increase 75 10/300 GL (Analytical SEC FPLC column) and Ni-NTA Agarose were purchased from GE Healthcare (Munich, Germany).

3.1.9 Genetically modified mice

Cotl1$^{+/-}$ mice were created by injection of embryonic stem cell clone Cotl1$^{tm1a(EUCOMM)Hmgu}$ (*European Conditional Mouse Mutagenesis Program* (EUCOMM)) into C57Bl/6 blastocysts. Germline transmission was achieved by backcrossing of the resulting chimeric mice with C57Bl/6 mice. These mice were further intercrossed with mice carrying the Flp-recombinase to generate *Cotl1*$^{fl/fl}$ mice, which were, in a final step, intercrossed with mice carrying the Cre-recombinase under the *platelet factor 4* (PF4) promoter [159] to generate animals lacking Cotl1 specifically in MKs and platelets. Conditional *Pfn1*$^{fl/f\text{-}Pf4Cre}$ mice have been generated by intercrossing *Pfn1*$^{fl/fl}$ mice (obtained from EUCOMM, Strain ID EM: 03711) with mice carrying the Cre-recombinase under the platelet factor 4 (*Pf4*) promoter [159]. *Tβ4*$^{-/-}$ mice were created by MRC mouse network by injection of embryonic stem cell clone Tmsb4x$^{tm2a(EUCOMM)Wtsi}$ into C57Bl/6/*129*/SvJ blastocysts and afterwards transferred to our animal facility where the KO mice were kept on the mixed background.

If not stated otherwise, 8- to 16-week-old mice of either sex were used in experiments. Animal studies were approved by the district government of Lower Frankonia (Bezirksregierung Unterfranken).

3.2 Methods

3.2.1 Genotyping of mice

3.2.1.1 Isolation of genomic DNA from mouse ears

A 5 mm^2 piece of mouse ear was incubated in 500 µL lysis buffer under constant shaking at 900 rpm o/N or at 1,400 rpm for 3 h at 56°C. Cellular proteins and lipids were removed by the addition of 500 µL of phenol/chloroform/isoamyl alcohol (25:24:1). Samples were mixed and centrifuged for 10 min at 10,000 rpm in an Eppendorf 5417R tabletop centrifuge at RT. After centrifugation, the aqueous nucleic acid containing upper phase was transferred into a new tube containing 500 µL isopropanol to precipitate the DNA. Subsequently, the nucleic acids were spun down at 14,000 rpm for 15 min. The pellet was washed and dehydrated by the addition of 500 µL 70% ethanol with subsequent centrifugation at 14,000 rpm for 10 min. Before dissolving the pellet in 50 µL TE buffer, the pellet was dried for 30 min at 37°C.

3.2.1.2 *Polymerase Chain Reaction* (PCR)

The pipetting scheme shown is representative for 1 sample (final volume: 25 µL) for the below described genotyping PCRs.

2.0 µL DNA sample
2.5 µL 2 x Dream Taq Buffer (+KCl, +$MgCl_2$)
0.5 µL dNTPs [10 mM]
1 µL forward Primer [1 µg mL^{-1}]
1 µL reverse Primer [1 µg mL^{-1}]
0.25 µL Dream Taq-Polymerase [5 U $µL^{-1}$]
18.75 µL H_2O

Detection of the Pfn1 floxed allele

- **Primer**

Pfn1_i2_f2: 5’ TTC TGA CTC TGG CTC CCC AG 3’
Pfn1_i2_r2: 5’ GCT AGG AAC GGC TGT GAT GC 3’

- **Program**

Temperature [°C]	Time [s]	Repeats
96	180	1
94	30	35
55.5	30	35
72	60	35
72	300	1
22	∞	1

- **Expected band sizes**

WT: 187 bp
Floxed allele: 221 bp

Detection of the Cotl1 floxed allele

- **Primer**

Cotl1_for: 5´ GGA GGA CGT GAG TGG ACT GCA GCG 3´
Cotl1_rev: 5´ TGA ACT GAT GGC GAG CTC AGA CC 3´
Cotl1_5´arm: 5´ GGGACATCGTCACCATGGGAACGG 3´
Cotl1_3´: 5´ TAG CTG GCG TAG ATG CAC ACC ACC 3´
Cotl1_LAR3: 5´ CAA CGG GTT CTT CTG TTA GTC C 3´

- **Program**

Temperature [°C]	**Time [s]**	**Repeats**
96	180	1
94	30	35
60	30	35
72	60	35
72	300	1
22	∞	1

- **Expected band sizes**

WT: 224 bp
Floxed allele: 354 bp & 450 bp for the LAR3 cassette

Detection of the Tβ4 transgene allele

- **Primer**

Tβ4_fw: 5´ GTG CTT TTG GAA CTG GGA GA 3´
Tβ4_rev: 5´ AGC CCG TTC TGA AAA TGG 3´
Tβ4_GT: 5´ GGC CTT CTT GAC GAG TTC TT 3´

- **Program**

Temperature [°C]	**Time [s]**	**Repeats**
96	180	1
94	30	35
63.5	30	35
72	60	35
72	300	1
22	∞	1

- **Expected band sizes**

WT: 190 bp
Genetrap+: 600 bp

Detection of the PF4 Cre transgene

- **Primer**

PF4_for: 5´ CCC ATA CAG CAC ACC TTT TG 3´
PF4_ rev: 5´ TGC ACA GTC AGC AGG TT 3´

- **Program**

Temperature [°C]	Time [s]	Repeats
96	300	1
94	30	35
54.1	30	35
72	45	35
72	30	1
22	∞	1

- **Expected band sizes**

WT allele: no PCR product
PF4-Cre+: 450 bp

3.2.1.3 Semiquantitative *reverse transcription* PCR (RT-PCR)

For reverse transcription of RNA, two different Mastermixes were prepared:

- **Mastermix 1 pipetting scheme**

1.0 µg RNA
2.0 µL oligo dT Primer [0.5 µg μL^{-1}]
add 20 µL H_2O

Mastermix 1 was denaturated for 10 min at 70°C and subsequently cooled on ice.

- **Mastermix 2 pipetting scheme**

5.0 µL 5x first strand buffer
2.0 µM DTT [0.1 M]
1.0 µL dNTPs [10 mM]
0.1 µL RNAse inhibitors [5 U mL^{-1}]

Mastermix 1 and 2 were pooled and 1 µL of SuperScript® II Reverse Transcriptase [200 U μL^{-1}] was added. Amplification was performed for 1 to 2 h at 42°C in a thermomixer and afterwards the reaction was aborted by incubation of the samples for 10 min at 70°C. The generated cDNAs were stored at -20°C. The mRNA expression levels were determined by

PCR, optimal annealing temperature for the used primers was identified via gradient PCR. *Gapdh* expression was determined as control.

- **Mastermix for semi-quantitative RT-PCR**

2.0 µL cDNA sample
2.0 µL 10x Taq Buffer (+KCl, -$MgCl_2$)
1.2 µL $MgCl_2$ [25 mM]
0.4 µL dNTPs [10 mM]
0.1 µL forward Primer [1 µg mL^{-1}]
0.1 µL reverse Primer [1 µg mL^{-1}]
0.125 µL native Taq-Polymerase [5 U $µL^{-1}$]
14.075 µL H_2O

- **Primer**

Tβ4_RT_for: 5´ GAG CAG ATC AGA CTC TCC TCG 3´ (annealing temperature 45°C)
Tβ4_RT_rev: 5´ GAA GGC AAT GCT CGT GGA ATG 3´ (annealing temperature 60.8°C)
GAPDH_RT_for: 5‘ GCA AAG TGG AGA TTG TTG CCA T 3‘
GAPDH_RT_rev: 5‘ CCT TGA CTG TGC CGT TGA ATT T 3‘

- **Program**

Temperature [°C]	**Time [s]**	**Repeats**
96	180	1
94	30	35
45-61	30	35
72	60	35
72	300	1
22	∞	1

- **Expected band sizes**

Tβ4: 280 bp.
GAPDH: 108 bp.

3.2.1.4 Agarose gel electrophoresis

PCR products were separated on agarose gels. A molecular weight marker with a range from 100 to 10,000 bp was run on the gels to control the size of the products. For a 1% agarose gel, 1.0 g of agarose per 100 mL TAE buffer was boiled in microwave until it was dissolved. The cooled (60°C) agarose was submitted with the DNA marker Midori Green™ [50 µL L^{-1}] and poured into a sleigh containing a comb. The cast gel was then laid into a chamber filled with 1x TAE buffer. 20 µL of the PCR products were loaded onto the gels. The samples were separated for 30-45 min at 140 V. For big gels, 4 g agarose in 400 mL TAE buffer were used.

The big gels were run at 160 V. Finally, the DNA was visualized under *ultra violet* (UV) light and pictures were taken with a GelDoc system (Herolab GmbH, Germany).

3.2.2 Biochemical analyses

3.2.2.1 UV/Vis spectrophotometry

The concentrations of purified DNA and proteins were determined by measuring the UV absorbance using a spectrophotometer (NanoDrop™, Thermo Scientific). Absorbance spectra in the wavelength range of 220-350 nm were recorded and corrected for the reference spectrum of the buffer solution devoid of DNA or protein. For DNA, the concentration was calculated based on the absorbance at 260 nm and the ratio of the absorbance at 260 nm and 280 nm was used to control for the purity of the DNA. For proteins, the concentration was calculated based on the absorbance at 280 nm and the specific extinction coefficient of the respective protein, which was calculated based on the amino acid sequence using the ProtParam tool (Expasy).

3.2.2.2 *Sodium Dodecyl Sulfate* (SDS)-*Polyacrylamide Gel Electrophoresis* (PAGE)

For SDS-PAGE under denaturing conditions, samples were mixed with an equal volume of reducing 2x Loading Dye and boiled for 5 min at 95°C. Afterwards, samples were separated by their molecular weight following the protocol described by Laemmli [160]. Protein samples and a molecular-weight size marker were loaded to the gel installed in the electrophoresis chamber filled with running buffer. Electrophoresis was performed at 25 mA per gel until the dye had nearly traversed the gel. For staining, gels were first stained in Coomassie staining solution for up to 30 min and afterwards destained in Destaining solution.

3.2.2.3 Immunoblotting

Samples were separated by SDS-PAGE as described above and afterwards blotted onto *polyvinylidene difluoride* (PVDF) membranes and incubated with the respective primary antibodies (section 3.1.6) o/N at 4°C. For visualization, *horseradish peroxidase* (HRP)-conjugated secondary antibodies were used and membranes were developed using an *enhanced chemiluminescence* (ECL) detection system with autoradiography films or digitally on a MultiImage® II FC Light Cabinet (Alpha Innotech cooperation) device.

3.2.3 Molecular Cloning

Classical cloning using restriction endonucleases was chosen as cloning strategy. For this, fragments with suitable overhangs containing the restriction endonuclease recognition site were amplified from cDNA by PCR.

3.2.3.1 PCR

- **Pipetting scheme (25 µL)**

10 ng template DNA
1 x HF-buffer
0.5 µM forward Primer
0.5 µM reverse Primer
0.5 µL dNTP mix
1 U Phusion® polymerase high-fidelity

- **Primer**

Tβ4_NcoI: 5´ TTC AGG GCG CCA TGG GCT CCG ATA AGC CTG ATA TGG CAG 3´
Tβ4_XhoI: 5´ GTG GTG GTG CTC GAG TTA AGA CTC TCC AGC TTG TTT C 3´

- **Program**

Temperature [°C]	**Time [s]**	**Repeats**
96	180	1
94	30	35
60	30	35
72	60	35
72	300	1
22	∞	1

- **Expected band size**

180 bp

The PCR product was purified using the NucleoSpin® Gel and PCR Clean-up kit according to the manufacturer's instructions.

3.2.3.2 Restriction Digestion

- **Pipetting scheme (50 µL)**

1 µg Tβ4 Insert
or 800 ng pETM-52
3 µL XhoI-HF®
3 µL NcoI-HF®
5 µL CutSmart buffer
Add H_2O to 50 µL

The DNA was digested for 4 h at 37°C. 10 U Fast Alkaline Phosphatase were added to the vector digestion reaction 15 min prior to the end of incubation. The products were separated by agarose gel electrophoresis and extracted using the NucleoSpin® Gel and PCR Clean-up kit.

3.2.3.3 Ligation

For ligation the digested Insert and the linearized vector were mixed in a 8:2 or 9:1 ratio (insert: vector), and incubated for 5 min at 45°C, followed by 3 min on ice. Subsequently, the ligation mix was combined with Quick Ligation Buffer and 2,000 U Quick T4 DNA Ligase, and incubated for 30 min at RT. Ligation products were either directly transformed into *E. coli* TOP10 cells or stored at -20°C.

3.2.3.4 Transformation of competent *E. coli* cells

For transformation, chemically competent TOP10 *E. coli* were incubated with 10 ng of the ligation for 30 min on ice. Transformation was triggered by a 90 s heat shock at 42°C with subsequent incubation for 3 min on ice. Thereafter, bacteria were supplied with 500 µL LB-medium and incubated at 450 rpm for 1.5 h at 37°C. Positive clones were selected by plating the transformation mixture on LB-agar plates containing the respective antibiotics.

3.2.3.5 Colony-PCR

To probe for positive clones, single colonies were studied in an analytical PCR following the protocol depicted below.

- **Pipetting scheme (50 µL)**

1 colony
2.5 µL 2x DreamTaq Buffer (+KCl, +$MgCl_2$)
0.5 µL dNTPs [10 mM]
0.1 µL forward Primer [1 µg mL^{-1}]
0.1 µL reverse Primer [1 µg mL^{-1}]
0.25 µL Dream Taq-Polymerase [5 U $µL^{-1}$]
21.55 µL H_2O

- **Primer**

Tβ4_NcoI: 5´ TTC AGG GCG CCA TGG GCT CCG ATA AGC CTG ATA TGG CAG 3´
Tβ4_XhoI: 5´ GTG GTG GTG CTC GAG TTA AGA CTC TCC AGC TTG TTT C 3´

- **Program**

Temperature [°C]	**Time [s]**	**Repeats**
98	30	1
98	10	30
60	30	30
72	10	30
72	300	1
22	∞	1

- **Expected band size**

180 bp fpr positive clones

Finally, all recombinant plasmids were verified by dideoxy sequencing executed by the company MWG (Eurofins Genomics, Ebersberg, Germany).

3.2.3.6 Amplification and isolation of plasmid DNA

Following sequencing, the desired clone was transformed into *E. coli* TOP10 cells and plated onto LB plates containing the respective antibiotics. On the next day, a single colony was transferred to 5 mL sterile LB medium with antibiotics and incubated under constant shaking at 220 rpm o/N at 37°C in an incubator shaker. Subsequently, cells were separated from the medium by centrifugation at 6,000 rpm for 15 min at 4°C. The plasmid DNA was isolated following the manufacturer's instructions with the NucleoSpin® Plasmid kit. The DNA content of the samples was determined using a NanoDrop (Thermo Scientific) device. For long-term storage, glycerol stocks of the respective plasmids were created. For this, 800 µL of an o/N culture was added to 200 µL of sterile 10% glycerol, shock-frozen in liquid N_2 and stored afterwards at -80°C.

3.2.4 Protein expression and purification

3.2.4.1 Small-scale expression

To test the influence of different temperatures and durations on the protein yield, small-scale expressions (125 mL) were performed. For this, the *E. coli* expression strains BL21 (DE3), BL21 (DE3) pLysS and Rosetta 2™ pRARE2 were transformed with the plasmid and used to inoculate 5 mL sterile LB medium containing the appropriate antibiotics. Cultures were incubated under constant shaking at 220 rpm o/N at 37°C. Expression cultures were started by transferring pre-cultured cells to fresh LB-medium containing antibiotics (125 mL). Cultures were grown under constant shaking at 220 rpm at 37°C, while the optical density at 600 nm ($O.D._{600}$) was monitored. When the desired $O.D._{600}$ of 0.4-0.6 was reached, expression was induced by addition of IPTG [0.5 mM], and the cultures were incubated at 220 rpm o/N at 20°C. At the end of the expression phase, the cells were harvested by centrifugation at 4,000 rpm for 10 min at 4°C (Beckman Coulter centrifuge, Rotor type JLA-16.250) and the cell pellets were stored at -80°C until further use.

3.2.4.2 Purification of small-scale expression

The harvested cell pellets were resuspended in 10 mL per g lysis buffer supplemented with 1 mM DTT. To separate the soluble and insoluble protein fraction, cells were first lysed mechanically by sonification (3x 30 sec) on ice. After centrifugation at 14,000 rpm for 15 min at 4°C, soluble and insoluble fractions were separated. The soluble fraction was subsequently

incubated with 0.1 mL Ni-NTA Agarose, which was previously washed 3x with lysis buffer, for 1 h at 4°C. The Ni-NTA Agarose was spun down by centrifugation at 1,000 rpm for 1 min at 4°C and the bound protein was eluted with 200 µL lysis buffer containing 250 mM Imidazol. 50 µL sample was taken at every step of the purification and thereafter all samples were analyzed by SDS-PAGE and staining with Coomassie. As these initial purification tests already indicated a strong overexpression in *E. coli* BL21 (DE3) cells at 20°C, further optimization was dispensable.

3.2.4.3 Large-scale expression

For larger expressions, *E. coli* BL21 (DE3) cells were transformed with the plasmid and used to inoculate 125 mL sterile LB medium containing the appropriate antibiotics. Cultures were grown o/N as described in section 3.2.4.1 and transferred to 2 L LB medium containing the appropriate antibiotics. After induction of expression at an $O.D._{600}$ of 0.4-0.6 with 0.5 mM IPTG, cells were grown as described in section 3.2.4.1. At the end of the expression phase, cells were harvested by centrifugation at 6,000 rpm for 15 min at 4°C (Beckman Coulter centrifuge, Rotor type JA-10)

3.2.4.4 Purification of large-scale expression

Cell pellets of the large-scale expression were resuspended as described in section 3.2.4.2 and lysed mechanically by sonification (5x 30 sec) on ice. The cell lysate was centrifuged at 16,000 rpm for 1 h at 4°C (Beckman Coulter centrifuge, Rotor type JA 25.50). The supernatant was subsequently subjected to *Immobilized Metal Affinity Chromatography* (IMAC), which was performed in a batch procedure. For this, 1 mL Ni-NTA Agarose, washed 3x in lysis buffer, was incubated with the supernatant under constant stirring for 1 h at 4°C. The Ni-NTA agarose was transferred to an Econo-Column® 2.5x 20 cm column body (Bio-Rad Laboratories), washed intensively with at least 100 mL lysis buffer before the bound protein was eluted with 25 mL lysis buffer supplemented with 250 mM Imidazol. The protein tag was cleaved off o/N at 4°C under constant stirring using 10 µg TEV Protease per mg protein. Next day, the untagged protein was separated from the cleaved His-DsbA tag by reverse IMAC. The protein was concentrated using Amicon Ultra® centrifugal filter units to a volume of 1 mL and further purified using size exclusion chromatography with a Superdex 75 10/300 GL column on an Äkta pure 25 system (GE Healthcare). Because of the potential *in vivo* use of the purified Tβ4, the size exclusion chromatography was performed in 1x PBS, pH 7.0. Afterwards the purified protein was concentrated using Amicon Ultra® centrifugal filter units and protein concentration was determined using a NanoDrop™ device (Thermo Scientific). The protein was stored until further usage at -80°C.

3.2.5 *In vitro* analysis of platelet function

3.2.5.1 Platelet preparation and washing

Mice were anesthetized using isoflurane and bled from the retro-orbital plexus up to 1 mL in 300 µL heparin [20 U mL^{-1}] or ACD buffer. 300 µL of heparin [20 U mL^{-1}] were added and the samples were centrifuged at 800 rpm for 6 min. Subsequently, the upper phase and the buffy coat with some erythrocytes were transferred into 300 µL heparin [20 U mL^{-1}]. To further purify the platelets, centrifugation was repeated (800 rpm, 6 min) and only the upper phase without any erythrocytes was pipetted into a new Eppendorf tube containing 2 µL of apyrase [0.02 U mL^{-1}, f.c.] and 5 µL PGI_2 [0.1 µg mL^{-1}, f.c.]. Platelets were spun down at 2,800 rpm for 5 min, resuspended in 1 mL of Tyrode's buffer without Ca^{2+}, containing 2 µL of apyrase [0.02 U mL^{-1}, f.c.] and 5 µL PGI_2 [0.1 µg mL^{-1}, f.c.] and allowed to rest for 5 min at 37°C. The washing step was repeated twice, before the pellet was resuspended in an appropriate volume of Tyrode's buffer without Ca^{2+} containing apyrase [0.02 U mL^{-1}, f.c.] and the platelets were allowed to rest for 30 min prior to experiments.

3.2.5.2 Plasma preparation

Mice were bled to 1 mL as described above. The heparinized blood was centrifuged at 2,800 rpm for 5 min and the supernatant was transferred into a new tube. After a second centrifugation step at 14,000 rpm for 5 min, the supernatant was collected. The plasma was either used directly or stored at -80°C.

3.2.5.3 RNA preparation from platelets

Animals were bled to 1 mL into 300 µL heparin [20 U mL^{-1}] and washed platelets were prepared (see 3.2.5.1). The platelet pellets were resuspended in a total volume of 250 µL IP-buffer supplied with 1% NP-40, vortexed and incubated for 10 min at RT. After the addition of 1 mL TRIzol® reagent, the samples were incubated for 10 min at RT. Then, 250 µL of chloroform were added and the samples were incubated for 10 min at RT and afterwards centrifuged at 10,000 rpm for 10 min at 4°C. The upper phase was then transferred into a tube containing 1 mL chloroform/isoamyl alcohol (24:1), vortexed for 2 min and centrifuged again at 10,000 rpm for 10 min at 4°C. Subsequently, the upper phase was pipetted into a new tube containing 1 mL of ice cold isopropanol, mixed well and incubated for 30 min on ice. The nucleic acids were pelleted by centrifugation at 14,000 rpm for 10 min at 4°C, washed once with 70% ethanol (14,000 rpm, 10 min, 4°C), dried at RT for 30 min and finally resuspended in 20 µL RNase free water. The RNA content of the samples was determined using a NanoDrop (Thermo Scientific) device.

3.2.5.4 Determination of platelet size and count

Mice were bled to 50 µL in 300 µL heparin [20 U mL^{-1}] as described in section 3.2.5.1. The sample was filled up with 650 µL Tyrode's buffer without Ca^{2+}. Platelet count and size were assessed by incubating diluted, heparinized blood with fluorophore-conjugated antibodies directed against platelet-specific epitopes and subsequently analyzed by flow cytometry (FACSCalibur, BD Biosciences). *Forward scatter* (FSC) and the counts per second were determined. Alternatively, platelet count and size were measured in heparinized blood using a Sysmex analyzer (Sysmex KX-21N automated hematology analyzer; Sysmex Corp., Kobe, Japan).

3.2.5.5 Platelet glycoprotein expression

Mice were bled to 50 µL in 300 µL heparin [20 U mL^{-1}] as described in 3.2.5.1 and blood was diluted using 650 µL Tyrode's buffer without Ca^{2+}. The expression levels of the most abundant platelet glycoproteins were determined by incubating the heparinized blood with fluorophore-conjugated monoclonal antibodies and *mean fluorescence intensities* (MFI) were analyzed by flow cytometry.

3.2.5.6 Platelet integrin activation and degranulation

50 µL of blood in 300 µL heparin [20 U mL^{-1}] were withdrawn, diluted and washed twice at 2,800 rpm for 5 min with 1 mL of Tyrode's buffer without Ca^{2+}. After the final washing step, the washed blood was resuspended in an appropriate volume of Tyrode's buffer with Ca^{2+} and incubated with fluorophore-conjugated antibodies directed against activated β1-integrins (9EG7-FITC) or αIIbβ3 integrins (PE-conjugated JON/A) and against P-selectin (FITC-labeled WUG 1.9). Subsequently, the samples were activated with different agonists. The reaction was stopped after an incubation for 7 min at 37°C and 7 min at RT by the addition of 500 µL PBS. Where stated, samples were pretreated with the calpain inhibitor MDL-28170 [200 µM] or the actin polymerization inhibitor cytochalasin D [5 µM].

3.2.5.7 Platelet fibrinogen binding

1 mL of blood in 300 µL heparin [20 U mL^{-1}] was withdrawn and platelets were washed as described (see section 3.2.5.1). Binding of fluorescently labeled fibrinogen [50 µg mL^{-1}] to washed platelets (18.000 per µL) was assessed over time in resting or activated samples. After the indicated time points the reactions were stopped by the addition of 500 µL of Tyrode´s buffer containing 3 mM Ca^{2+}.

3.2.5.8 Aggregometry

Mice were bled to 1 mL into 300 µL heparin [20 U mL^{-1}] and platelets were washed as described before in section 3.2.5.1. The light transmission of a washed platelet suspension

(1.5x 10^5 platelets per µL) in 150 µL Tyrode's buffer with Ca^{2+} supplied with 100 µg mL^{-1} human fibrinogen was monitored for 10 min using a four-channel aggregometer (APACT, Laborgeräte und Analysensysteme, Hamburg) following activation with different agonists. For stimulation with thrombin, Tyrode's buffer without human fibrinogen was used. Aggregation studies with ADP were performed in platelet-rich plasma (1.5x 10^5 platelets per µL). Aggregation is displayed as arbitrary units with the light transmission of 160 µL Tyrode's buffer with Ca^{2+} and fibrinogen set as 100%.

3.2.5.9 Western Blot analysis of platelets

For Western blotting of platelets, mice were bled and platelets were prepared as described in section 3.2.5.1, but washed twice in PBS/EDTA [5 mM] to remove residual serum albumin. Platelet counts were adjusted to 1.0 x 10^6 platelets per µL in IP Buffer using a Sysmex KX 21-N cell analyzer (Sysmex Deutschland GmbH). After an incubation time of 30 min on ice, the samples were mixed with an equal volume of reducing 2x Loading Dye and boiled for 5 min at 95°C and then subsequently were subjected to SDS-PAGE and immunoblotting as described in section 3.2.2.2 and 3.2.2.3.

3.2.5.10 Tyrosine phosphorylation studies

For identification of tyrosine phosphorylated proteins in platelets, washed platelets (1.4x 10^8 platelets per µL) were used. Platelets were prepared as described in section 3.2.5.1, but were washed only once with Tyrode's buffer containing BSA, whereas all subsequent washing steps were carried out in Tyrode's buffer without BSA. To prevent aggregation, apyrase [2 U mL^{-1}], EDTA [5 mM] and indomethacin [10 µM] were added to the platelet suspension. Platelets were stimulated with different agonists under stirring. Reaction was stopped at different time points by the addition of ice-cold 2x lysis buffer and samples were lysed for 30 min on ice. Afterwards, the samples were mixed with an equal volume of reducing 2 x Loading Dye, boiled for 5 min at 95°C and were subsequently subjected to SDS-PAGE and immunoblotting as described in section 3.2.2.2 and 3.2.2.3. Densitometry was conducted by volume analysis using ImageJ (version 1.46r, ImageJ software, National Institutes of Health, Bethesda, MD, USA).

3.2.5.11 Determination of platelet vWF content and secretion by ELISA

For the determination of total vWF levels, platelet lysates were prepared as described in section 3.2.5.9. Samples were stored at -80°C until further use. For the determination of vWF secretion, washed platelets were prepared as described in section 3.2.5.1, diluted in Tyrode's buffer with Ca^{2+} (5x 10^5 μL^{-1}) and stimulated with thrombin [0.1 U mL^{-1}] under stirring conditions for 15 min at 37°C. Samples were centrifuged at 2,800 rpm for 5 min and platelet aggregate-free supernatants were spun down at 14,000 rpm for 5 min. Supernatants were stored at

-80°C. vWF levels were subsequently assessed by ELISA. For this, Nunc® 96 DeepWell™ plates MediSorb (Nunc, Roskilde, Denmark) were coated with 10 µg mL^{-1} rabbit anti-human antibody o/N at 4°C and blocked with 5% BSA for 90 min at 37°C on the next day. Serial sample dilutions were incubated for 2 h at 37°C. After extensive washing with TBS-T, samples were incubated with an HRP-coupled rabbit anti-human vWF antibody, which was shown to cross-react with mouse vWF. After washing, ELISA plates were developed using TMB substrate and the reaction was stopped by the addition of 0.5 M H_2SO_4.

3.2.5.12 Determination of TxB_2 and total LT release

Washed platelets were obtained as described in section 3.2.5.1, adjusted to a concentration of 5x 10^5 platelets per µL and stimulated with different agonists for 5 min. The reaction was stopped by adding 5 mM EDTA and 1 mM aspirin. Platelets were removed by centrifugation at 14,000 rpm for 5 min and the supernatant was collected. TxB_2 concentrations in the supernatant were measured using the TxB_2 ELISA kit according to the manufacturer's instructions (DRG, Marburg, Germany). Total LT concentrations in the supernatant were measured with the total LT ELISA kit according to the manufacturer's instructions (My Biosource, San Diego, USA).

3.2.5.13 Determination of ATP release

Washed platelets were resuspended to a concentration of 5x 10^5 per µL in Tyrode's buffer without Ca^{2+}. 80 µL of this platelet suspension were diluted into 160 µL Tyrode's buffer with 2 mM Ca^{2+}. After addition of 25 µL Chrono-lume luciferase reagent, agonists were added to the continuously stirred (1,000 rpm) platelet suspension. Light transmission and luminescence were recorded on a 700 Whole Blood/Optical Lumi-Aggregometer (Chrono-log) over 10 min. Results were shown in arbitrary units with buffer representing 100% transmission and washed platelet suspension 0% transmission. ATP release was calculated using an ATP standard and the AggroLink 8 software.

3.2.5.14 Intracellular Ca^{2+} measurements

For intracellular calcium measurements, washed platelets (0.6x 10^6 per µL) were prepared in Tyrode's buffer without Ca^{2+} and loaded with Fura-2/AM [5 µM] together with Pluronic F-127 [0.2 µg mL^{-1}] for 30 min at 37°C. After labeling, platelets were washed once and resuspended in Tyrode's buffer containing 0.5 mM EGTA to measure store release or 1 mM Ca^{2+} to assess Ca^{2+} entry. Platelets were activated with the indicated agonists and the fluorescence signal was measured with a fluorimeter (LS 55; PerkinElmer). Each measurement was calibrated using Triton X-100 (Roth) and EGTA.

3.2.5.15 Platelet adhesion under flow conditions

For flow adhesion experiments on collagen, rectangular coverslips (24x 60 mm) were coated o/N at 37°C with 70 µg mL^{-1} fibrillar type I collagen and prior to the experiment blocked for 1 h with 1% BSA. Mice were bled up to 1 mL in 300 µL heparin [20 U mL^{-1}], the blood was diluted 3:1 with Tyrode's buffer with Ca^{2+} and incubated for 5 min at 37°C with a DyLight488-conjugated anti-GPIX derivative [0.2 µg mL^{-1}]. A transparent flow chamber with a slit depth of 50 µm was covered with the prepared cover slip and perfused for 4-10 min with the blood using a pulse-free pump with different shear rates (150, 1,000, 1,700 and 3,000 s^{-1}), reflecting the blood flow in different vessel types. Subsequently, the chamber was perfused under the same conditions with Tyrode's buffer with Ca^{2+} and at least five phase-contrast and fluorescent pictures were taken using a Zeiss Axiovert 200 inverted microscope (40x/0.60 objective) equipped with a CoolSNAP-EZ camera (Visitron). The recorded phase-contrast and fluorescence pictures were analyzed using Metavue software.

For experiments on immobilized vWF, rectangular coverslips (24x 60 mm) were coated o/N at 4°C with 200 µL 1:500 diluted polyclonal rabbit anti-human vWF antibody (A0082; Dako) in coating buffer. Prior to the experiment slides were blocked for 1 h with 1% BSA and incubated with 200 µL heparinized wild-type mouse plasma for 2 h at 37°C and placed within the flow chamber. Afterwards, mice were bled up to 1 mL in 300 µL heparin [20 U mL^{-1}], the blood was diluted 2:1 with Tyrode's buffer with Ca^{2+} and subsequently perfused over the slides for 4 min at 1,700 s^{-1}. Afterwards, the chamber was perfused for the same time and at the same shear rate with Tyrode's buffer and at least five phase-contrast and fluorescent pictures were taken.

3.2.5.16 Analysis of PS exposing platelets

Under flow conditions

Rectangular cover slips (24x 60 mm) were coated with 70 µg mL^{-1} fibrillar type I collagen o/N at 37°C and blocked with 1% BSA. Heparinized whole blood was supplemented with additional 5 U mL^{-1} heparin and perfused over the coverslips through a transparent flow chamber at a shear rate of 1000 s^{-1} as described above. The flow chamber was rinsed for 4 min with Tyrode's buffer supplemented with 5 U mL^{-1} heparin and 0.25 µg mL^{-1} Annexin A5-DyLight488. After additional washing for 2 min with Tyrode's buffer containing Ca^{2+} and 5 U mL^{-1} heparin, phase-contrast and fluorescence images were taken. Procoagulant activity was defined as the ratio of surface coverage of PS-exposing platelets (Annexin A5-DyLight488 staining of platelets) to the total surface covered by platelets.

Under static conditions

Washed platelets were diluted into Tyrode's buffer with Ca^{2+} (50 µL with 0.5x 10^5 platelets per µL) and incubated with different agonists for 15 min at 37°C in the presence of saturating

amounts of Alexa F488-coupled Annexin A5. Reactions were stopped by the addition of 500 µL Tyrode's buffer with Ca^{2+}, and data were immediately collected on a FACSCalibur (BD Biosciences, Heidelberg, Germany) and analyzed using FlowJo v7 software (FlowJo, LLC, Ashland OR, USA).

3.2.5.17 Platelet clot retraction

Mice were bled up to 700 µL in 70 µL sodium citrate [0.129 mM] and PRP was isolated by centrifugation at 1,800 rpm for 5 min. Plasma was collected and platelets were resuspended in 1 mL Ca^{2+}-free Tyrode's buffer supplemented with 2 µL of apyrase [0.02 U mL^{-1}] and 5 µL PGI_2 [0.1 µg mL^{-1}]. Platelet count was determined and 7.5x 10^7 platelets were resuspended in 250 µL plasma. PRP (3x 10^5 platelets per µL) was recalcified by adding 20 mM $CaCl_2$ and supplemented with 1 µL of red blood cells to visualize the clot. Clot formation was initiated by the addition of 4 U mL^{-1} thrombin (Sigma). Clot formation and retraction was recorded up to 4 h and the residual serum volume was determined.

3.2.5.18 Measurement of coagulation factors (Central Laboratory)

Mice were bled under isoflurane anesthesia from the retro-orbital plexus to 700 µL blood into 70 µL sodium citrate. Plasma was prepared as described above. For measurement of PTT and for single measurements of FVIII, FIX, FXI and FXII, undiluted samples were used. For the Quick index, samples were diluted 1:3 in 0.9% NaCl. Measurements were performed in collaboration with Dr. Sabine Herterich from the Central Laboratory.

3.2.5.19 Thrombin generation assay

Thrombin generation was quantified in citrate-anticoagulated PRP (1 x 10^5 platelets per µL), which was prepared as described above and measured according to the calibrated automated thrombogram method as previously described [161]. Assays were performed in collaboration with Sarah Beck in our laboratory.

3.2.5.20 Platelet spreading on fibrinogen

Rectangular coverslips (24x 50/60 mm) were coated with 100 µL of 100 µg mL^{-1} human fibrinogen o/N at 4°C in a humid chamber. Slides were blocked with 1% BSA for 1 h at RT. 30-50 µL of washed platelets (3x 10^5 per µL) were mixed with 50-70 µL Tyrode's buffer with Ca^{2+}, activated with 0.01 U mL^{-1} thrombin and immediately allowed to spread on the fibrinogen-coated coverslips. After different time intervals, the adherent platelets were fixed with 300 µL 4% PFA in PBS for 5 min and *differential interference contrast* (DIC) microscopy pictures were taken using an inverted microscope Zeiss HBO 100 (Axiovert 200M, Zeiss). For analysis, the phase abundance of the different spreading stages (1, resting; 2, formation of filopodia; 3, formation of filopodia and lamellipodia; 4, fully spread) was determined.

3.2.5.21 *Immunofluorescence* (IF) stainings of platelets

After the spreading assays on fibrinogen or vWF, platelets were fixed and permeabilized in PHEM complete buffer for 20 min at RT and blocked for at least 30 min at 37°C with 5% BSA. Slides were further incubated o/N with primary antibodies or for 2 h with fluorophore-labeled primary antibodies (section 3.1.6). After intense washing unlabeled primary antibodies were detected with the respective fluorophore-conjugated secondary antibodies. Analysis was performed by confocal microscopy with a 100x oil objective on a Leica TCS SP5. Where indicated, washed platelets were pretreated (10 minutes at 37°C) with the calpain inhibitor MDL-28170 [200 µM]. To visualize the cytoskeleton of resting platelets, 30 µL washed platelets (3x 10^5 per µL) were mixed with 70 µL PHEM complete buffer and allowed to adhere to poly-L-lysine-coated coverslips and processed as described above. Images were further processed using Image J software (National Institute of Health, USA).

3.2.5.22 F-actin assembly

The ability of platelets to incorporate G-actin monomers into F-actin filaments was assessed using the F-actin assembly assay. Washed platelets (5x 10^5 per µL) were prepared as described before, diluted (1:1) in Tyrode's buffer with Ca^{2+} and stained with 10 µL DyLight649-labeled anti-GPIX antibody derivative by incubation at 400 rpm for 3 min at 37°C in a thermomixer (Eppendorf). Subsequently, the samples were divided into two sets: a resting control and an activated sample. Activation was induced by different agonists at 400 rpm for 2 min at 37°C. After activation, the platelets were fixed with 10% PFA at 400 rpm for 10 min at 37°C and spun down by centrifugation at 2,800 rpm for 5 min. The pellets were permeabilized in 55 µL of Tyrode's buffer supplied with Ca^{2+} and 0.1% Triton X-100 and stained with 10 µM phalloidin-FITC for 30 min at RT. The reaction was stopped by addition of 500 µL PBS. Platelets were spun down at 2,800 rpm for 5 min, resuspended in 500 µL PBS, stored on ice and measured immediately. MFI was assessed by flow cytometry using a FACSCalibur (BD Biosciences, Heidelberg, Germany). To assess the ability of platelets to assemble F-actin after stimulation, the ratio between resting and activated sample was calculated.

3.2.5.23 Sedimentation of the actin and microtubule cytoskeleton

Washed platelets (3x 10^5 per µL) were prepared as described in section 3.2.5.1. 190 µL of resting platelets in Tyrode´s without Ca^{2+} were lysed by addition of 20 µL 10x PHEM buffer containing 1% Triton X-100, 60 µM taxol, 20 µM phalloidin and protease inhibitors. One set (105 µL) served as whole cell lysate. The other set (105 µL) was separated into polymerized and soluble fraction by centrifugation at 56,000 rpm (microtubules) or 75,000 rpm (actin) for 30 min at 37°C in a TLA-100 rotor (Beckman Coulter). Total platelet lysates (T), soluble *supernatant* (S) and insoluble *pellets* (P) were supplemented with 2x Loading Dye and

subjected to subjected to SDS-PAGE and immunoblotting as described in section 3.2.2.2 and 3.2.2.3.

3.2.5.24 Cold-induced microtubule disassembly

Washed platelets (3x 10^5 per µL) were prepared as described before and microtubules were depolymerized by incubation of platelets in Tyrode´s without Ca^{2+} for 3 h at 4°C. Microtubule reassembly was then allowed by subsequent rewarming at 37°C for 30 min. Samples maintained at 4°C and 37°C, as well as rewarmed platelets were allowed to adhere to poly-L-lysine-coated coverslips and subsequently fixed and permeabilized in PHEM buffer supplemented with 4% PFA and 0.1% TritonX-100. Samples were stained with the respective antibodies as described in section 3.2.5.21 and visualized with a Leica TCS SP5 confocal microscope (Leica Microsystems).

3.2.6 *In vivo* analysis of platelet function

3.2.6.1 Determination of platelet life span

The clearance of platelets from the circulation was determined by the retro-orbital injection of 5 µg DyLight488-labeled anti-GPIX derivative in PBS per mouse. The percentage of labeled platelets was determined by daily blood withdrawal (50 µL) and subsequent analysis by flow cytometry.

3.2.6.2 Anesthesia (Triple narcotics)

Mice were anesthetized by intraperitoneal injection of a combination of Midazolam, Medetomidine and Fentanyl [5, 0.5 and 0.05 mg kg^{-1} body weight]. Mice were placed on a heating mat to prevent hypothermia. Before performing any experiment, absence of corneal and crossed extensor reflexes was ensured.

3.2.6.3 Tail bleeding time

Mice were anesthetized by intraperitoneal injection of triple narcotics and a 1 mm segment of the tail tip was removed using a scalpel. Tail bleeding was monitored by gently absorbing blood on filter paper at 20 s intervals without touching the wound site. Bleeding was determined to have ceased when no blood was observed on the paper. Experiments were stopped at latest after 20 min by euthanization.

3.2.6.4 $FeCl_3$-induced injury of mesenteric arterioles

The mesentery of 3- to 4-week old anesthetized mice (triple narcotics) was exteriorized by a midline abdominal incision. Endothelial damage in mesenteric arterioles was induced by application of a 3 mm^2 filter paper soaked with 20/13% $FeCl_3$. Arterioles were visualized using a Zeiss Axiovert 200 inverted microscope equipped with a 100-W HBO fluorescent lamp source

and a CoolSNAP-EZ camera (Visitron). Digital images were recorded and analyzed using the Metavue software. Adhesion and aggregation of fluorescently labeled platelets (Dylight488-conjugated anti-GPIX derivative) was monitored until complete occlusion occurred (blood flow stopped for > 2 min). Experiments were performed in collaboration with Sarah Beck.

3.2.6.5 Mechanical injury of the abdominal aorta

The abdominal cavity of 12-weeks-old anesthetized mice was opened by a longitudinal incision. An ultrasonic flow probe (Transonic Flowprobe 0.5, Transonic Systems) was placed around the exposed abdominal aorta. Thrombosis was induced by a single firm compression of the aorta using forceps. Blood flow was monitored until complete blood vessel occlusion occurred for a minimum of 5 min. Otherwise the experiment was stopped after 30 min. Aorta injury experiments shown in this study were performed and evaluated in collaboration with Sarah Beck in our laboratory.

3.2.6.6 *Transient Middle Cerebral Artery Occlusion* (tMCAO) model

tMCAO was induced in 12 weeks-old male mice under isoflurane inhalation anesthesia using the intraluminal filament technique [162]. Briefly, a midline neck incision was made and a standardized silicon rubber-coated 6.0 nylon monofilament (6021PK10, Doccol, Redlands, CA, USA) was inserted into the right common carotid artery and advanced via the internal carotid artery to occlude the origin of the middle cerebral artery. After 60 min, the filament was removed to allow reperfusion. 24 h after tMCAO the global neurological status was assessed using the Bederson score [163], motor function and coordination were evaluated using the grip test [164]. For determination of the ischemic brain infarct volume, mice were euthanized 24 h after induction of tMCAO and brain sections were stained with 2% *2,3,5-triphenyltetrazoliumchloride* (TTC). Planimetric measurements were performed using ImageJ software to calculate lesion volumes, which were corrected for brain edema as described [165]. Experiments were conducted in collaboration with Dr. Michael Schumann in the group of Prof. Dr. Guido Stoll (Department of Neurology, University Hospital, Würzburg) according to the recommendations for research in mechanism-driven basic stroke studies [166].

3.2.7 MK analysis

3.2.7.1 Sample preparation for histology

Spleen and femora of 12-week-old KO and wild-type mice were isolated and fixed in 4% PFA in PBS o/N at 4°C. Femora were decalcified for 3 d in decalcification buffer. Afterwards, spleens and femora were dehydrated in an automated tissue processor (Leica ASP200S) and embedded in paraffin.

3.2.7.2 *Hematoxylin and Eosin* (H&E) staining on paraffin sections

After embedding in paraffin, 3 µm thick sections of the formalin-fixed paraffin embedded spleens and femora were prepared, immobilized on glass slides and allowed to dry o/N at 37°C. On the following day, deparaffinization and rehydration was performed using xylene (2 x 5 min), followed by a graded alcohol series (100%, 96%, 90%, 80% and 70%, each 2 min) and finally the slides were transferred into H_2O bidest (2 min). Sections were stained with hematoxylin for 15 s and washed intensively at least for 10 min with tap water. 0.05% Eosin was used as counterstaining. Slides were washed once with H_2O bidest and dehydrated by a graded alcohol series (70%, 80%, 90%, 96% and 100%, each 2 min) followed by xylene incubation (2 times 5 min). The sections were mounted using Eukitt®, a xylene-based mounting medium. Analysis was performed with an inverted Leica DMI 4000 B microscope.

3.2.7.3 IF staining on cryosections

Femora and spleen of mice were isolated, fixed with 4% PFA and 5 mM sucrose for 1 h under agitation, transferred into 10% sucrose in PBS and dehydrated using a graded sucrose series (each 24 h in 10%, 20% and 30% sucrose in PBS, respectively). Subsequently, the samples were embedded in Cryo-Gel and shock frozen in liquid nitrogen. Frozen samples were stored at -20°C. 7 µm thick cryosections were generated using the CryoJane tape transfer system (Leica Biosystems) and probed with AlexaF488-conjugated anti-GPIb antibodies (7A9 and 13G12 [1.33 µg mL^{-1}]), to specifically label platelets and MKs, and AlexaF647-conjugated anti-CD105 antibody [3.33 µg mL^{-1}] to stain the endothelium. Nuclei were stained using DAPI [1 µg mL^{-1}]. Samples were visualized with a Leica TCS SP5 confocal microscope (Leica Microsystems).

3.2.8 *Transmission electron microscopy* (TEM)

3.2.8.1 TEM analysis of resting platelets in suspension

PRP was prepared as described before and mixed in a 1:2 ratio with 5% glutaraldehyde in PBS for 10 min at 37°C and for 1 h at RT. Platelets were spun down at 2,800 rpm for 5 min, washed three times with cacodylate buffer and incubated for 1 h at RT with 1% OsO_4 in cacodylate buffer. Afterwards, the samples were washed twice with cacodylate buffer and H_2O bidest and 2% uranyl acetate (in H_2O) was added for 1 h at 4°C. Then, platelets were dehydrated by a graded ethanol series (3x 70%, 5 min; 3x 95%, 15 min; 3x 100%, 15 min), incubated twice for 10 min with propylenoxide and afterwards transferred in a 1:1 mixture of propylenoxide and epon for 1 h under rotation. After this step, epon was added twice and samples were incubated o/N at RT. Epon was hardened for 48 h at 60°C. Ultrathin sections were prepared, stained with 2% uranyl acetate (in ethanol) and lead citrate (in H_2O) and examined at 80 kV under a EM900 (Zeiss).

3.2.8.2 TEM analysis of BM MKs *in situ*

For TEM on BM samples, the femora of 12-weeks old mice were isolated and fixed o/N at 4°C in Karnovsky fixation buffer. Subsequently, femora were decalcified for three consecutive days. Contrasting, embedding and analysis of the samples was performed as described above for platelets.

3.2.9 Data analysis

The presented results are mean ± *standard deviation* (SD) from at least three independent experiments per group, if not stated otherwise. Differences between wild-type and KO mice were statistically analyzed using the unpaired Student's *t*-test. Infarct volumes and functional data obtained from tMCAO experiments were tested for Gaussian distribution with the D'Agostino and Pearson omnibus normality test and then analyzed using the two-tailed Student's t test. Differences between more than two groups were analyzed by one-way analysis of variance (ANOVA) with Dunnetts T3 as post-hoc test. *P*-values < 0.05 were considered as statistically significant: ****P*< 0.001; ***P*< 0.01; **P*< 0.05. Results with a *P*-value > 0.05 were considered as non-significant (NS).

4. RESULTS

4.1 Coactosin-like 1 is a regulator of thrombosis and hemostasis in mice

4.1.1 Cotl1 is dispensable for platelet production and structure

Rearrangements of the actin cytoskeleton play a crucial role for platelet formation and reactivity and thus several actin-binding proteins have already been reported to be critically involved in these processes, e.g. the ADF-H family members Cof and Twf2a [82, 99]. Therefore, we were interested to investigate another ADF-H family member, Coactosin-like 1 (Cotl1) and its implication in thrombopoiesis and platelet reactivity using transgenic mice.

Preliminary experiments had indicated that the constitutive Cotl1 depletion was perinatally lethal between day P14 and P17 (Stritt *et al.*, unpublished observations). Conditional MK- and platelet-specific Cotl1-deficient (*Cotl1*$^{fl/fl\text{-}Pf4Cre}$) mice, however, were viable and fertile and were therefore used in this study. Absence of Cotl1, which was confirmed by Western Blotting (Fig. 11 A), did not alter the expression of prominent platelet surface receptors (Table 1).

	WT	***Cotl1*$^{-/-}$**
GPIb	268±36	294±16
GPV	213±4	222±5
GPIX	384±10	396±10
CD9	668±20	661±21
GPVI	36±2	36±2
CLEC-2	110±6	113±5
α2	43±4	45±3
β1	131±2	136±4
αIIbβ3	438±31	425±21

Table 1. Platelet surface glycoprotein expression in *Cotl1*$^{-/-}$ platelets. Diluted whole blood was stained with fluorophore-labeled antibodies and analyzed on a FACSCalibur (Becton Dickinson, Heidelberg). Platelets were gated by FSC/SSC characteristics. Results are given as the *mean fluorescence intensity* (MFI) ± SD of 6-12 mice per group.

In contrast to Twf2a- or Cof-deficient platelets, depletion of Cotl1 did not affect peripheral platelet count and size as assessed by flow cytometry (Fig. 11 B). Analysis of the morphology of resting platelets (Fig. 11 C) using *transmission electron microscopy* (TEM) confirmed the unaltered platelet size and revealed no differences in the distribution of α- and dense granules in *Cotl1*$^{-/-}$ mice. In agreement with these observations, MK numbers in spleen and BM were unaltered in *Cotl1*$^{-/-}$ mice (data not shown). Consistently, the life span of *Cotl1*$^{-/-}$ platelets was comparable to wild-type platelets (Fig. 11 D).

Thus, *Cotl1*$^{-/-}$ mice represent the first KO mouse model of an ADF-H family member with unaltered platelet number and size.

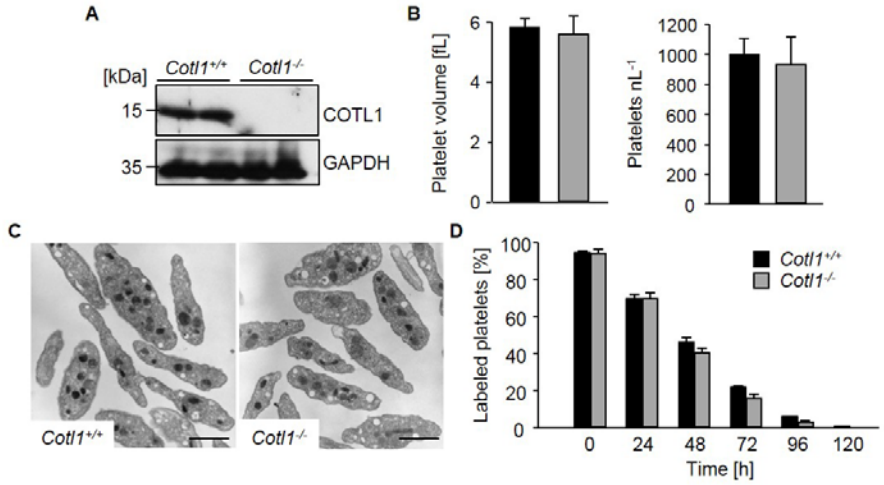

Figure 11. Cotl1 is dispensable for platelet formation, survival and structure. (A) Immunoblot on platelet lysates proved the complete loss of Cotl1 in mutant platelets. GAPDH served as loading control. (B) Peripheral platelet count and size was assessed by flow cytometry (n= 6 per group). (C) Representative TEM pictures of wild-type and *Cotl1*$^{-/-}$ platelets. Bar, 2 µm. (D) Platelet life span was assessed by i.v. injection of a Dylight488-coupled anti-GPIX-IgG derivative [0.5 µg g^{-1} body weight] and monitoring of fluorescently-labeled platelets over 5 days by flow cytometry.

4.1.2 Cotl1-deficiency does not affect cytoskeletal dynamics in platelets

A common feature of ADF-H family members is, besides their ability to bind actin, their involvement in cytoskeletal dynamics. Cof-deficiency was shown to downregulate stimulus-dependent F-actin assembly, whereas Twf2a-deficient mice displayed enhanced actin dynamics [82, 99]. Therefore, it was assumed that a deletion of Cotl1 would have effects on the cytoskeletal organization, too.

First, agonist-induced actin polymerization was assessed and found to be unaltered in Cotl1-deficient platelets (Fig. 12 A). In line with this, total tubulin and actin content was unaltered in *Cotl1*$^{-/-}$ platelets (Fig. 12 C, D), which was further confirmed by immunofluorescence stainings of resting platelets on poly-L-lysine (Fig. 12 B, left). Consistently, actin and tubulin reorganization of Cotl1-deficient platelets during spreading on fibrinogen was comparable to wild-type platelets (Fig. 12 B, right). Together, these results suggest that Cotl1 has no impact on cytoskeletal dynamics in platelets *in vitro*.

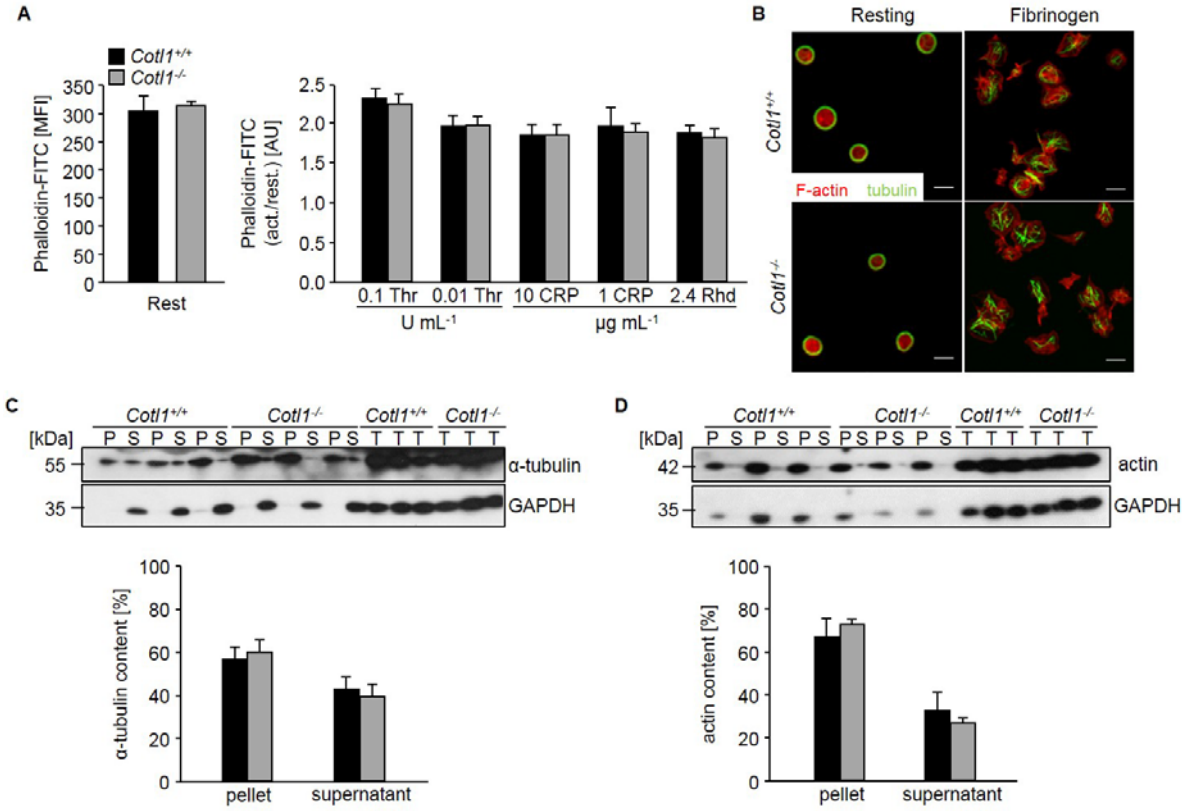

Figure 12. Cotl1-deficiency does not affect cytoskeletal function in platelets. (A) F-actin content of resting and agonist-stimulated platelets was measured by flow cytometry after incubation with phalloidin-FITC. The ratio of MFI from activated and resting platelets ± SD of 4 mice per group is shown. (B) Visualization of the cytoskeleton of resting platelets on poly-L-lysine and spread platelets (15 min) on fibrinogen, which were stained with Phalloidin-atto647N (red) and α-tubulin antibody-AlexaF488 (green) and analyzed by confocal microscopy. Bar, 2 µm. (C, D) The tubulin (C) and actin (D) cytoskeleton was isolated by ultracentrifugation, immunoblotted with anti-α-tubulin and anti-β-actin antibodies and analyzed for the content of monomeric/polymeric tubulin (C) or monomeric/polymeric actin (D) using densitometry. GAPDH served as loading control. Values are mean ± SD (n= 3). P: pellet, S: supernatant, T: total protein.

4.1.3 Increased Cofilin phosphorylation in *Cotl1*$^{-/-}$ platelets

Since Cotl1-deficiency did not affect cytoskeletal dynamics, the hypothesis arises that other actin-binding proteins compensated for the lack of Cotl1. To test a possible effect of Cotl1-deficiency on other cytoskeletal regulators, expression levels of the ADF-H members Twf and Cof, the Cof upstream effector Cdc42, as well as the actin-sequestering protein Pfn1 were assessed by western blotting.

Analysis of total protein expression revealed no differences in Twf, Cof, Pfn1 or Cdc42 levels between wild-type and *Cotl1*$^{-/-}$ platelets. Since Cof is known to be regulated by (de)-phosphorylation at the highly conserved amino acid serine 3, phosphorylation levels were assessed in addition. In platelets, approximately 90% of n-cofilin is phosphorylated at position serine 3 in the resting state [82].

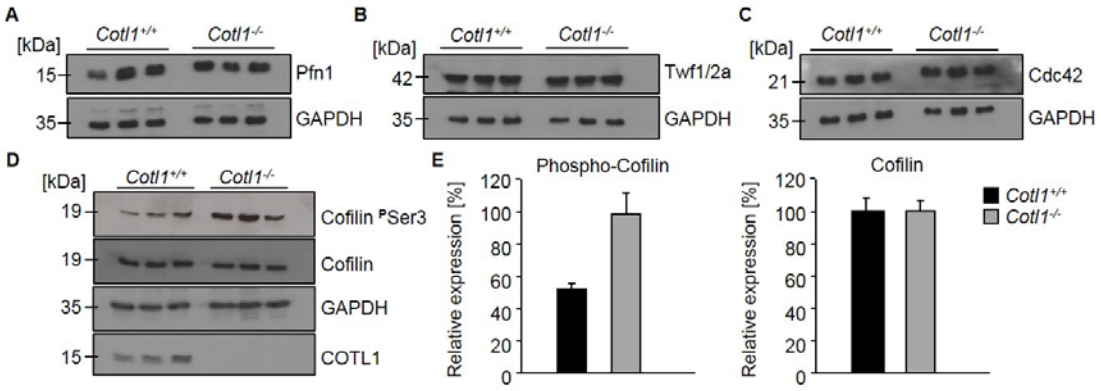

Figure 13. Increased Cofilin phosphorylation in *Cotl1*$^{-/-}$ platelets. Western blots of lysates from resting wild-type and *Cotl1*$^{-/-}$ platelets using antibodies against (A) Pfn1, (B) Twf1/2a, (C) Cdc42 and (D) Cofilin´s Phospho-Ser as well as total Cofilin. GAPDH served as loading control. (E) Densitometric analysis of relative expression levels of Phospho-Cofilin (left) and total Cofilin (right) in unstimulated wild-type and *Cotl1*$^{-/-}$ platelets.

Strikingly, a strong, 2-fold increase in expression of the (inactive) phosphorylated form of Cof could be detected in Cotl1-deficient platelets. As described by Kim *et al.* Cotl1 antagonizes Cof´s actin severing function, resulting in reduced F-actin depolymerization [104]. Therefore, the increased phosphorylation of Cof in the absence of Cotl1, ultimately causing reduced F-actin severing, might act as a compensatory mechanism.

4.1.4 Unaltered integrin activation in Cotl1-deficient platelets

Next it was tested whether Cotl1-deficiency might affect platelet reactivity as it was shown for *Twf2a*$^{-/-}$ platelets [99]. Therefore, agonist-induced αIIbβ3 integrin activation using the JON/A-PE antibody [152], which specifically binds to activated αIIbβ3 integrins, as well as degranulation-dependent surface exposure of P-selectin, a marker for α-granule release, were determined by flow cytometry. Interestingly, *Cotl1*$^{-/-}$ platelets showed unaltered αIIbβ3 integrin activation in response to all tested agonists (Fig. 14 A). Likewise, agonist-induced P-selectin exposure was indistinguish-able between wild-type and *Cotl1*$^{-/-}$ platelets (Fig. 14 B).

In line with this data, *Cotl1*$^{-/-}$ platelets showed unaltered aggregation in response to all tested agonists (Fig. 14 C). Spreading assays on fibrinogen showed the functionality of αIIbβ3 integrin outside-in signaling, which is critically important for cytoskeletal rearrangements upon platelet activation. Although Cotl1 was recently described as a regulator of T cell spreading at the immune synapse by preventing cofilin-mediated depolymerization of actin filaments [104], Cotl1-deficiency in platelets did not affect their spreading ability on fibrinogen (Fig. 14 D). In summary, these results showed that Cotl1 is dispensable for platelet reactivity *in vitro* under static conditions.

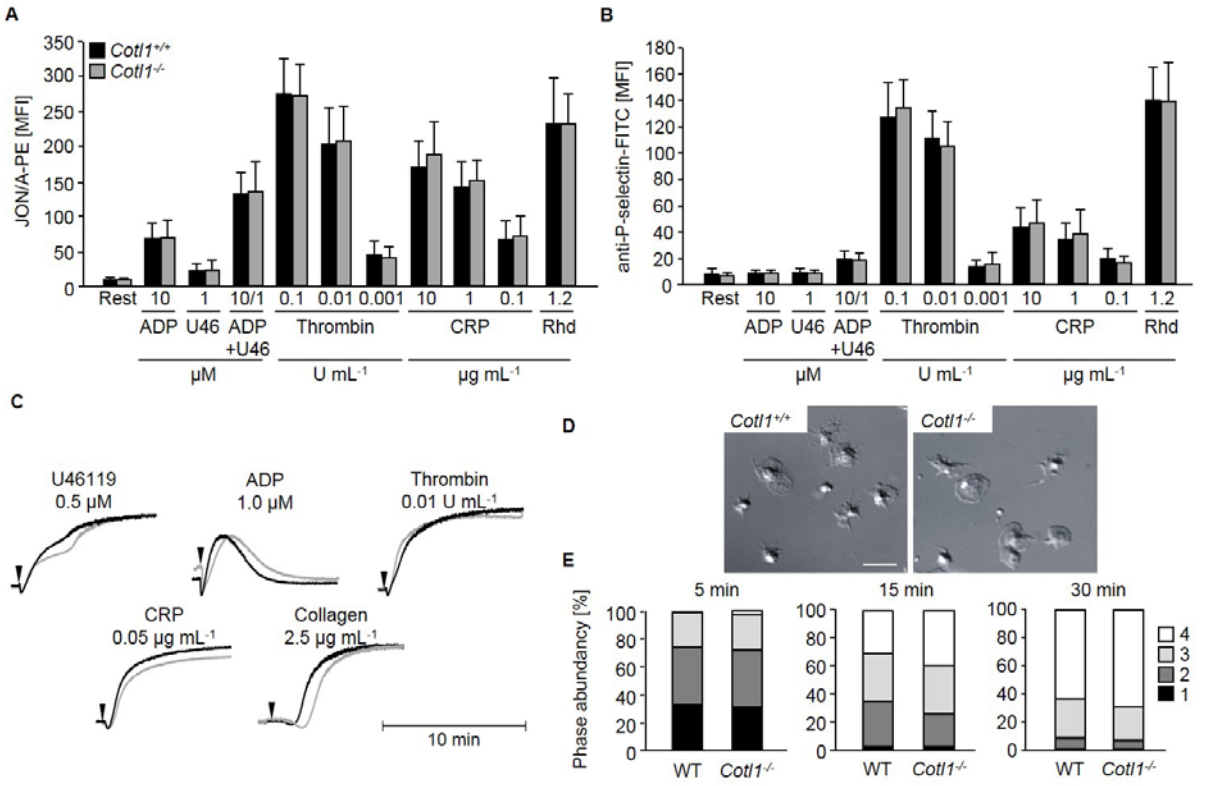

Figure 14. Unaltered integrin activation in Cotl1-deficient platelets. (A) Activation of platelet αIIbβ3 integrin (JON/A-PE) and (B) degranulation (α-P-selectin-FITC) in *Cotl1*$^{-/-}$ platelets as determined by flow cytometry. (C) Aggregation responses in turbidometric aggregometry after stimulation with the indicated agonists. (D, E) Washed platelets were stimulated with 0.01 U mL^{-1} thrombin and allowed to spread on fibrinogen. (D) Representative *Differential Interference Contrast* (DIC) microscopy images of 3 individual experiments at t= 15 min and (E) statistical evaluation of the percentage of spread platelets at different spreading stages. Bar, 3 µm.

4.1.5 Unaltered thromboxane secretion in *Cotl1*$^{-/-}$ platelets

Besides its interaction with F-actin, Cotl1 was shown to upregulate *5-lipoxygenase* (5-LO) activity, a key enzyme in *leukotriene* (LT) biosynthesis [110]. LTs are derivatives of *arachidonic acid* (AA) and act as inflammatory lipid mediators, which cause leukocyte chemotaxis and increased vascular permeability. 5-LO catalyzes the two initial steps of LT biosynthesis, (1) the oxygenation of AA to 5-HPETE and (2) the subsequent dehydration into the epoxide LTA_4 [106, 167]. Likewise, 5-HPETE can be reduced to 5-HETE, which is metabolized to 5-oxo-ETE. Moreover, AA is converted to thromboxanes (TxA/B_2), prostacyclin (PGI_2) and prostaglandines (PGE/F_2) by cyclooxygenases [168, 169].

To test the effect of Cotl1-deficiency on LT and TxA/B_2 production, their resting levels as well as the amount of released LT and TxB_2 were assessed in Cotl1-deficient platelets using commercially available ELISA kits. As shown in Figure 15, neither resting thromboxane levels nor TxB_2 release upon platelet stimulation was altered in Cotl1-deficient platelets as compared to wild-type levels.

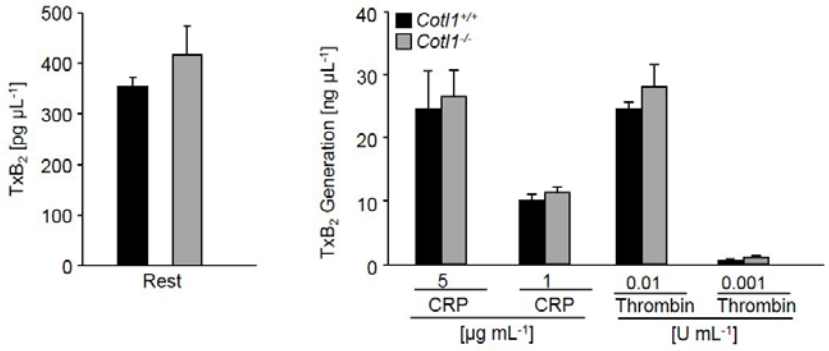

Figure 15. Unaltered TxA_2 and LT production in Cotl1-deficient mice. TxA_2 levels were measured in the supernatant of resting (A) and stimulated washed platelets (B) by ELISA. Results are expressed as mean TxB_2 generation [ng mL^{-1}] ± SD of 4 mice per group.

LT levels of resting or agonist-stimulated platelets (A23187, CRP, thrombin) were not detectable with the ELISA kit used in this study, presumably due to low concentration of these mediators in platelets. A study from Evangelista *et al.* detected 52.7 ng LTB_4 after stimulation of 5 mL rabbit whole blood with the calcium ionophore A23187 [170]. Thus, more sensitive methods are necessary to detect LT levels in platelets. To this end, analysis of the LT content of wild-type and Cotl1-deficient platelets is meanwhile performed by our collaboration partner Dr. Robert Ahrends from ISAS (Düsseldorf, Germany) using a Lipidomics approach.

4.1.6 Decreased aggregate formation of *Cotl1*$^{-/-}$ platelets under flow

At sites of vessel wall injury, release of secondary mediators from activated platelets at the exposed subendothelium plays a crucial role for the recruitment and activation of further platelets to promote thrombus formation.

To study the effect of Cotl1 on aggregate formation under flow, whole blood was perfused over a collagen-coated surface at different shear rates, reflecting the blood flow in different vessel sizes. Interestingly, less *Cotl1*$^{-/-}$ platelets adhered to the collagen-coated surface (Fig. 16 A, B) and thrombus formation was significantly reduced (Fig. 16 C). Notably, the reduction in aggregate formation was most striking at medium and high shear rates as surface coverage and thrombus formation of *Cotl1*$^{-/-}$ platelets at a low shear rate of 150 s^{-1} was unaltered as compared to wild-type platelets (data not shown).

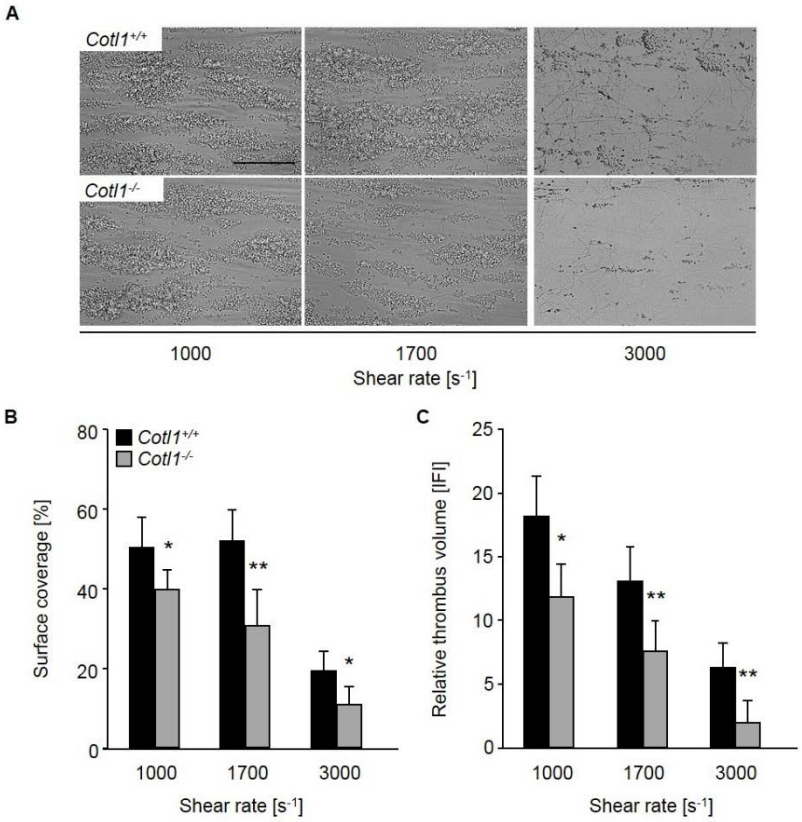

Figure 16. Impaired adhesion and thrombus formation of *Cotl1*$^{-/-}$ platelets on collagen under flow. Heparinized whole blood of *Cotl1*$^{-/-}$ and wild-type mice was perfused over a collagen-coated surface for 4 min at shear rates of 1,000, 1,700 and 3,000 s^{-1}. (A) Representative phase contrast images taken at the end of the perfusion time, (B) analysis of the surface area covered by platelets (%) and (C) the relative thrombus volume ± SD (n= 6 per group) are depicted. Unpaired Student's *t*-test: ***P*< 0.01; **P*< 0.05. Bar, 50 µm.

4.1.7 *Cotl1*$^{-/-}$ mice are protected from arterial thrombus formation and ischemic stroke

To test whether the observed thrombus formation defect on collagen *in vitro* translates into an *in vivo* phenotype, *Cotl1*$^{-/-}$ and wild-type mice were subjected to the thrombosis model of the mechanically injured abdominal aorta, where blood flow is monitored until vessel occlusion using an ultrasonic perivascular Doppler flow meter (Fig. 17 A, B). After a transient increase directly following injury, blood flow progressively decreased for several minutes in all animals. In all wild-type mice (8/8), this decrease resulted in complete and irreversible occlusion of the vessel within maximally 7 min after injury (mean occlusion time 3.37 ± 0.72 min). In sharp contrast, while a progressive reduction in blood flow was observed during the first minutes after injury in *Cotl1*$^{-/-}$ mice, blood flow afterwards normalized and 9 of 11 mice displayed normal flow rates through the injured vessel at the end of the observation period (30 min). Notably, thrombus formation of *Cotl1*$^{-/-}$ mice in smaller arterioles was unaltered as compared to wild-type mice, which was assessed using a second thrombosis model, the $FeCl_3$-induced injury of the mesenteric arterioles (data not shown). This is in line with the observed *in vitro* data under

flow, as it is well documented that collagen is the main driver of thrombus formation in bigger vessels, whereas in smaller vessels thrombosis is predominantly driven via TF-dependent mechanisms [171]. Supporting the reduced thrombotic activity in *Cotl1*$^{-/-}$ mice, these animals also exhibited mildly prolonged bleeding times (Fig. 17 C). Notably, bleeding times were highly variable suggesting thrombus instability.

To analyze whether Cotl1-deficiency would also improve outcome in a model of thrombo-inflammatory brain infarction, wild-type and *Cotl1*$^{-/-}$ mice were subjected to the *transient middle cerebral artery occlusion* (tMCAO) model of acute stroke, where the origin of the middle cerebral artery is occluded by a filament [162]. After 60 min, the filament was removed to allow reperfusion. 24 h after tMCAO the global neurological status was assessed using the Bederson score [163], motor function and coordination were evaluated using the grip test [164]. Additionally, *2,3,5-triphenyltetrazolium chloride* (TTC) staining of the brains was performed to differentiate between metabolically active and inactive tissue. Of note, infarct volumes of *Cotl1*$^{-/-}$ mice were significantly reduced (Fig. 17 D, E). The neurological outcome and motoric function, however, was not improved in Cotl1-deficient mice (Fig. 17 F).

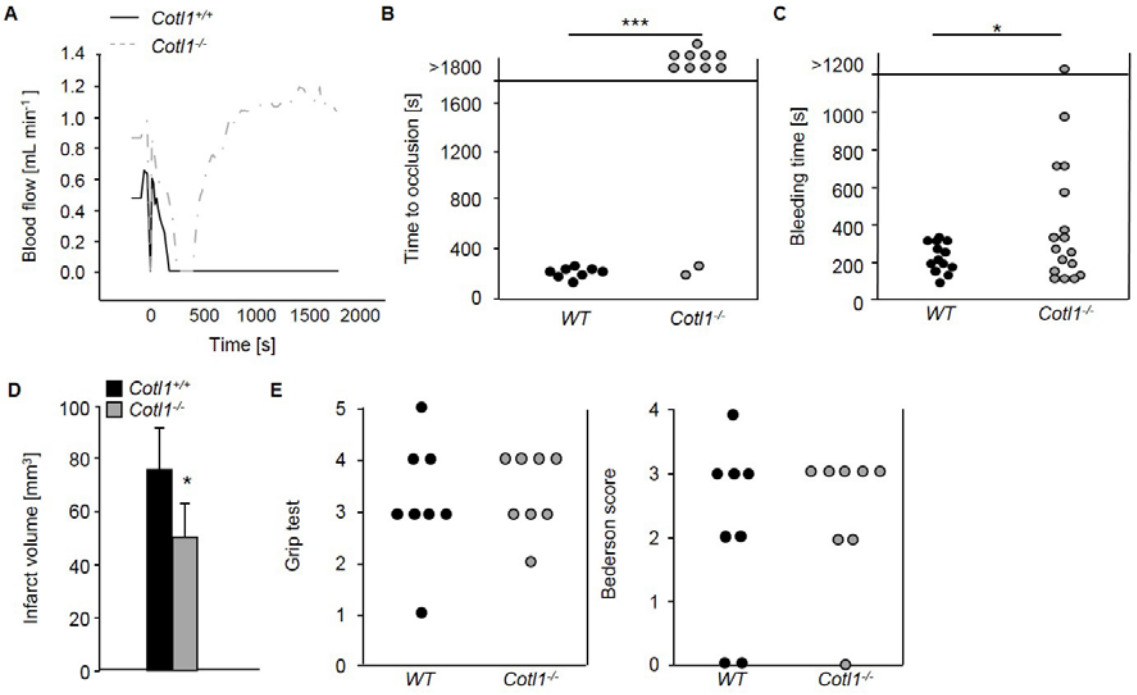

Figure 17. *Cotl1*$^{-/-}$ mice are protected from arterial thrombus formation. (A, B) Aorta thrombosis model. (A) Representative graph of blood flow of a wild-type and a *Cotl1*$^{-/-}$ mouse after mechanical injury of the abdominal aorta at t= 0. (B) Occlusion time after mechanical injury of the abdominal aorta. Experiments were performed in collaboration with Sarah Beck in our laboratory. (C) Tail bleeding times on filter paper in wild-type and *Cotl1*$^{-/-}$ mice. Each symbol represents one individual. (D) Brain infarct volumes of wild-type and *Cotl1*$^{-/-}$ mice which were subjected to 1 h tMCAO. Data are mean ± SD of 8 mice per group. (E) Neurological outcome tested by Grip test and Bederson score 24 h after tMCAO. Experiments were performed in collaboration with Dr. Michael Schumann (Department of Neurology, University Hospital, Würzburg). Unpaired Student's *t*-test: ****P*< 0.001; **P*< 0.05.

Taken together, it was shown that Cotl1-deficiency had no effect on cytoskeletal dynamics and platelet function under static conditions. Nevertheless, *in vitro* under flow lack of Cotl1 resulted in reduced thrombus formation, which translated into protection from arterial thrombus formation *in vivo*. Overall, these findings show that Cotl1 contributes to thrombotic activity and hemostasis. However, the underlying mechanism remains elusive, which was addressed in further experiments. The protection from thrombus formation of Cotl1-deficient mice in the mechanically injured aorta model as well as the decreased aggregate formation, especially under high shear rates, in the *in vitro* flow chamber model, pointed towards altered GPIb-vWF interactions in *Cotl1*$^{-/-}$ platelets.

4.1.8 Altered GPIb-vWF interaction of Cotl1-deficient platelets

GPIbα is part of the GPIb-V-IX complex and plays a crucial role for the initial platelet tethering at sites of vascular injury through binding to its ligand vWF [172]. Upon blockade of GPIb-vWF interactions, a reduced lesion progression after experimentally induced tMCAO has been described [162, 173]. Moreover, blockade of the vWF binding site on GPIbα by p0p/B-Fab treatment significantly reduced platelet tethering and thus abolished aggregate formation at sites of vascular injury [153].

Platelet tethering to vWF-coated surfaces under flow was assessed to analyze GPIb-vWF interactions in Cotl1-deficient platelets. Strikingly, adhesion of *Cotl1*$^{-/-}$ platelets was significantly reduced, which was most prominent at a shear rate of 3000 s^{-1} (Fig. 18). Of note, this defect was not caused by altered GPIb expression levels (see Table 1).

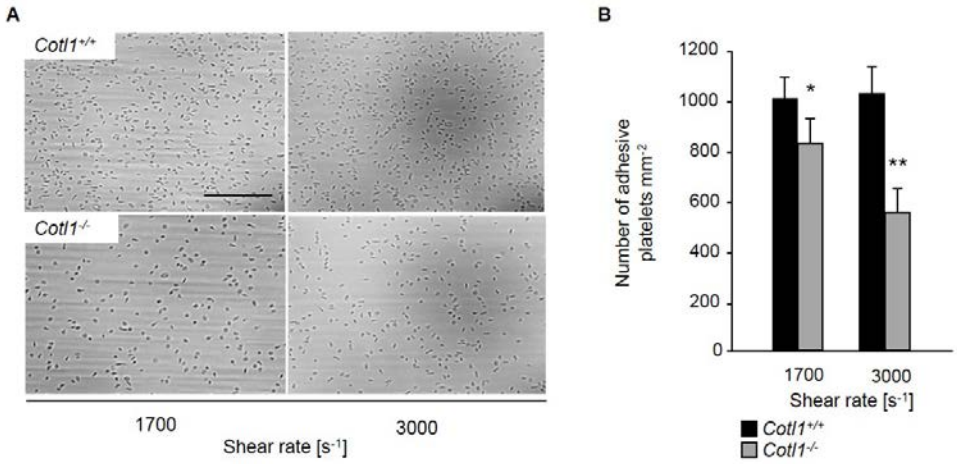

Figure 18. Impaired adhesion of *Cotl1*$^{-/-}$ platelets to vWF under flow. Heparinized whole blood of *Cotl1*$^{-/-}$ and wild-type mice was perfused over a vWF-coated cover slip for 4 min at 1,700 and 3,000 s^{-1}. (A) Representative phase contrast images taken at the end of the perfusion time and (B) analysis of the number of adherent platelets per mm^2 ± SD (n= 6 per group). Bar, 50 µm. Unpaired Student's *t*-test: ***P*< 0.01; **P*< 0.05.

These results demonstrate that Cotl1 is an important mediator of GPIb-vWF-interactions under shear flow suggesting that the decreased GPIb-vWF interaction may account for the observed *in vivo* phenotypes.

4.1.9 Slightly altered granule content and release in Cotl1-deficient platelets

Second wave mediators, such as ADP or TxA_2, potentiate thrombus formation at sites of vascular injury by further recruitment of platelets into the growing thrombus [14]. To assess whether impaired release of second wave mediators contributed to the defective thrombus formation of *Cotl1*$^{-/-}$ mice, agonist-induced granule secretion of wild-type and Cotl1-deficient platelets was assessed. Unexpectedly, dense granule ATP release was significantly enhanced in Cotl1-deficient platelets (Fig. 19 A), but, indeed, α-granular vWF secretion was slightly decreased in Cotl1-deficient platelets (Fig. 19 B). To elucidate granule secretion of Cotl1-deficient platelets further, it will be interesting to determine ADP and P-selectin content as well as the amount of released serotonin.

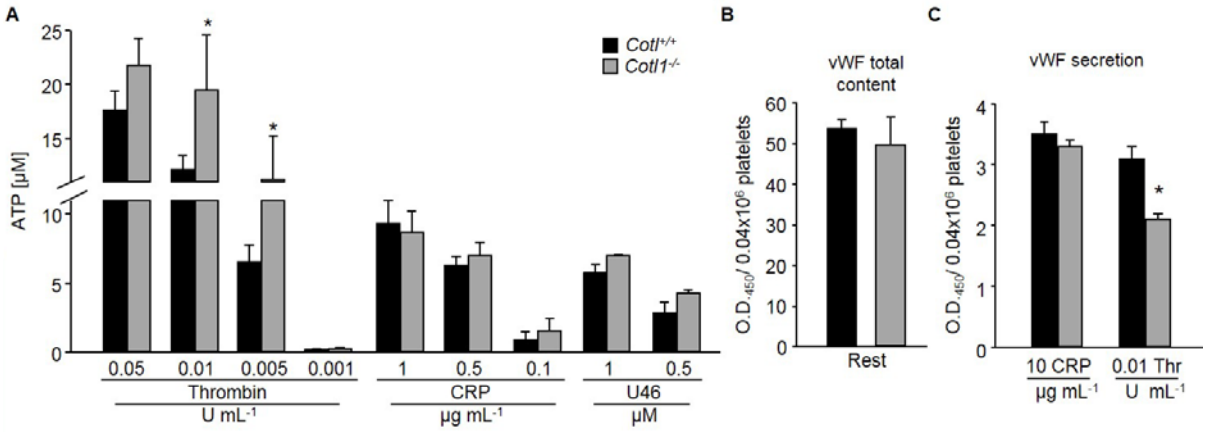

Figure 19. Moderately altered granule release of *Cotl1*$^{-/-}$ platelets. (A) Luminometric measurement of released ATP of activated wild-type and *Cotl1*$^{-/-}$ platelets. Results are given as mean ATP concentration [µM] ± SD (n= 3 per group). (B) Platelet α-granular vWF content in wild-type and *Cotl1*$^{-/-}$ platelets as assessed by ELISA. Results are expressed as mean $O.D._{450}$/0.04 x 10^6 platelets ± SD of 4 mice per group. (C) vWF release upon platelet activation. Results are expressed as mean $O.D._{450}$/0.04x 10^6 platelets ± SD of 3 mice per group. Unpaired Student's *t*-test: **P*< 0.05.

4.1.10 Addition of second wave mediators partially restores the defective thrombus formation of *Cotl1*$^{-/-}$ mice

To assess whether the observed altered second wave mediator release of Cotl1-deficient platelets contributed to the defective thrombus formation, ADP and the TxA_2 analogue U46619 were co-infused into *Cotl1*$^{-/-}$ blood using the *in vitro* flow chamber model [174].

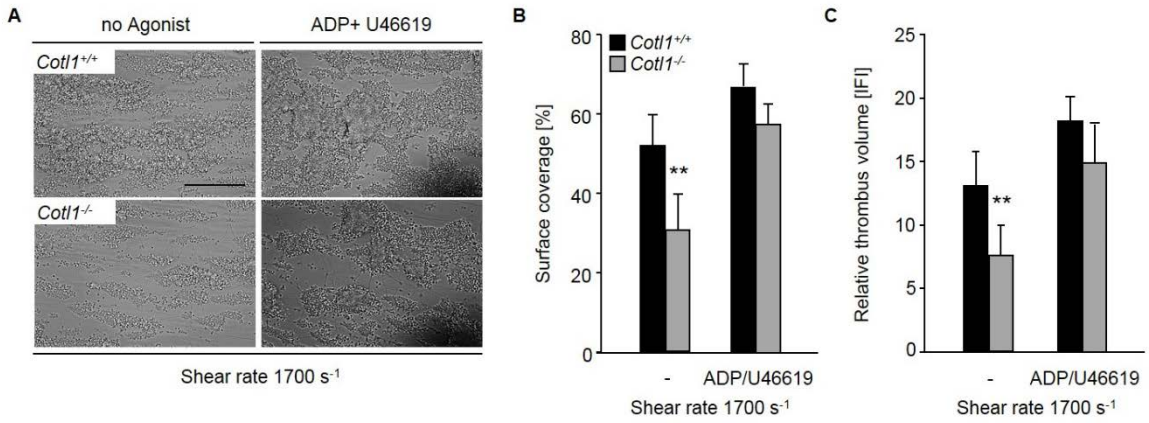

Figure 20. Defective thrombus formation of *Cotl1*$^{-/-}$ mice under shear flow is partially restored by exogenous addition of second wave mediators. Heparinized whole blood of *Cotl1*$^{-/-}$ and wild-type mice was perfused over a collagen-coated surface for 4 min at a shear rate of 1700 s^{-1}. Where stated, 10 µM ADP and 1 µM U46619 were co-infused into the blood. (A) Representative phase contrast images taken at the end of the perfusion time, (B) analysis of the surface area covered by platelets (%) and (C) relative thrombus volume ± SD (n= 6 per group) are depicted. Unpaired Student's *t*-test: ***P*< 0.01. Bar, 50 µm.

Strikingly, exogenous addition of these agonists could restore the thrombus formation defect of *Cotl1*$^{-/-}$ platelets as Cotl1-deficient platelets were able to build larger thrombi compared to untreated *Cotl1*$^{-/-}$ platelets (Fig. 20 A, C), although the defect could not be restored to wild-type levels. These results suggest that both the altered GPIb-vWF interaction and a decreased second wave mediator release contribute to the protection from thrombus formation of Cotl1-deficient mice *in vitro* under flow and *in vivo*.

4.1.11 Increased procoagulant activity of *Cotl1*$^{-/-}$ platelets under shear flow

Platelet adhesion at high shear rates to sites of vascular injury depend on GPIb-vWF interactions. Platelet deceleration subsequently enables the binding of collagen to GPVI, which initiates a powerful intracellular signaling cascade characterized by a rise in cytosolic Ca^{2+} concentration, cytoskeletal rearrangements, mobilization of α- and dense granules and subsequent release of secondary platelet agonists as well as surface exposure of negatively charged procoagulant *phosphatidylserine* (PS) [175, 176]. PS exposure further enhances TF-triggered thrombin generation and second wave mediators together with locally generated thrombin reinforce cellular activation and recruit additional circulating platelets to the growing thrombus.

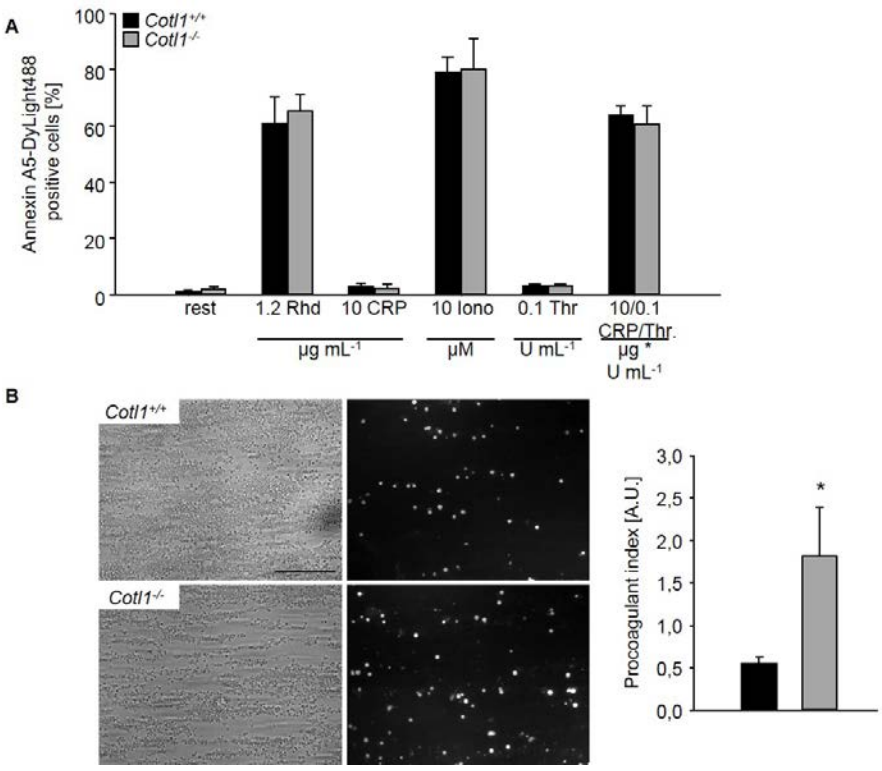

Figure 21. Cotl1-deficiency increases platelet procoagulant activity under flow. (A) Washed platelets were stimulated with the indicated agonists, stained with saturating amounts of Annexin A5-DyLight488 and analyzed by flow cytometry. Results are expressed as MFI ± SD (n= 4 mice per group). (B) Whole blood was perfused over a collagen-coated surface at a shear rate of 1,700 s^{-1} for 4 min. Adherent platelets were stained with Annexin A5-AlexaF488 [0.25 mg mL^{-1}]. Representative phase contrast and fluorescence images and mean relative amount of Annexin-A5 positive platelets ± SD of at least 6 mice. Unpaired Student's *t*-test: **P*< 0.05.

Since *Cotl1*$^{-/-}$ platelets displayed impaired GPIb-vWF interactions as well as altered second wave mediator release, it was assessed whether procoagulant activity might be affected by Cotl1-deficiency. To this end, binding of fluorescently-labeled Annexin A5 to PS exposed on the platelet surface upon stimulation was analyzed by flow cytometry [177]. Notably, no differences in procoagulant activity between wild-type and Cotl1-deficient platelets could be observed (Fig. 21 A). However, under flow, procoagulant activity of Cotl1-deficient platelets as assessed by binding of Annexin A5 to PS was significantly increased, although collagen-induced platelet adhesion was decreased in Cotl1-deficient blood (Fig. 21 B). This result again emphasizes that the effect of Cotl1-deficiency is most prominent under shear flow *in vitro* and *in vivo* suggesting reduced thrombus stability.

In summary, it was very surprising to find that Cotl1 as a member of the ADF-H protein family and regarding its actin-binding capability [68] was dispensable for thrombopoiesis and actin dynamics, but that it shows major impact on thrombosis and hemostasis.

4.2 Profilin 1 regulates integrin function in mouse platelets by mediating cytoskeletal rearrangements

4.2.1 Pfn1-deficiency leads to microthrombocytopenia

The MK- and platelet-specific Pfn1 KO mouse model (*Pfn1*$^{fl/fl\text{-}Pf4Cre}$) has previously been described. Briefly, Pfn1-deficiency resulted in a microthrombocytopenia due to cytoskeletal alterations, an accelerated platelet clearance as well as premature platelet release into the BM. Pfn1-deficient platelets displayed a thicker marginal band and a partially disrupted actin cytoskeleton. The severely misarranged and hyperstable microtubules detected in Pfn1-deficient platelets were also found in platelets isolated from WAS patients, which established Pfn1 as a new regulator of microtubule stability and reorganization [178]. However, the impact of Pfn1-deficiency on platelet function has not been addressed in this study. Therefore, platelets from *Pfn1*$^{fl/fl\text{-}Pf4Cre}$ mice were investigated concerning platelet reactivity, aggregation and thrombotic activity.

Western Blot analysis of platelet lysates confirmed effective ablation of Pfn1 expression in mutant platelets (Fig. 22 A). Assessment of platelet count and size by flow cytometry revealed a microthrombocytopenia, which was already described by Bender, Stritt *et al.* [178] (Fig. 22 B, C) and is caused by accelerated clearance and premature release of platelets into the BM compartment. In line with the decreased platelet size, the surface expression of major platelet glycoproteins was decreased (Fig. 22 D).

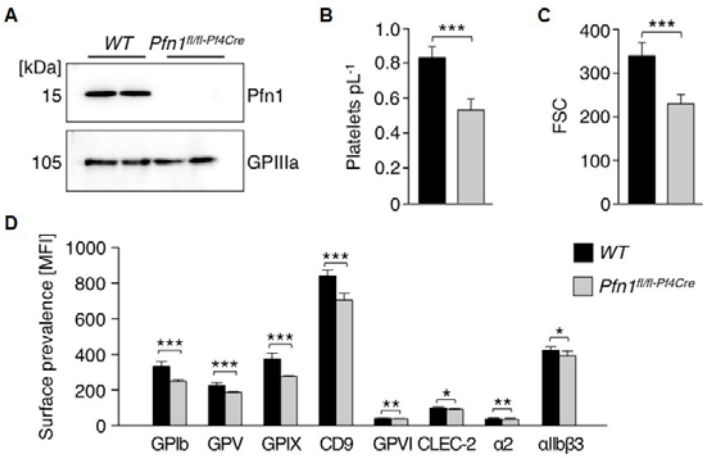

Figure 22. *Pfn1*$^{fl/fl\text{-}Pf4Cre}$ mice display microthrombocytopenia. (A) Immunoblot on platelet lysates proved lack of Pfn1 expression in mutant platelets. GPIIIa served as loading control. (B-D) Platelet count (B), size (C) and surface prevalence of major platelet glycoproteins (D) were assessed by flow cytometry. Values are ± SD (n= 6 vs. 6). Unpaired Student's t-test: ***P< 0.001; **P< 0.01; *P< 0.05. (Stritt, Birkholz *et al.*, **Blood Adv**, 2018 [179])

4.2.2 Impaired inside-out integrin activation in *Pfn1*$^{fl/fl\text{-}Pf4Cre}$ platelets

To study whether the smaller sized platelets show altered reactivity, agonist-induced platelet β1 (9EG7-FITC)- and β3 (JON/A-PE)-integrin activation was assessed by flow cytometry (Fig. 23 A, B). Strikingly, *Pfn1*$^{fl/fl\text{-}Pf4Cre}$ platelets showed impaired activation of β1- and β3-integrins in response to all tested agonists. Degranulation as assessed by P-selectin exposure was, however, unaltered in Pfn1-deficient platelets (Fig. 23 C).

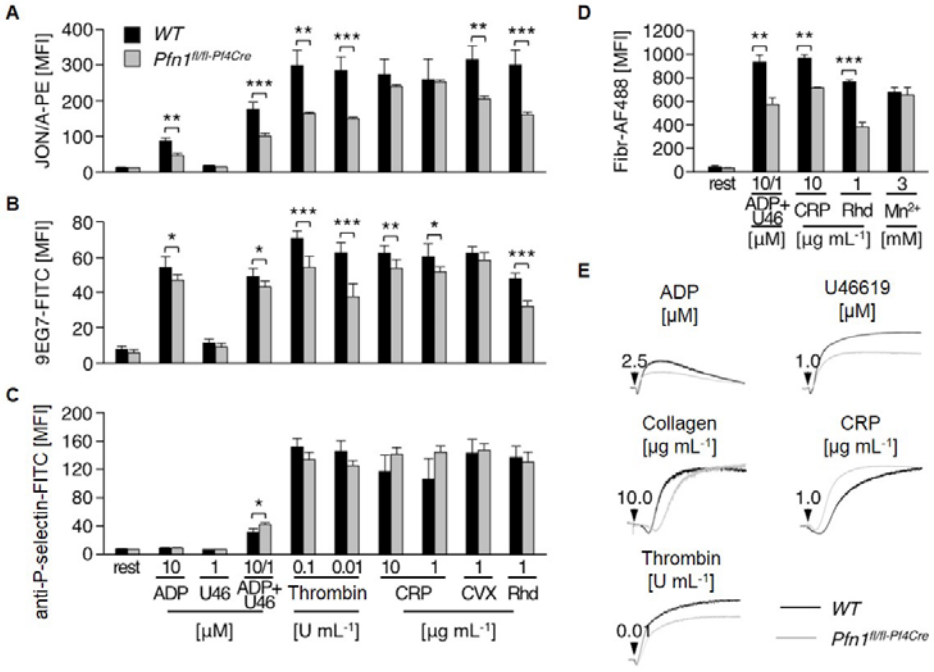

Figure 23. Impaired integrin activation in *Pfn1*$^{fl/fl\text{-}Pf4Cre}$ platelets. Activation of platelet (A) αIIbβ3- (JON/A-PE) and (B) β1-integrins (9EG7-FITC), as well as (C) α-granule release (α-P-selectin-FITC) and (D) platelet fibrinogen-binding (Fibr-AF488) in response to different agonists were assessed by flow cytometry. Values are presented as mean ± SD (n= 6 per group). (E) Aggregation responses in turbidometric aggregometry. Unpaired Student's *t*-test: ***P< 0.001; **P< 0.01; *P< 0.05. (Stritt, Birkholz *et al.*, **Blood Adv**, 2018 [179])

In line with the decreased integrin activation, agonist-stimulated *Pfn1*$^{fl/fl\text{-}Pf4Cre}$ platelets showed reduced binding to AlexaF488-conjugated fibrinogen (Fig. 23 D). Unexpectedly, aggregation responses of *Pfn1*$^{fl/fl\text{-}Pf4Cre}$ platelets were only slightly affected by the impaired integrin activation (Fig. 23 E).

4.2.3 Defective outside-in signaling in *Pfn1*$^{fl/fl\text{-}Pf4Cre}$ platelets

Integrin outside-in signaling was assessed in a spreading assay on fibrinogen to further assess the integrin activation defect of Pfn1-deficient platelets (Fig. 24). Consistently, Pfn1-deficient platelets displayed severely reduced outside-in activation, which was characterized by significantly impaired filopodia and lamellipodia formation. Strikingly, Pfn1-deficient platelets displayed only few "normal looking" filo- and lamellipodia, hence, two new spreading phases,

"leaky" (a stage between filopodia and lamellipodia formation) and "rough" (the stage between lamellipodia formation and fully spread platelets) were defined. Of note, this spreading defect is probably not only caused by impaired integrin signaling, but can additionally be attributed to the grossly disrupted actin cytoskeleton as described by Bender, Stritt *et al.* [178].

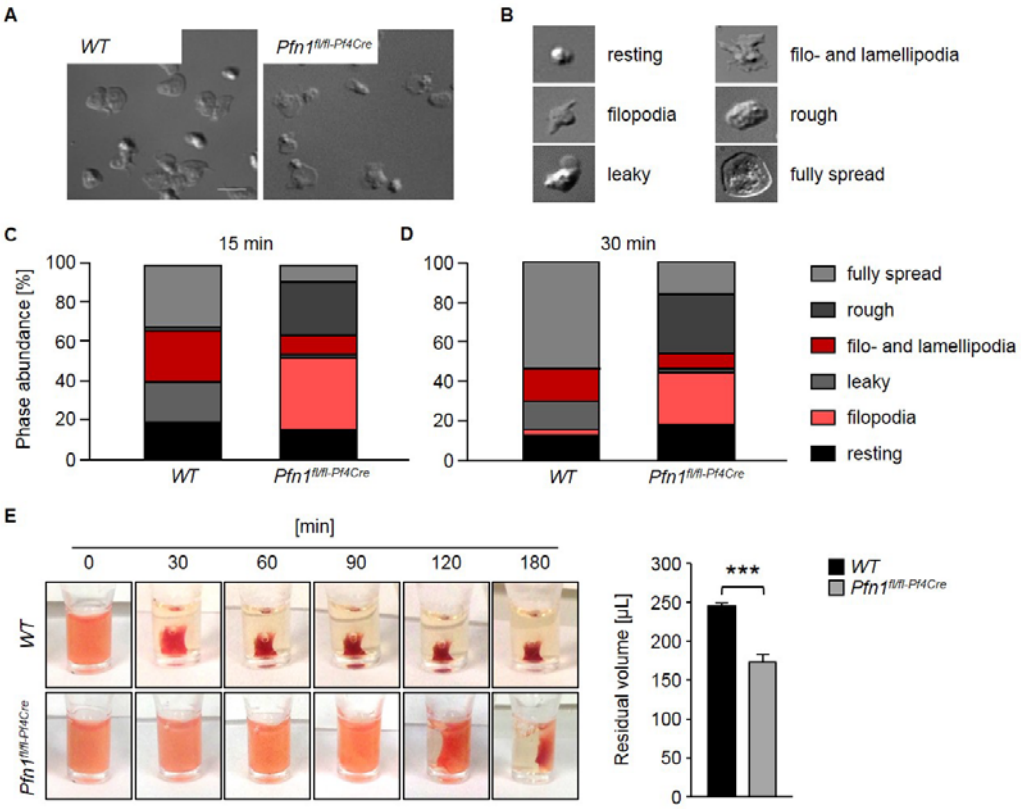

Figure 24. Impaired filopodia and lamellipodia formation of *Pfn1*$^{fl/fl\text{-}Pf4Cre}$ platelets. Washed wild-type and *Pfn1*$^{fl/fl\text{-}Pf4Cre}$ platelets were allowed to spread on fibrinogen-coated coverslides after stimulation with 0.01 U mL^{-1} thrombin. (A) Representative DIC images at t= 30 min after thrombin stimulation. Bars, 3 µm. (B) Overview of newly defined spreading phases. (C) Quantification of the different spreading phases after 15 (C) and 30 min (D) from DIC images (Zeiss Axiovert 200 inverted microscope (100x/1.4 oil objective, Zeiss)). Images are representative of at least 6 animals per group. Values are mean ± SD. (E) Platelet clot retraction was determined over time in response to 5 U mL^{-1} thrombin. Values are mean ± SD (n= 6 mice per group). ***P< 0.001. (Stritt, Birkholz *et al.*, **Blood Adv**, 2018 [179])

In line with the defective spreading of *Pfn1*$^{fl/fl\text{-}Pf4Cre}$ platelets, they showed severely delayed and less effective clot retraction (Fig. 24 E), further reflecting impaired integrin function.

4.2.4 Pfn1 is a regulator of thrombosis and hemostasis

To investigate whether the integrin activation defect of *Pfn1*$^{fl/fl\text{-}Pf4Cre}$ platelets does translate into a thrombus formation defect under flow, aggregate formation on collagen using the *in vitro* flow chamber model, was assessed. Indeed, Pfn1-deficient platelets displayed markedly reduced adhesion and aggregate formation (Fig. 25 A, B) at an intermediate shear rate of 1000 s^{-1}. This

translated into a profound protection from *in vivo* thrombus formation as upon induction of arterial thrombosis by mechanical injury of the abdominal aorta all control mice formed occlusive thrombi, whereas 5 out of 6 *Pfn1*$^{fl/fl\text{-}Pf4Cre}$ mice did not form stable occlusions (Fig. 25 C, D). In line with the *in vitro* data, *Pfn1*$^{fl/fl\text{-}Pf4Cre}$ mice displayed prolonged bleeding times as compared to wild-type mice, since two out of nine *Pfn1*$^{fl/fl\text{-}Pf4Cre}$ mice failed to cease bleeding within the observation period (Fig. 25 D). Altogether, these results highlight Pfn1 as a critical factor for platelet integrin activation and thus as regulator of hemostasis and thrombosis.

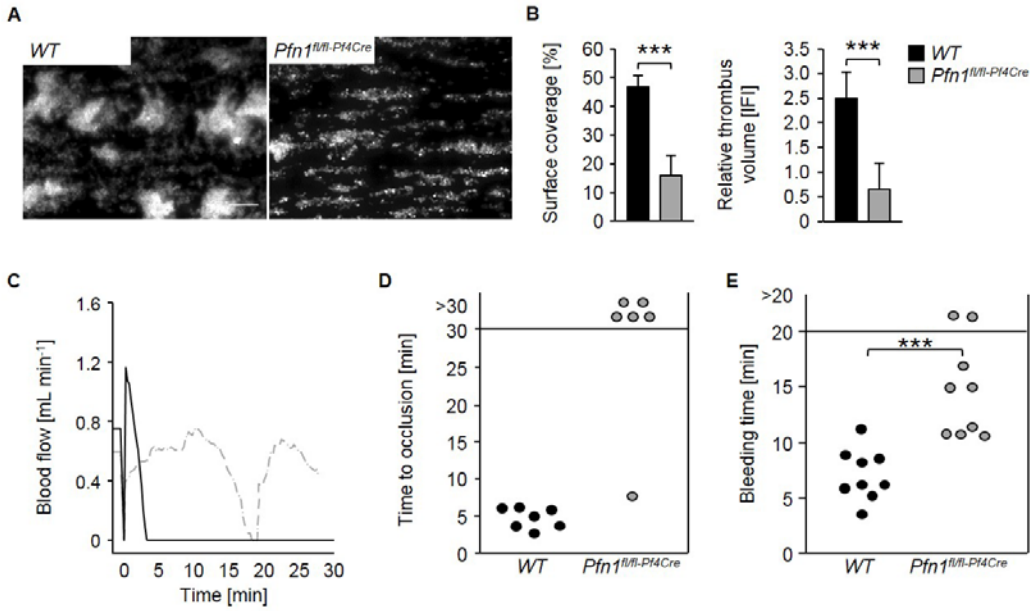

Figure 25. Impaired thrombosis and hemostasis in *Pfn1*$^{fl/fl\text{-}Pf4Cre}$ mice. Assessment of platelet adhesion and aggregate formation on collagen-coated coverslides under flow (1,000 s^{-1}) of wild-type and platelet count-adjusted *Pfn1*$^{fl/fl\text{-}Pf4Cre}$ samples. (A) Representative phase contrast images taken at the end of the perfusion time, (B) analysis of the surface area covered by platelets (%) and the relative thrombus volume ± SD (n= 6 per group) are depicted. Values are mean ± SD (n= 12 mice per group). (C) Aorta thrombosis model. Representative graph of blood flow of a wild-type and a *Pfn1*$^{fl/fl\text{-}Pf4Cre}$ mouse after mechanical injury of the abdominal aorta at t= 0. (B) Occlusion time after mechanical injury of the abdominal aorta (n= 7 vs. 6 mice). Experiments were performed in collaboration with Sarah Beck in our laboratory. (E) Hemostasis as assessed by a tail bleeding time assay (n= 9 mice per group). Unpaired Student's *t*-test (B, E) and Fisher's exact test (D): ***P< 0.001. (Stritt, Birkholz *et al.*, **Blood Adv**, 2018 [179])

4.2.5 Altered β3-integrin and Talin-1 localization in *Pfn1*$^{fl/fl\text{-}Pf4Cre}$ platelets

Talin-1 (Tln1) recruitment to the tails of β-integrin subunits represents a key step in integrin activation. To analyze if altered Tln1 recruitment causes the defective integrin activation observed in *Pfn1*$^{fl/fl\text{-}Pf4Cre}$ platelets, Tln1 and β3-integrin localization was assessed by immunostaining of platelets spread on fibrinogen. Whereas in wild-type platelets Tln1 and β3-integrins localized mainly at the cell cortex (Fig. 26 A, upper part, B), *Pfn1*$^{fl/fl\text{-}Pf4Cre}$ platelets displayed a diffuse localization pattern throughout the entire platelet cytoplasm (Fig. 26 A,

lower part, B). These results suggested that lack of Pfn1 impairs Tln1 and β3-integrin localization, possibly due to an integrin defect or the disrupted actin cytoskeleton, also interfering with proper spreading of the platelets, or both.

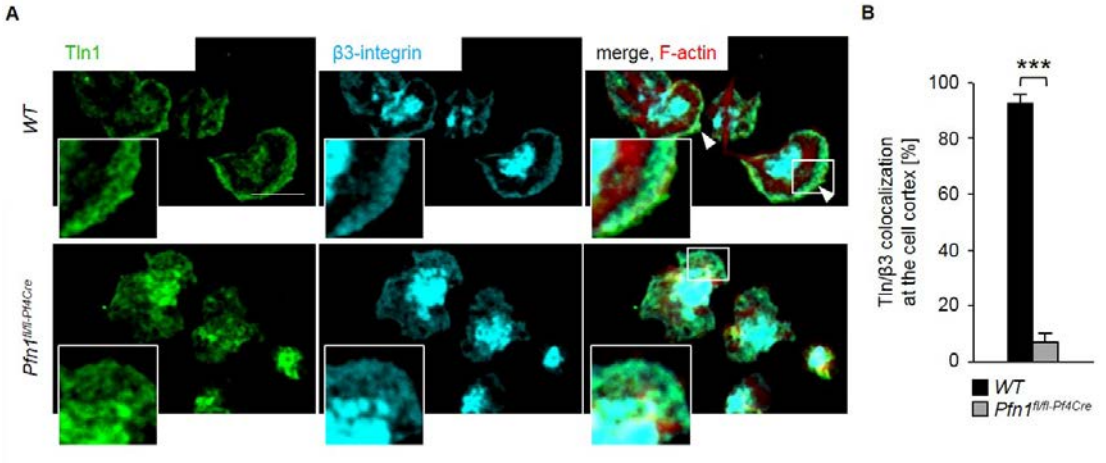

Figure 26. Altered integrin and Tln1 localization in *Pfn1*$^{fl/fl\text{-}Pf4Cre}$ platelets. (A) Tln1 localization to β3-integrin tails was assessed by immunostaining and confocal microscopy (Leica TCS SP5, 100x/1.4 oil STED WHITE objective, Leica Microsystems) of spread platelets on fibrinogen (t= 30 min) of 6 vs. 6 animals. Bar, 3 µm. (B) Assessment of the Tln1 and β3-integrin distribution pattern in at least 70 platelets of 6 animals per group. Values are mean ± SD. ****P*< 0.001. (Stritt, Birkholz *et al.*, **Blood Adv**, 2018 [179])

4.2.6 Accelerated integrin closure in *Pfn1*$^{fl/fl\text{-}Pf4Cre}$ platelets

The integrin activation defect in Pfn1-deficient platelets was further addressed by analysis of the activation status of β3-integrins. It has previously been reported that the switch of β3-integrin from its high- to low-affinity state, the so-called integrin closure, is triggered by activation of the Ca^{2+}-dependent cytosolic cysteine proteinase calpain, which cleaves off the β3-integrin tail. Sustained Ca^{2+} signaling, in turn, leads to exposure of PS on the outer leaflet of platelets, which critically links PS exposure and integrin closure [99, 180-182].

To assess the role of Pfn1 in the dynamics of integrin closure, time course experiments were performed and the percentages of platelets with activated β3-integrins (measured by JON/A-PE binding, quadrant Q1), PS exposure (assessed by Annexin A5-FITC binding, Q3), or both (Q2), were determined. In line with the increased Ca^{2+} signaling (data not shown), *Pfn1*$^{fl/fl\text{-}Pf4Cre}$ platelets displayed a significantly increased percentage of PS-positive platelets with inactivated integrins (JON/A$^-$ Annexin A5$^+$; lower right quadrant Q3) after 5 minutes (Fig. 27 A, B) which was further increased 30 min after stimulation (Fig. 27 A, C).

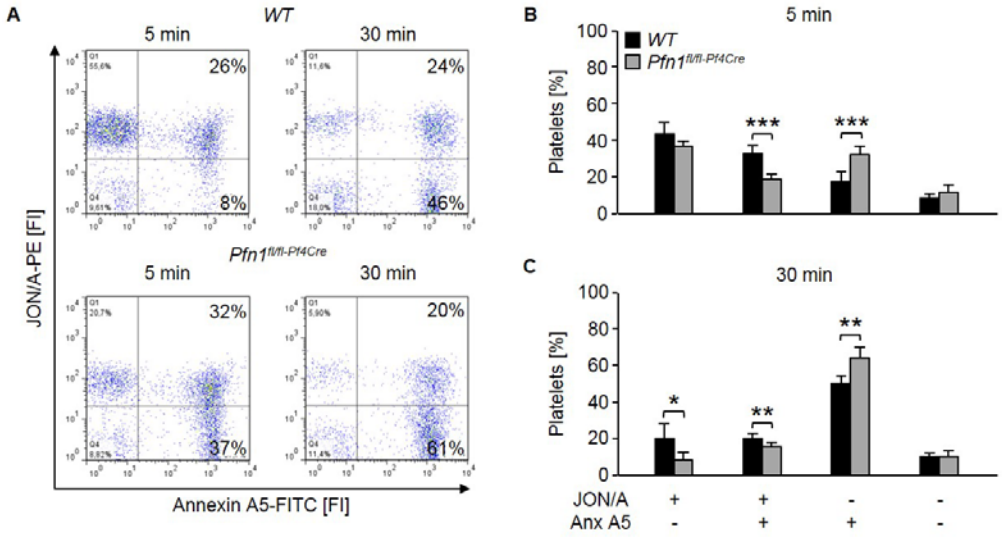

Figure 27. Accelerated integrin closure in *Pfn1*$^{fl/fl\text{-}Pf4Cre}$ mice. (A) Washed platelets were stimulated for 5 or 30 minutes with 0.1 U mL^{-1} Thr and 10 µg mL^{-1} CRP. Activation of β3-integrins and PS exposure on the outer leaflet of the platelet membrane were determined by JON/A-PE antibody and Annexin A5 protein (Anx A5-FITC). Analysis was performed by flow cytometry. Plots are representative of at least 6 animals per group. (B, C) Percentage of platelets (mean ± SD of 6 vs. 7 animals) per quadrant (Q); Q1, JON/A$^+$ Anxa5$^-$ (upper left); Q2, JON/A$^+$ Anxa5$^+$ (upper right); Q3, JON/A$^-$ Anxa5$^+$ (lower right); Q4, JON/A$^-$ Anxa5$^-$ (lower left). Unpaired Student's *t*-test: ***P< 0.001; **P< 0.01; *P< 0.05. (Stritt, Birkholz *et al.*, **Blood Adv**, 2018 [179])

These results revealed that Pfn1-deficiency leads to accelerated integrin closure and is consequently a reason for the integrin activation defect observed in Pfn1-deficient platelets.

4.2.7 Increased calpain activity in *Pfn1*$^{fl/fl\text{-}Pf4Cre}$ platelets

Stritt *et al*. previously showed that altered calpain activity can impair integrin closure [99]. Therefore, it was assessed next whether accelerated integrin closure in Pfn1-deficient platelets was the reason of increased calpain activity. Immunoblotting of stimulated wild-type and *Pfn1*$^{fl/fl\text{-}Pf4Cre}$ platelets showed that cleavage of β3-integrin tails and hence dissociation of the integrin-cytoskeleton linkage was increased in stimulated *Pfn1*$^{fl/fl\text{-}Pf4Cre}$ platelets independent of the used agonist. A23187 (Fig. 28 A, lane 2), a Ca^{2+} ionophore which increases Ca^{2+} levels and hence activates calpain, served as activation-independent control. Increased calpain cleavage of β3-integrin in *Pfn1*$^{fl/fl\text{-}Pf4Cre}$ platelets was detectable upon stimulation with thrombin and CRP. As control, the cleavage of two additional calpain targets, Tln1 and *Filamin A* (Fln A) was assessed in Pfn1-deficient platelets. Again, similar results were obtained as increased calpain cleavage of these targets was observed in *Pfn1*$^{fl/fl\text{-}Pf4Cre}$ platelets (Fig. 28 B, C, lanes 2+3). Of note, when calpain was chemically inhibited using the compound MDL-28170, the accelerated cleavage of calpain targets in Pfn1-deficient platelets was reversed to wild-type levels (Fig. 28 A-C, lane 4).

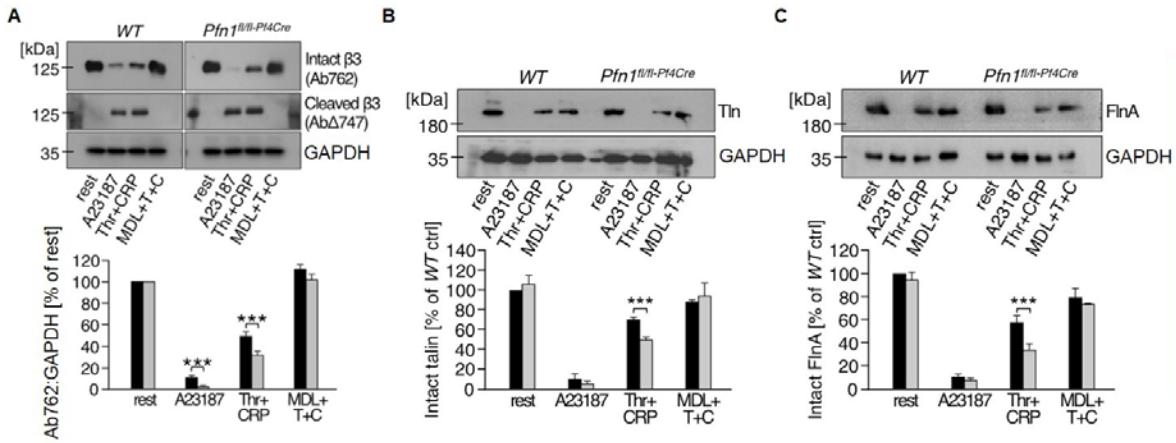

Figure 28. Increased calpain-mediated cleavage of β3-integrin, Talin and Filamin A in *Pfn1*$^{fl/fl\text{-}Pf4Cre}$ platelets. (A-C) Where indicated, platelets were pre-incubated for 10 min with the calpain inhibitor MDL-28170 [200 µM]. Subsequently, resting platelets were left untreated or were stimulated with A23187 [10 µM] or thrombin [0.1 U mL^{-1}] and CRP [10 µg mL^{-1}] (T+C), lysed and processed for immunoblotting. Full-length (Ab762) and calpain-cleaved (AbΔ747) β3-integrin, as well as Tln1 and Fln A were probed with the respective antibodies and analyzed by densitometry (n = 7 vs. 6 animals). Immunoblots are representative of at least 6 animals per group. (Stritt, Birkholz *et al.*, **Blood Adv**, 2018 [179])

As pretreatment with MDL-28170 could revert the enhanced calpain-mediated cleavage of β3-integrins in Pfn1-deficient platelets, it was assessed next whether it would also restore the impaired β3-integrin localization. To this end, platelets were pre-treated with MDL-28170 10 min prior to spreading on fibrinogen. Inhibition of calpain could indeed restore β3-integrin and Tln1 localization (Fig. 29) and significantly improved spreading of *Pfn1*$^{fl/fl\text{-}Pf4Cre}$ platelets.

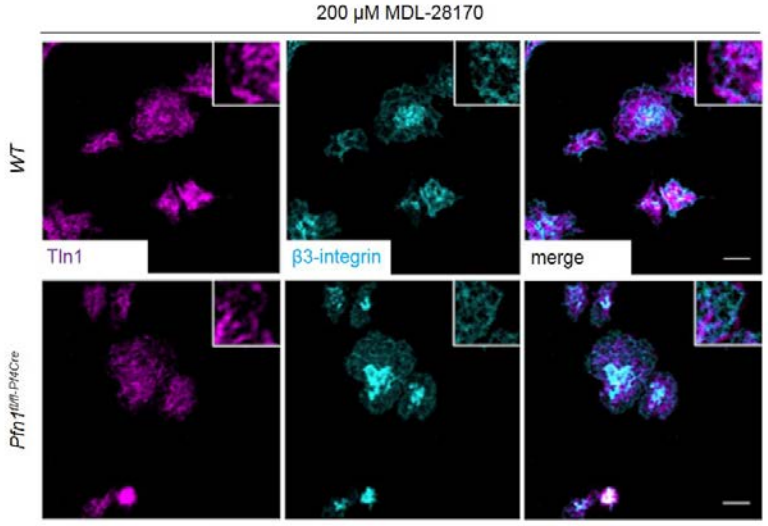

Figure 29. Restored integrin and Tln1 localization in *Pfn1*$^{fl/fl\text{-}Pf4Cre}$ platelets upon MDL-28170 treatment. Platelets were pretreated with the calpain inhibitor MDL-28170 [200 µM] and localization of β3-integrin (cyan) and Tln1 (magenta) was assessed by immunostaining and confocal microscopy (Leica TCS SP5, 100x/1.4 oil STED WHITE objective, Leica Microsystems) of spread platelets on fibrinogen (t= 30 min) of 4 animals per group. Bar, 3 µm. (Stritt, Birkholz *et al.*, **Blood Adv**, 2018 [179])

In summary, accelerated integrin closure caused by enhanced calpain activity, leads to reduced levels of activated integrins in Pfn1-deficient platelets. Moreover, these results support the previously described mechanism of calpain-mediated integrin closure.

4.2.8 Defective actin dynamics in *Pfn1*$^{fl/fl\text{-}Pf4Cre}$ platelets modulate calpain activity

Stritt *et al.* proposed that the organization of the circumferential actin cytoskeleton modulates calpain-mediated β3-integrin closure and thereby also controls their localization [99]. Therefore, it was assessed whether pretreatment with the actin polymerization inhibitor Latrunculin A could normalize the increased calpain activity of Pfn1-deficient platelets. Strikingly, inhibition of actin polymerization could revert the increased calpain-mediated cleavage of β3-integrin tails in Pfn1-deficient platelets to wild-type levels as assessed by immunoblotting of stimulated platelets pretreated with Latrunculin A (Fig. 30, A, B).

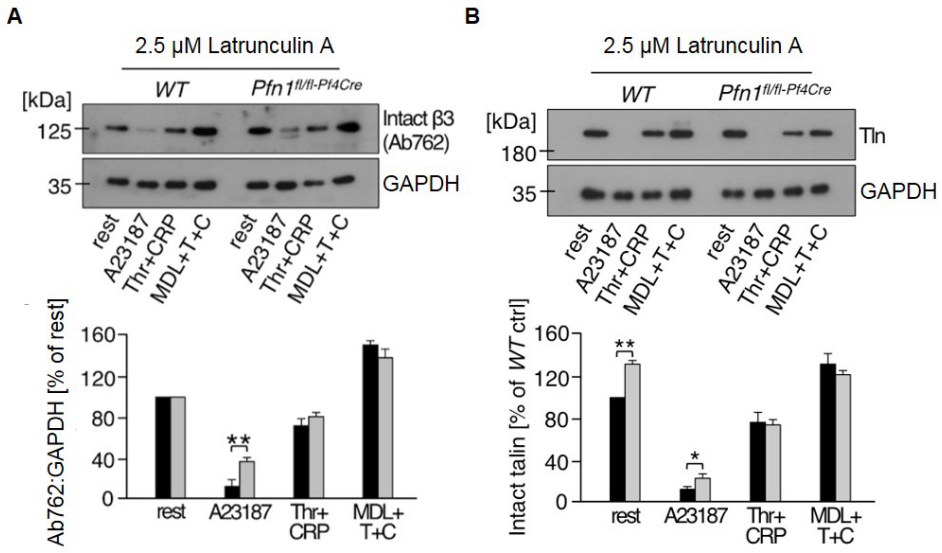

Figure 30. Increased calpain-mediated cleavage of β3-integrin and Talin-1 is restored by inhibition of actin polymerization. Latrunculin A-pretreated platelets ([2.5 µM], 10 min) were left untreated or pre-incubated for 10 min in the presence of the calpain inhibitor MDL-28170 [200 µM]. Subsequently, samples were stimulated with A23187 [10 µM] or thrombin [0.1 U mL^{-1}] and CRP [10 µg mL^{-1}], lysed and processed for immunoblotting. Full-length β3-integrin (Ab762) and Talin-1 (Tln) was probed with the respective antibody and analyzed by densitometry. Immunoblots are representative of 3 animals per group. Values are mean ± SD. Unpaired Student's *t*-test: ***P*< 0.01; **P*< 0.05. (Stritt, Birkholz *et al.*, **Blood Adv**, 2018 [179])

In summary, these findings reveal that lack of Pfn1 in platelets perturbs the organization of the adhesion-dependent circumferential actin network and thereby causes accelerated integrin closure translating into defective hemostatic and thrombotic function *in vitro* and *in vivo*.

4.3 Thymosin β4 regulates reactivity and procoagulant activity of platelets

4.3.1 Tβ4-deficient mice show a mild thrombocytopenia

Tβ4 is a moonlighting protein as it exerts various paracrine effects on the one hand, including cardiac protection, angiogenesis, wound healing and immunomodulatory effects [129]. On the other hand, it is, together with Pfn1, the major G-actin sequestering protein within cells of higher eukaryotes. While intensive research has investigated the beneficial impact of recombinant Tβ4 in a variety of disease models, its function for cytoskeletal dynamics is still poorly studied. Moreover, a distinction between endo- and exogenous protein function, its uptake and release mechanisms and its mode of action have remained elusive. Therefore, the aim was to investigate the effect of a constitutive Tβ4 KO on platelet physiology and thrombosis and to shed light on the underlying signaling network by analyzing the effect of recombinant Tβ4 in wild-type and Tβ4-deficient mice. Constitutive deletion of X-chromosomal Tβ4 (*Tβ4*$^{y/-}$ (male), *Tβ4*$^{-/-}$ (female)) in mice has previously been described by Rossdeutsch *et al.* [183]. Briefly, Tβ4-deficiency induced hemorrhages in the vessel wall (referred to as vascular hemorrhage) and reduced smooth muscle cell coverage [183], which reveals Pfn1 as regulator of mural cell development and vessel wall stability. The constitutive *Tβ4*$^{y/-}$ and *Tβ4*$^{-/-}$ mice (further referred to as *Tβ4*$^{-/-}$) were further investigated in this thesis to assess the effect of Tβ4 deletion for cytoskeletal dynamics and its other moonlighting properties.

Deletion of Tβ4 was confirmed by RT-PCR (Fig. 32 A), as a detection of protein levels using western blotting was not possible so far due to the small protein size of 5 kDa.

	wild-type	*Tβ4*$^{-/-}$
GPIb	276±11	260±21
GPV	155±11	171±9
GPIX	263±29	270±24
CD9	599±42	644±56
GPVI	27±2	25±1
CLEC-2	97±12	103±8
α2	41±1	43±2
αIIbβ3	270±23	283±6
WBC [nL^{-1}]	6,9±2	7,9±3
RBC [pL^{-1}]	8,4±1	8,9±2
Hb [g dL^{-1}]	11,9±2	12,9±4
HCT [%]	39,8±4	43,3±6

Table 2. Platelet membrane glycoprotein expression in *Tβ4*$^{-/-}$ platelets. Diluted whole blood was stained with fluorophore-labeled antibodies at saturating concentrations for 15 min at RT and analyzed on a FACSCalibur (Becton Dickinson, Heidelberg). Platelets were gated by FSC/SSC characteristics. Results are given as *mean fluorescence intensity* (MFI) ± SD of 6-12 mice per group. Basal blood parameters were assessed using the Sysmex automated hematology analyzer (Sysmex KX-21N, Sysmex Corp., Kobe, Japan).

Tβ4-deficiency did affect neither viability or fertility nor expression of prominent surface receptors or basal blood parameters (Table 2). Analysis of platelet count and size by flow cytometry revealed a moderate thrombocytopenia in *Tβ4*$^{-/-}$ mice, resulting in a 30% reduction

of platelet count compared to wild-type animals. However, the size of *Tβ4*$^{-/-}$ platelets was only slightly increased (Fig. 31 B). To test whether the thrombocytopenia was associated with altered MK numbers, H&E staining of spleen and BM sections was performed, which revealed normal MK numbers and morphology in *Tβ4*$^{-/-}$ mice compared to wild-type mice (Fig. 31 C)

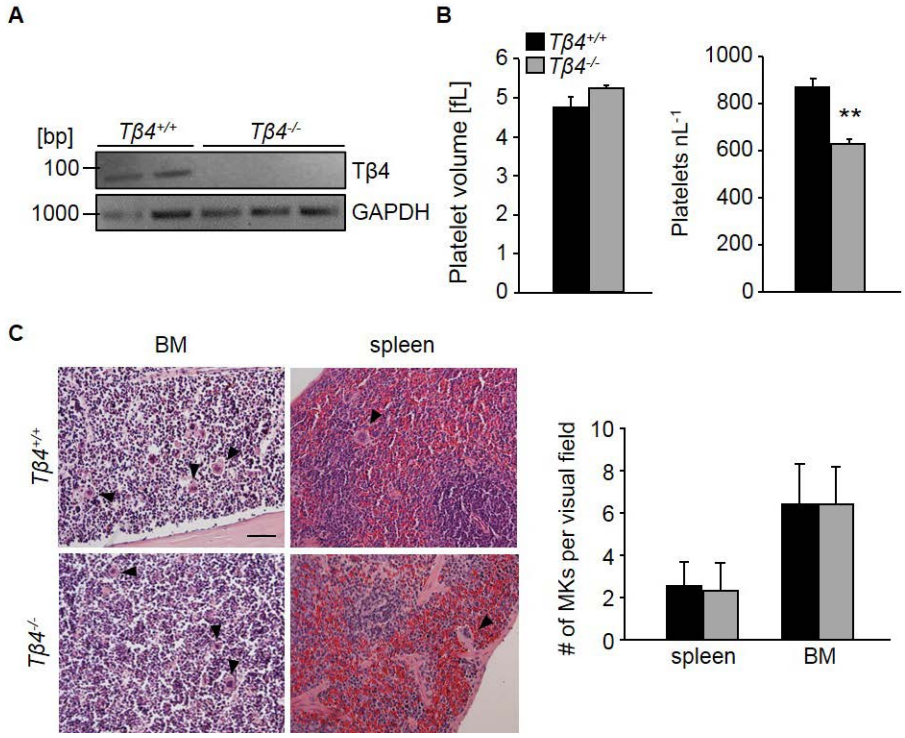

Figure 31. Tβ4-deficient platelets display a mild macrothrombocytopenia. (A) Agarose gel of RT-PCR products from wild-type and *Tβ4*$^{-/-}$ platelet lysates proved the efficient ablation of Tβ4 expression in mutant platelets. Platelet size and count (B) were assessed by flow cytometry (n= 6 per group). (C) Representative pictures and analysis of MK numbers on H&E stained BM and spleen sections from wild-type and *Tβ4*$^{-/-}$ mice. Bar, 50 µm. Unpaired Student's t-test: ***P*< 0.01.

This suggested that the thrombocytopenia was not attributed to BM failure. Reduced platelet numbers in *Tβ4*$^{-/-}$ mice could also result from accelerated platelet clearance or impaired platelet production. Hence, it will be interesting to determine *in vivo* platelet life span, platelet clearance and proplatelet-formation of *Tβ4*$^{-/-}$ mice, which have not been addressed here.

4.3.2 Altered cytoskeletal structure and function of Tβ4-deficient platelets

Tβ4 is, together with Pfn1, one of the major actin-sequestering molecules in cells. Pfn1-deficient platelets displayed severely misarranged, hyperstable microtubules and a partially disrupted actin cytoskeleton, as described by Bender, Stritt *et al.* [178]. Therefore, a detailed analysis of the actin and tubulin cytoskeleton of *Tβ4*$^{-/-}$ platelets was performed.

First, agonist-induced actin polymerization was assessed and, strikingly, *Tβ4*$^{-/-}$ platelets exhibited an increased F-actin content already in the resting state and assembled significantly

less F-actin after platelet stimulation (Fig. 32 A). Of note, pretreatment of platelets with the actin polymerization inhibitor Latrunculin A, diminished the differences between *Tβ4*$^{-/-}$ and wild-type platelets (Fig. 32 B).

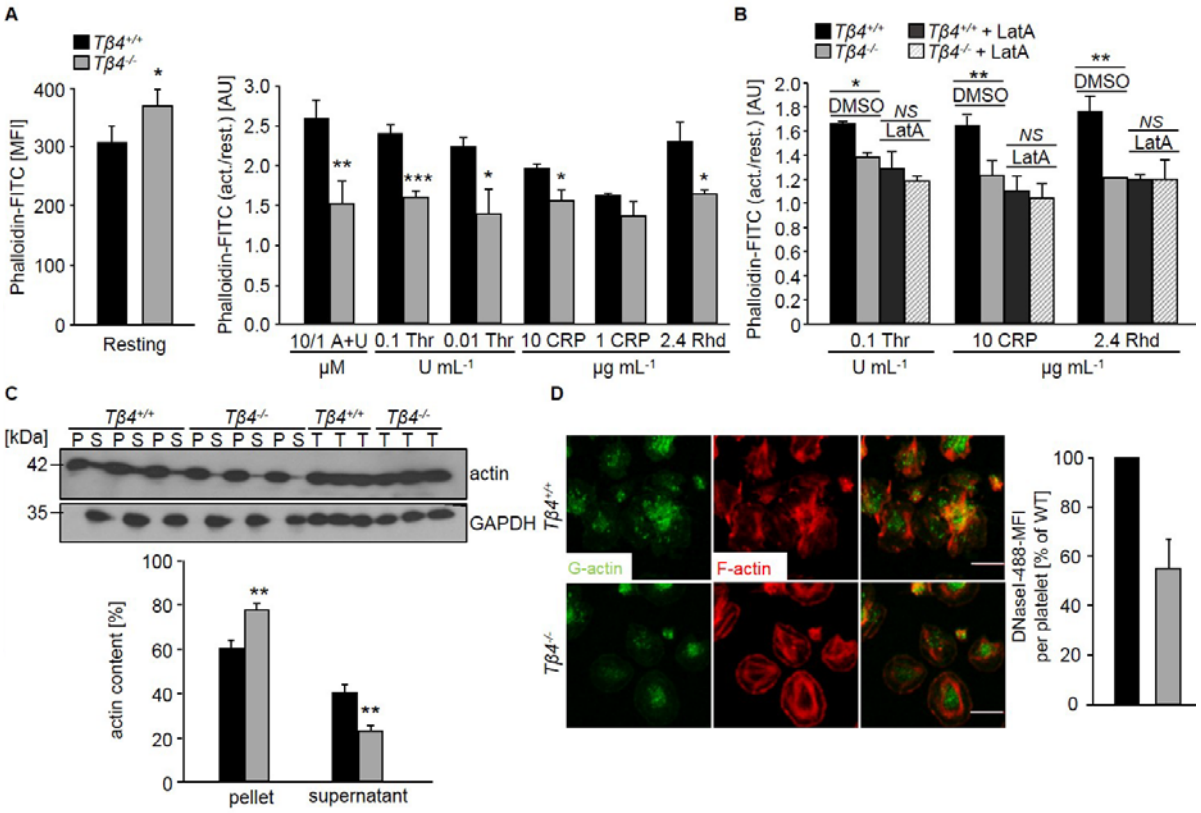

Figure 32. Increased levels and altered assembly of F-actin in *Tβ4*$^{-/-}$ platelets. (A-B) F-actin content of resting platelets and agonist-induced F-actin assembly was measured by flow cytometry after incubating the platelets with phalloidin-FITC and, where stated, with Latrunculin A (LatA) [2.5 μM] or with the same volume DMSO as control. The ratio of MFI from activated and resting platelets ± SD of 4 mice per group is shown. A: ADP; U: U46619; AU: arbitrary units. (C) The actin cytoskeleton was isolated by ultracentrifugation, immunoblotted with anti-β-actin antibody and analyzed for the content of monomeric vs. polymeric actin using densitometry. GAPDH served as loading control. Values are mean ± SD (n= 3). P: pellet, S: supernatant, T: total protein. (D) Visualization of the cytoskeleton of spread platelets (15 minutes) on fibrinogen, which were stained with DNase I-AlexaF488 (green) to label G-actin and Phalloidin-atto647N (red) for visualization of F-actin and analyzed by confocal microscopy. Bar, 2 μm. Unpaired Student's *t*-test: ***P< 0.001; **P< 0.01; *P< 0.05; *NS* = non-significant.

In a sedimentation assay, the above-mentioned results were confirmed. Resting Tβ4-deficient platelets contained 30% more F-actin compared to wild-type platelets, which was accompanied by a concomitant decrease in G-actin levels (Fig. 32 C). These observations are in line with studies suggesting that Tβ4 complexes about half of the total amount of G-actin in resting cells [184]. Moreover, specific G-actin staining of spread platelets on fibrinogen with fluorescently labelled DNase I [185], revealed a similar reduction in the content of monomeric actin (Fig. 32 D). In summary, this data shows that lack of Tβ4 impairs the equilibrium between actin monomers and polymers in platelets as Tβ4-deficient platelets displayed a decreased G-actin

pool concomitant with increased F-actin levels. Hence, due to the lack of actin monomers, less F-actin is assembled upon agonist-induced stimulation in Tβ4-deficient platelets.

Analysis of the tubulin cytoskeleton revealed a significant increase in microtubule numbers (Fig. 33 A) in *Tβ4*$^{-/-}$ platelets.

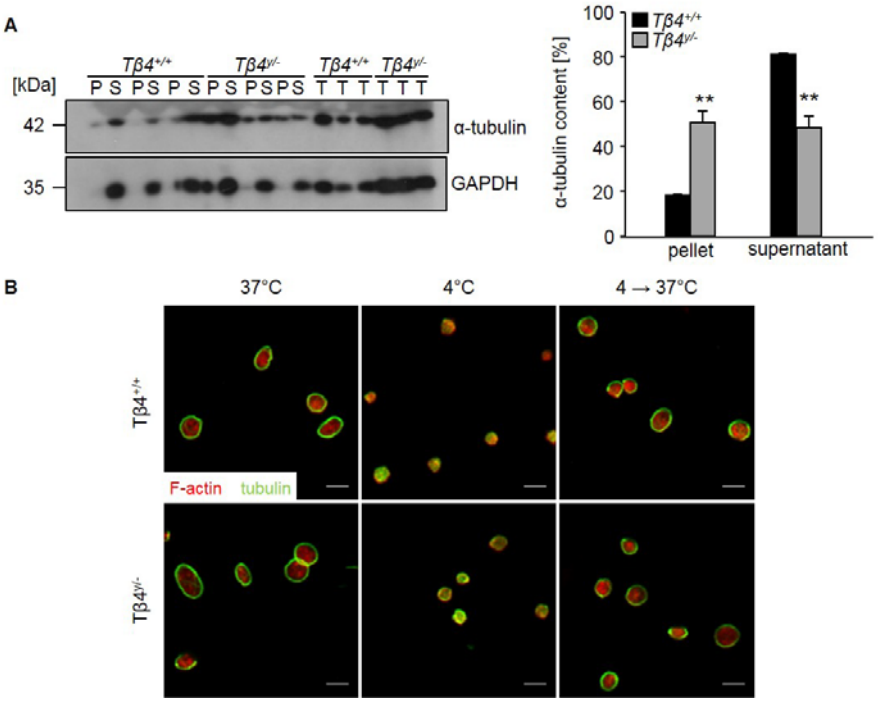

Figure 33. Increased levels of polymeric tubulin in *Tβ4*$^{-/-}$ platelets. (A) The tubulin cytoskeleton was isolated by ultracentrifugation, immunoblotted with an anti-α-tubulin antibody and analyzed for the content of monomeric vs. polymeric tubulin using densitometry. GAPDH served as loading control. Values are mean ± SD (n= 3). P: pellet, S: supernatant, T: total protein. (B) Platelets were either incubated at 37 or 4°C or were first incubated at 4°C and then allowed to reassemble their microtubules at 37°C. Platelets were subsequently fixed on a poly-L-lysine-coated surface. F-actin is shown in red and α-tubulin in green. Bars, 2 µm. Images are representative of at least 3 individuals. Unpaired Student's *t*-test: ***P*< 0.01.

Notably, this phenomenon was also described for Pfn1-deficient platelets [178], suggesting that impaired actin dynamics additionally affect the microtubule cytoskeleton. However, microtubule structure (Fig. 33 B and 36 B) as well as their cold-induced depolymerization (Fig. 33 B) was unaltered in *Tβ4*$^{-/-}$ platelets, indicating a minor role of Tβ4 for microtubule functionality. The increased number of microtubules might rather act as a compensatory mechanism to guarantee a grossly normal platelet structure and shape.

4.3.3 Unaltered expression of other actin-binding proteins in *Tβ4*$^{-/-}$ platelets

To exclude compensatory mechanisms of other actin-binding proteins in *Tβ4*$^{-/-}$ platelets, expression levels of the actin-sequestering protein Pfn1, and the ADF-H family members Twf1/2a and Cof were assessed by Western Blot analysis (Fig. 34). Interestingly, Tβ4-deficiency did not affect the expression of any of these proteins.

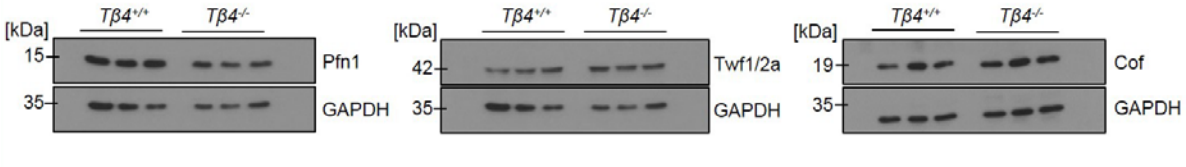

Figure 34. Unaltered expression levels of other cytoskeletal regulators in *Tβ4*$^{-/-}$ platelets. Western blots of lysates from unstimulated wild-type and *Tβ4*$^{-/-}$ platelets using antibodies against Pfn1, Twf1/2a or Cof. GAPDH served as loading control.

4.3.4 Altered integrin activation of Tβ4-deficient platelets

As altered cytoskeletal dynamics have been shown to influence platelet reactivity, e.g. for *Twf2a*$^{-/-}$ platelets [99], integrin activation was assessed next. To this end, β1- and β3-integrin activation as well as degranulation were assessed by flow cytometry (Fig. 35 A-C).

Tβ4$^{-/-}$ platelets showed impaired activation of β3-integrins (JON/A-PE) in response to all tested agonists, whereas β1-integrin activation (9EG7-FITC) was only moderately decreased after high doses of thrombin and CRP (Fig. 35 A, B). Degranulation as assessed by P-selectin exposure (Fig. 35 C) was generally slightly increased, despite a significant decrease upon high doses of CRP. In line with this, *Tβ4*$^{-/-}$ platelets showed impaired aggregation in response to thrombin and the GPVI-coupled agonists CRP and CVX, whereas aggregation in response to ADP and U46619 was unaltered (Fig. 35 D). Surprisingly, *Tβ4*$^{-/-}$ platelets showed a profound hyper-responsiveness towards collagen, which was most evident at low and intermediate concentrations. To exclude that this effect was caused by altered second wave mediator release, platelets were pre-incubated with apyrase [2 U mL^{-1}] and indomethacin [10 µM] to block these mediators and then stimulated with high concentrations of collagen [20 µg mL^{-1}]. This could, however not revert the hyperresponsiveness of *Tβ4*$^{-/-}$ platelets towards collagen. Moreover, a blockade of the collagen-binding receptor $\alpha_2\beta1$ using the antibody 23C11, did not affect the hyperreactivity either (data not shown).

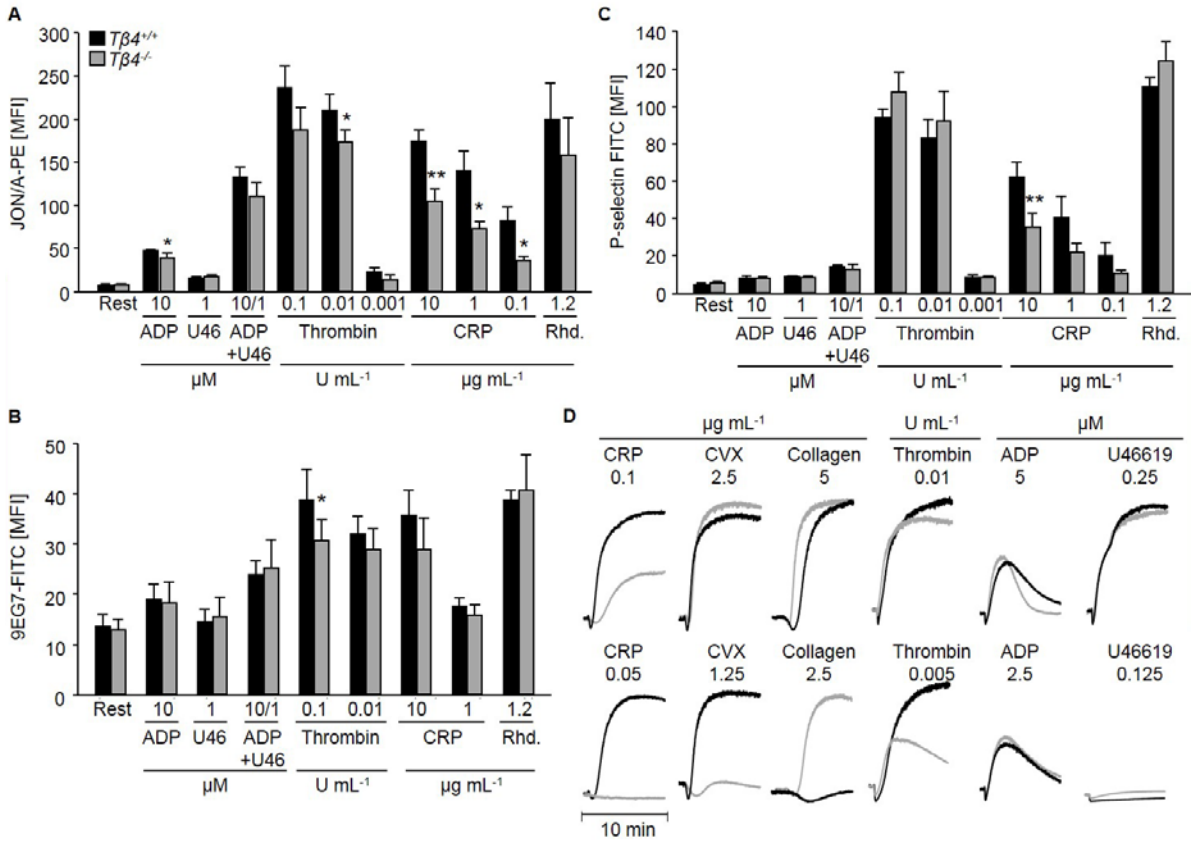

Figure 35. Altered integrin activation in *Tβ4*$^{-/-}$ platelets. Activation of platelet (A) αIIbβ3- (JON/A-PE) and (B) β1-integrins (9EG7-FITC), as well as (C) α-granule release (α-P-selectin-FITC) in response to different agonists were assessed by flow cytometry. Values are mean ± SD (n= 6 mice per group). (D) Aggregation responses of wild-type and *Tβ4*$^{-/-}$ platelets to different agonists. Values are mean ± SD of at least 4 mice per group. Unpaired Student's *t*-test: ***P*< 0.01; **P*< 0.05.

Next, the impact of Tβ4-deficiency on platelet integrin outside-in signaling was assessed in a clot retraction assay (Fig. 36 A) and spreading experiments on fibrinogen-coated surfaces (Fig. 36 B, C). *Tβ4*$^{-/-}$ platelets displayed significantly accelerated clot retraction, as well as faster lamellipodia formation already after 5 min and a higher abundance of fully spread platelets after 15 min. Pre-incubation of *Tβ4*$^{-/-}$ platelets with apyrase [2 U mL^{-1}] and indomethacin [10 μM] could not slow down the accelerated spreading back to wild-type levels (data not shown).

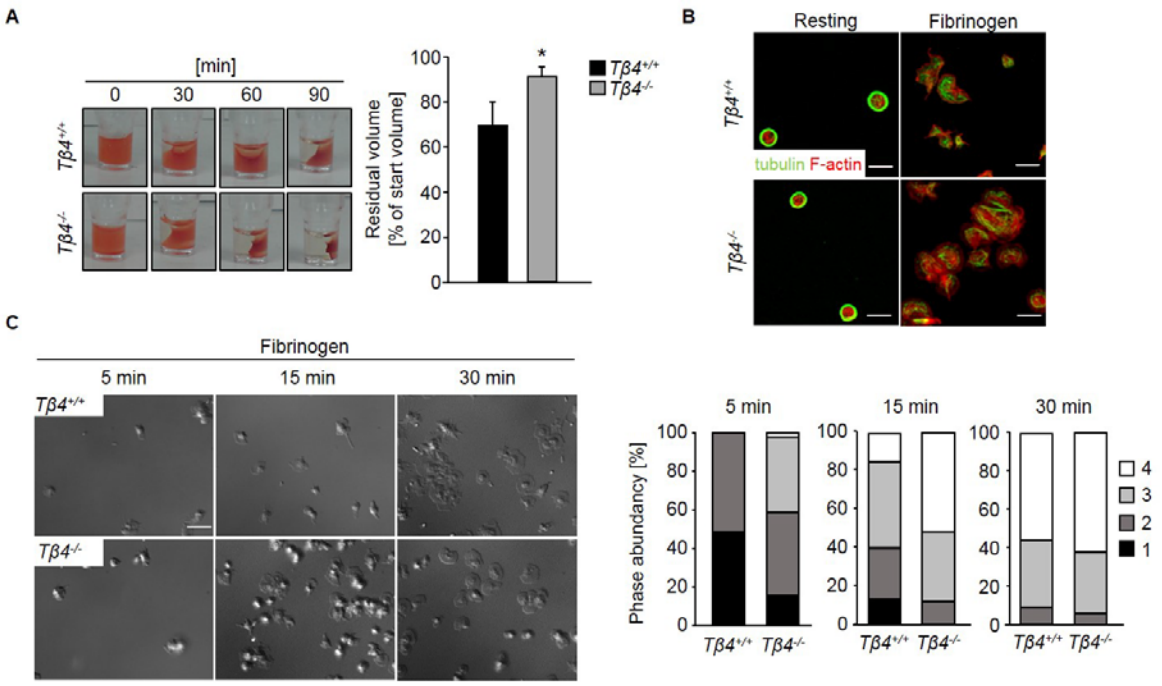

Figure 36. Altered integrin outside-in signaling in *Tβ4*$^{-/-}$ platelets. (A) Clot retraction of wild-type and Tβ4-deficient PRP was determined in response to 5 U mL^{-1} thrombin and monitored over time. Values are mean ± SD (n= 6 per group). (B) Visualization of the cytoskeleton of resting platelets on poly-L-lysine and spread platelets (t= 15 min) on fibrinogen, which were stained with Phalloidin-atto647N (red) and α-tubulin antibody-Alexa 488 (green) and analyzed by confocal microscopy microscopy (Leica TCS SP5, 100x/1.4 oil STED WHITE objective, Leica Microsystems). Bars, 2 µm. (C) Quantification of the different spreading phases at 5, 15 and 30 min after stimulation with 0.01 U mL^{-1} thrombin from DIC images. Images are representative of at least 6 animals per group. Unpaired Student's *t*-test: **P*< 0.05.

4.3.5 Defective thrombus formation of Tβ4-deficient platelets on collagen under flow

Platelet adhesion and thrombus formation of *Tβ4*$^{-/-}$ platelets on collagen using the *in vitro* flow chamber model was assessed to investigate whether the altered reactivity of *Tβ4*$^{-/-}$ platelets *in vitro* under static conditions would affect thrombus formation under flow. Indeed, Tβ4-deficiency resulted in a markedly reduced (up to 50%) adhesion and thrombus formation compared to wild-type levels at both low and high shear rates (Fig. 37 A, B).

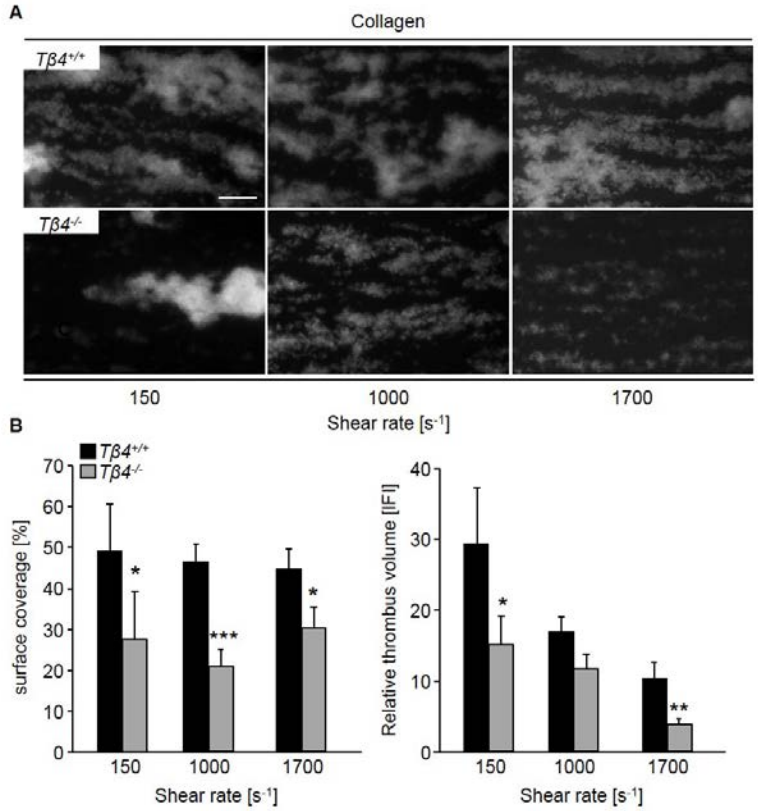

Figure 37. Impaired adhesion and defective thrombus formation of *Tβ4*$^{-/-}$ platelets on collagen under flow. (A) Representative phase contrast images taken at the end of the perfusion time after heparinized whole blood of *Tβ4*$^{-/-}$ and wild-type mice was perfused over a collagen-coated surface for 10 min at shear rates of low (150 s^{-1}) and for 4 min at shear rates of intermediate shear forces (1000, 1,700 s^{-1}). (B) Analysis of the surface area covered by platelets (%) and the relative thrombus volume ± SD of at least 6 animals per group. Unpaired Student's *t*-test: ***P< 0.001; **P< 0.01; *P< 0.05. Bar, 50 µm.

4.3.6 Tβ4-deficient mice are protected from arterial thrombus formation *in vivo*

To test whether the observed thrombus formation defect translates into an *in vivo* phenotype, *Tβ4*$^{-/-}$ and wild-type mice were subjected to two well-established *in vivo* thrombosis models. In the first model, mesenteric arterioles were injured by topical application of $FeCl_3$. The time to appearance of first thrombi, as well as the time to stable vessel occlusion was slightly prolonged in *Tβ4*$^{-/-}$ mice compared to wild-type animals (Fig. 38 A).

In the second model, injury is mechanically induced in the aorta. Notably, it is well established that thrombus formation occurs mainly through collagen-dependent mechanisms under these experimental conditions [171]. After a transient increase directly after injury, blood flow progressively decreased for several minutes in all animals. In all wild-type mice, this decrease resulted in complete and irreversible occlusion of the vessel within 7 min after injury (Fig. 38 B). Out of the 14 tested *Tβ4*$^{-/-}$ mice, 7 displayed a transient decrease in blood flow, which increased again to normal and led to essentially normal flow rates through the injured

vessel at the end of the observation period. The other group of *Tβ4*$^{-/-}$ mice showed a progressive decrease in blood flow, which resulted in full occlusion of the vessel transient within 8 minutes after injury, almost comparable to wild-type mice. Consistent with the *in vitro* data under flow, the protection of *Tβ4*$^{-/-}$ mice was more pronounced when using the collagen-dependent *in vivo* model.

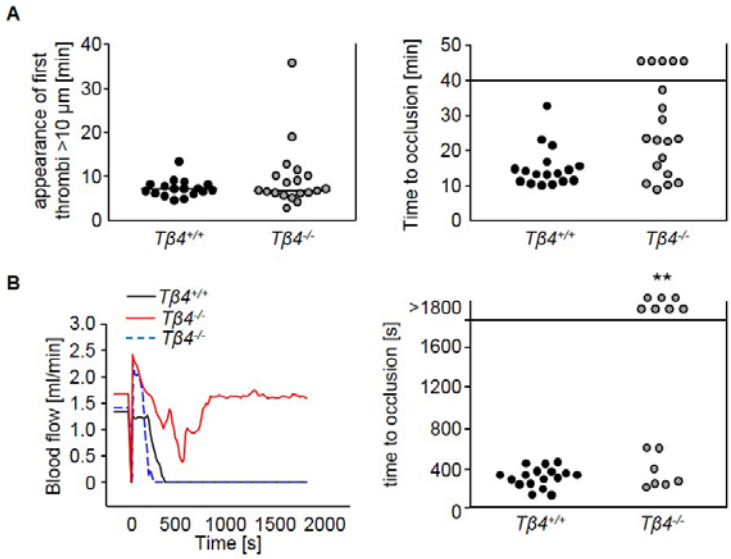

Figure 38. *Tβ4*$^{-/-}$ mice are protected from arterial thrombus formation *in vivo*. (A) $FeCl_3$-induced arterial thrombus formation of the mesenteric arterioles. Adhesion and thrombus formation of fluorescently-labeled platelets was monitored *in vivo* by fluorescence microscopy and time to appearance of first thrombus as well as time to occlusion was assessed. Each symbol represents one individual. (B) Aorta occlusion model. Representative graph of blood flow of a wild-type and two *Tβ4*$^{-/-}$ mice after mechanical injury of the aorta at t= 0 and occlusion time after injury of the aorta. Fisher´s exact test: ***P*< 0.01. Experiments were performed in collaboration with Sarah Beck in our laboratory.

4.3.7 Altered secretion of Tβ4-deficient platelets

At sites of vessel wall injury, release of secondary mediators from activated platelets at the exposed subendothelial matrix plays a crucial role for the recruitment and activation of further platelets to promote thrombus formation. To test whether the impaired thrombus formation *in vitro* and *in vivo* was caused by altered second wave mediator release, agonist-induced granule secretion of Tβ4-deficient platelets was assessed. Strikingly, a profound increase in ATP secretion upon stimulation with U46619 and thrombin, as well as the GPVI agonist collagen could be detected in Tβ4-deficient platelets (Fig. 39). In contrast, as seen in other assays (Fig. 35 A, D), Tβ4-deficient platelets were hyporesponsive towards CRP-stimulation, which resulted in a significant decrease in dense granule ATP release (Fig. 39). Notably, in line with this, α-granule release was generally slightly increased in Tβ4-deficient platelets, despite a significant decrease after CRP stimulation (Fig. 35 C). Hence, it will be interesting to

determine ATP and P-selectin content in Tβ4-deficient platelets to exclude that the effects observed here are caused by increased storage of these mediators.

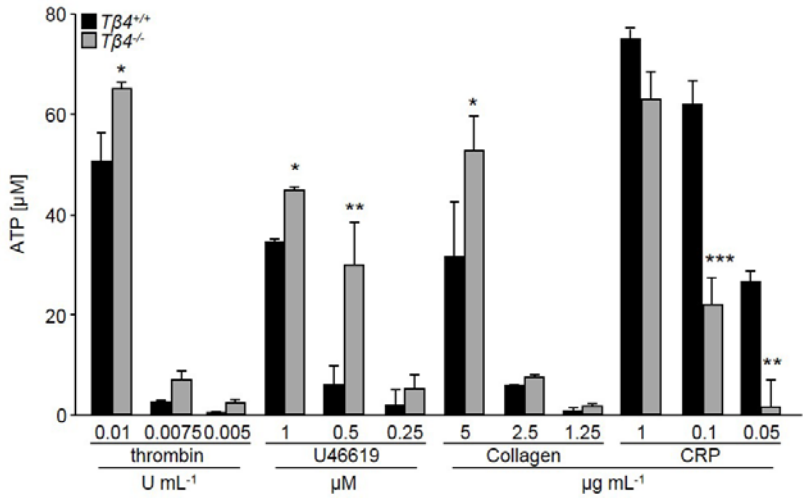

Figure 39. Altered dense granule secretion of *Tβ4*$^{-/-}$ platelets. Luminometric measurement of released ATP of activated wild-type and *Tβ4*$^{-/-}$ platelets. Results are given as mean ATP concentration [µM] ± SD (n = 12 per group). Unpaired Student's *t*-test: ****P*< 0.001; ***P*< 0.01; **P*< 0.05.

4.3.8 Increased procoagulant activity in Tβ4-deficient platelets

Sustained platelet activation leads to a marked increase in cytosolic Ca^{2+} concentrations, subsequent surface exposure of procoagulant PS and resultant thrombin generation [176] [186]. To assess whether the hyperresponsiveness towards collagen or the hypo-responsiveness towards CRP would predominate the procoagulant potential of *Tβ4*$^{-/-}$ platelets, binding of fluorescently-labeled Annexin A5 to PS exposed on the platelet surface upon stimulation was analyzed by flow cytometry [177]. Notably, no differences in procoagulant activity between wild-type and *Tβ4*$^{-/-}$ platelets could be observed (Fig. 40 A).

Next, whole blood from wild-type and *Tβ4*$^{-/-}$ mice was perfused over immobilized collagen at a shear rate of 1700 s^{-1} and PS exposure was determined by Annexin A5-staining. Although the surface covered by collagen-adherent platelets was strongly reduced in *Tβ4*$^{-/-}$ samples, PS exposure was markedly increased (Fig. 40 B), indicating that Tβ4 regulates procoagulant activity of platelets.

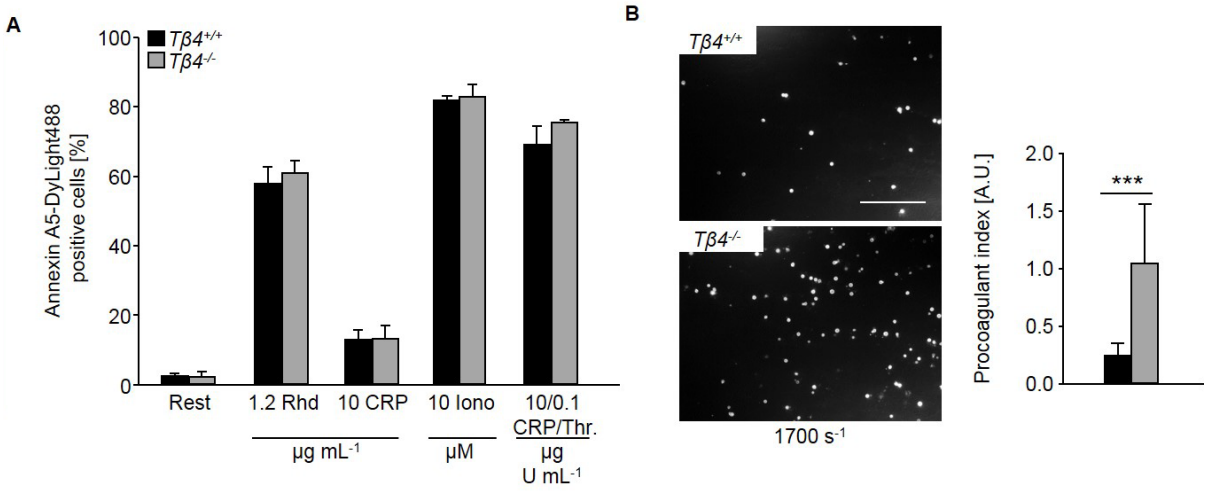

Figure 40. Increased procoagulant activity of *Tβ4*$^{-/-}$ platelets on collagen under shear flow. (A) Washed platelets were stimulated with the indicated agonists and stained with saturating amounts of Annexin A5-DyLight488 and directly analyzed by flow cytometry. Results are expressed as MFI ± SD (n= 4 mice per group). (B) Whole blood was perfused over a collagen-coated [0.2 mg mL^{-1}] surface at a shear rate of 1,700 s^{-1} for 4 min. Adherent platelets were stained with Annexin A5-AlexaF488 [0.25 mg mL^{-1}]. Representative phase contrast, fluorescence images and mean relative amount of Annexin A5 positive platelets ± SD of at least 6 mice per group is shown. Unpaired Student's *t*-test: ****P*< 0.001.

Surface-exposed PS triggers procoagulant activity of platelets and propagates coagulation by facilitating assembly and activation of the tenase and prothrombinase complexes [186] and leads to rapid thrombin generation [187]. In agreement with the enhanced PS exposure, lack of Tβ4 resulted in an altered maximal amount of generated thrombin (Fig. 41 B), which was signify-cantly accelerated upon stimulation with (hem)ITAM-specific agonists. The overall amount of produced thrombin (ETP), however, was comparable to wild-type samples (Fig. 41 A). In line with this, Tβ4-deficient mice showed a shortened *activated plasma thromboplastin time* (aPTT), a global test for the intrinsic coagulation pathway. When single factors were assessed, levels of FXII as initiator of the intrinsic cascade were unaltered. Strikingly, however, levels of FXI, the second factor of the intrinsic coagulation pathway, and the subsequent factor IX together with its cofactor VIII were significantly increased in Tβ4-deficient mice (Fig. 41 D, F-H). The extrinsic coagulation pathway as assessed by Quick was, however, unaltered in Tβ4-deficient mice. Taken together, the results establish Tβ4 as an important regulator of thrombin generation and coagulation.

In summary, the results of this thesis highlight Tβ4 as an important regulator of cytoskeletal dynamics on the one hand and of platelet reactivity, *in vivo* thrombus formation, granule release and procoagulant activity on the other hand. However, differences between endo- and exogenous protein function have not been addressed and therefore require further investigation.

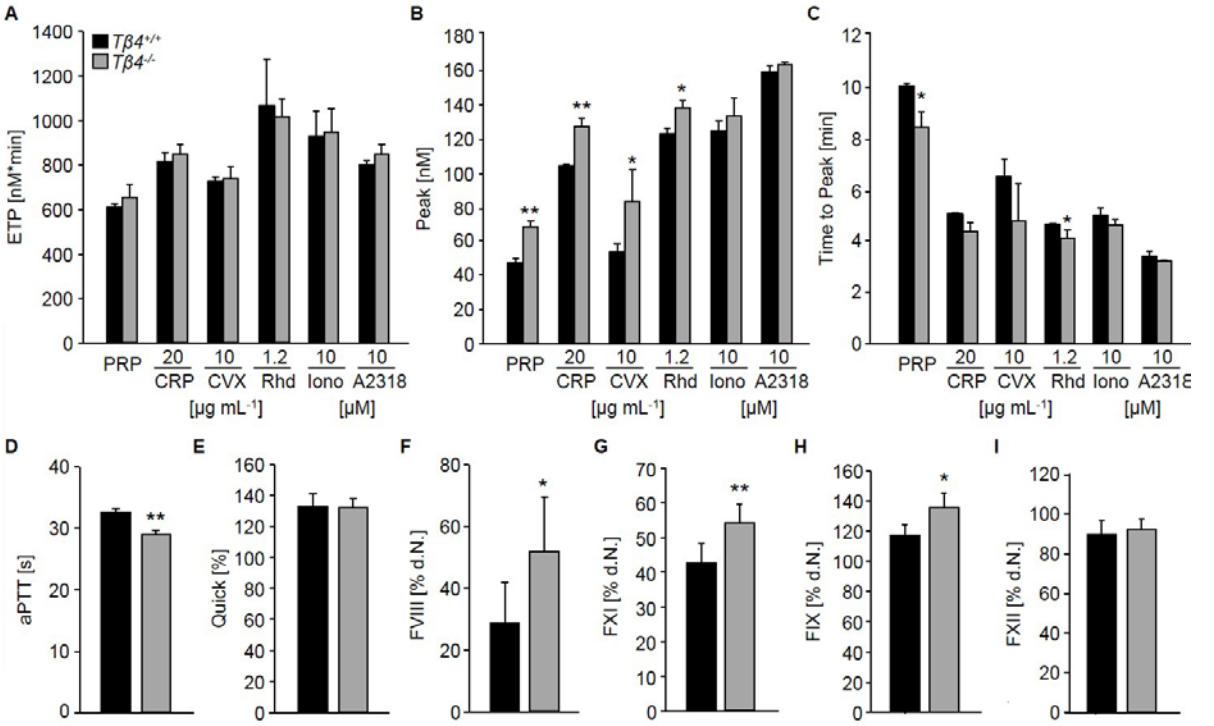

Figure 41. Tβ4-deficiency resulted in accelerated thrombin formation and enhanced intrinsic coagulation. (A-C) Citrate-anticoagulated PRP was left unstimulated (PRP), or platelets were activated by incubation with CRP [20 µg mL^{-1}], CVX [10 µg mL^{-1}], Rhd [1 µg mL^{-1}] or the Ca^{2+} ionophores A23187 and *ionomycin* (Iono) [10 µM] for 10 min at 37°C. Thrombin generation was triggered with tissue factor. (A) *Endogenous thrombin potential* (ETP). (B) Quantification of thrombin peak height. (C) Quantification of time to peak. Results are mean ± SD of at least 4 animals per group. Experiments were performed in collaboration with Sarah Beck in our laboratory. (D-I) Coagulation was assessed using the two global tests aPTT (D) and Quick (E). Measurement of single factors FVIII (F), XI (G), IX (H), XII (I). Results are mean of two independent experiments with 5 vs. 5 animals. Experiments were performed in collaboration with Dr. Sabine Herterich from the Central Laboratory, University Clinics Würzburg. Unpaired Student's *t*-test: $^{**}P < 0.01$; $^{*}P < 0.05$.

4.3.9 Assessment of the function of recombinant Tβ4

4.3.9.1 Recombinant Tβ4 rescues the thrombus formation defect of Tβ4-deficient platelets

Several studies investigated the anti-inflammatory, angiogenic and cardioprotective function of recombinant Tβ4 in a variety of disease models. Administration of Tβ4 following myocardial infarction in mice protected heart tissue from cell death and enabled heart myocytes to survive after hypoxia by upregulating PINCH-ILK-Akt survival pathways [144]. However, a distinction between endo- and exogenous protein function and especially its release and uptake mechanisms have remained elusive. Therefore, the aim was to investigate whether exogenously added recombinant Tβ4 would revert (at least in part) some of the observed effects of Tβ4-deficiency. To this end, several of the previously described assays were

repeated after pre-incubation of wild-type and *Tβ4*$^{-/-}$ platelets with commercial recombinant Tβ4 (Peprotech; Rocky Hill, USA) *in vitro*.

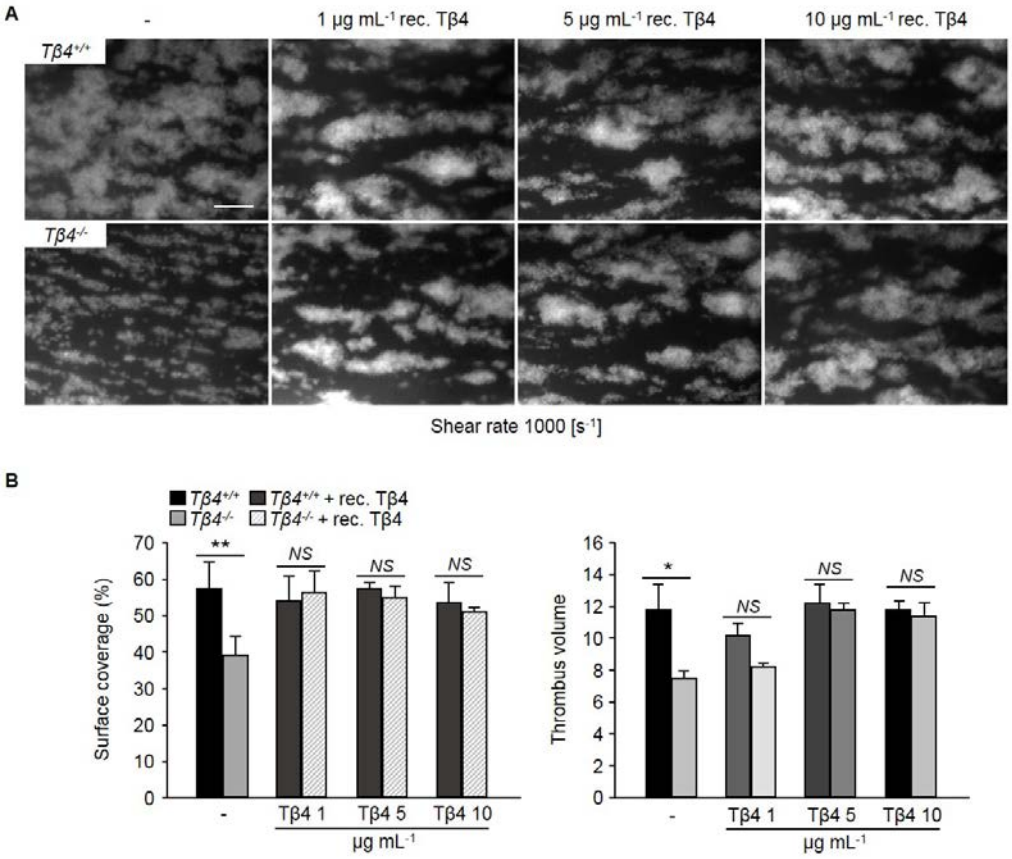

Figure 42. Recombinant Tβ4 rescued the thrombus formation defect of Tβ4-deficient platelets on collagen under flow. Heparinized whole blood of *Tβ4*$^{-/-}$ and wild-type mice was either pre-incubated with recombinant Tβ4 [1, 5, 10 µg mL^{-1}] for 5 min at 37°C or left untreated and afterwards perfused over a collagen-coated surface [0.2 mg mL^{-1}] for 4 min at an intermediate shear rate of 1000 s^{-1}. (A) Fluorescent images taken at the end of the perfusion period. Images are representative of at least 6 animals per group. (B) Analysis of the surface area covered by platelets (%) and the relative thrombus volume ± SD. Unpaired Student's *t*-test: ***P*< 0.01; **P*< 0.05; *NS* = non-significant. Bar, 50 µm.

As the described Tβ4 concentration in human plasma was estimated to 0.03-0.4 µg mL^{-1} [139], a concentration range of 0.1 to 10 µg mL^{-1} was chosen for the *in vitro* pre-incubation of platelets and the working concentration was titrated for each experiment. Similarly, different incubation times (5-30 min) were tested and showed an effect of the protein as early as after 5 minutes. Since the effect of Tβ4-deficiency was most pronounced under flow, activity of the recombinant protein was first tested using the *in vitro* flow chamber system. At concentrations of 0.1, 0.5 and 1 µg mL^{-1} recombinant Tβ4 showed no effect on thrombus formation under flow, strikingly, however, it could fully revert the thrombus formation defect of Tβ4-deficient blood to wild-type levels at a concentration of 5 and 10 µg mL^{-1} (Fig. 42 A, B and data not shown). Of note, although a concentration of 1 µg mL^{-1} was insufficient to fully restore thrombus volume, it could

rescue platelet adhesion to collagen in *Tβ4*$^{-/-}$ mice. In wild-type samples pre-incubation with recombinant Tβ4 had no obvious effect on surface coverage or thrombus formation (Fig. 42 A, B and data not shown). The results suggest a direct interaction between Tβ4 and collagen, which might be facilitated by its highly adoptive structure as an *intrinsically unstructured protein* IUP [132]. In line with this hypothesis, Tβ4 is released from activated platelets and partially crosslinked to fibrin by FXIIIa, a transglutaminase [133]. A possible interaction between collagen and Tβ4 will be addressed in further experiments.

4.3.9.2 Recombinant Tβ4 has differential influence on αIIbβ3 integrin activation

Besides the reduced thrombus formation *in vitro* under flow, *Tβ4*$^{-/-}$ platelets exhibited defective αIIbβ3 integrin activation. Therefore, it was investigated whether pre-incubation of *Tβ4*$^{-/-}$ platelets with recombinant Tβ4 (5 min at 37°C with 0.05, 0.1, 0.5, 1 and 5 µg mL^{-1}) could revert the impaired integrin activation as assessed by flow cytometry and aggregometry.

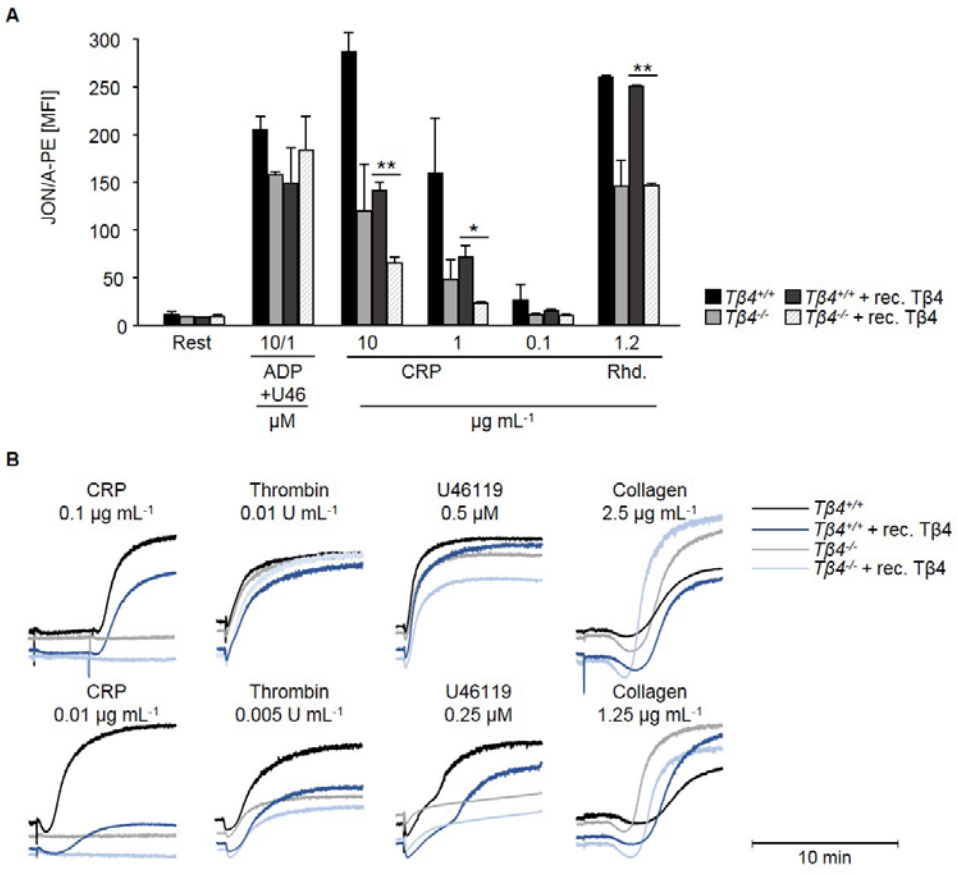

Figure 43. Recombinant Tβ4 cannot rescue the altered integrin activation of *Tβ4*$^{-/-}$ platelets. Washed platelets were pre-incubated with 5 µg mL^{-1} recombinant Tβ4 for 5 min or left untreated prior to stimulation. (A) Activation of platelet αIIbβ3-integrins (JON/A-PE) in response to different agonists was assessed by flow cytometry. Values are mean ± SD of 4 mice per group. (B) Aggregation responses to different agonists. Values are mean ± SD of at least 4 animals per group. Unpaired Student's *t*-test: ***P*< 0.01; **P*< 0.05.

At concentrations less than 0.1 µg mL^{-1} recombinant Tβ4 had no effect on wild-type or *Tβ4*$^{-/-}$ platelets (data not shown). However, at concentrations of 0.1 µg mL^{-1} or higher, αIIbβ3 integrin inside-out activation was decreased in comparison to untreated controls of both wild-type and *Tβ4*$^{-/-}$ platelets (Fig. 43 A and data not shown). Strikingly, the integrin activation defect of *Tβ4*$^{-/-}$ platelets pre-incubated with recombinant Tβ4 was even more pronounced. Similarly, pre-incubation with 1 and 5 µg mL^{-1} recombinant Tβ4 could neither enhanced aggregation of *Tβ4*$^{-/-}$ platelets upon stimulation with CRP and thrombin nor revert the hyperresponsiveness of *Tβ4*$^{-/-}$ platelets towards collagen stimulation (Fig. 43 B). Interestingly, recombinant protein further enhanced aggregation of both wild-type and *Tβ4*$^{-/-}$ platelets in comparison to the untreated controls upon collagen stimulation. Next, the effect of recombinant Tβ4 on integrin outside-in signaling was assessed by performing spreading assays on fibrinogen. Recombinant Tβ4 could not slow down the enhanced spreading of *Tβ4*$^{-/-}$ platelets to levels of wild-type platelets.

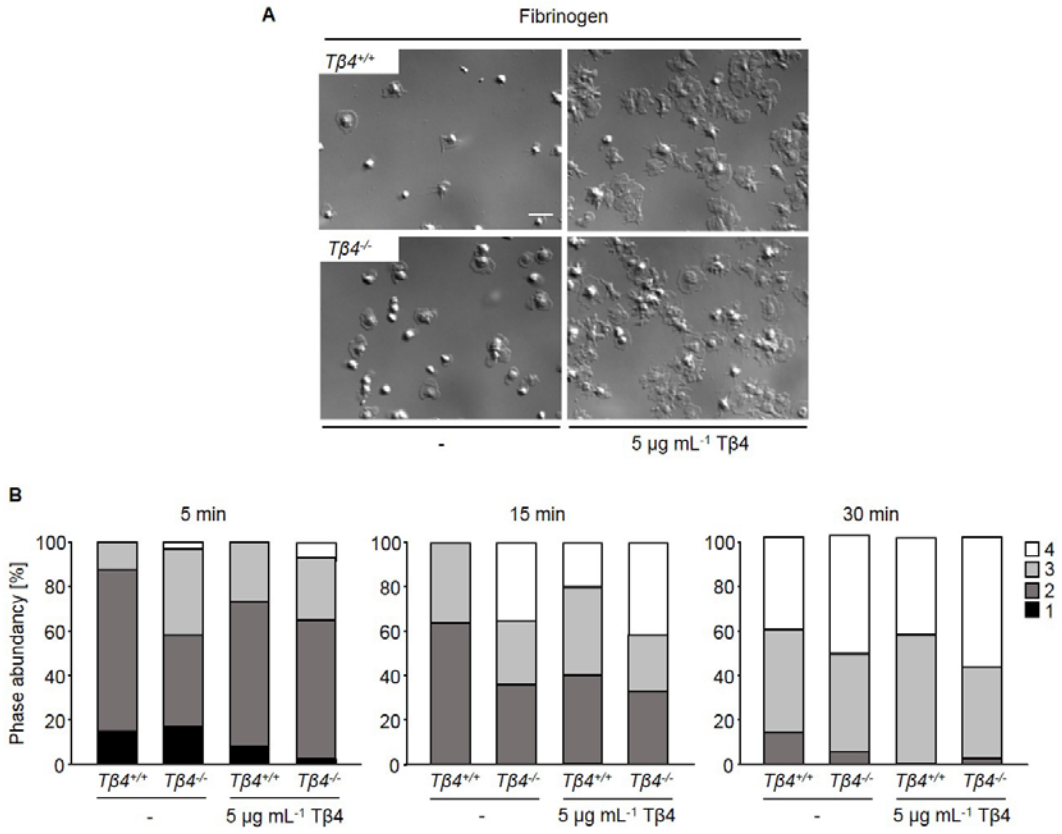

Figure 44. Recombinant Tβ4 accelerates spreading of wild-type and Tβ4-deficient platelets. Washed platelets were pre-incubated with 5 µg mL^{-1} recombinant Tβ4 or left untreated prior to stimulation with 0.01 U mL^{-1} thrombin. Platelets were allowed to spread on fibrinogen [100 µg mL^{-1}]. (A) Representative DIC images of 2 individual experiments at t= 15 min and (B) statistical evaluation of the percentage of spread platelets at different spreading stages. Bar, 3 µm.

Pre-treatment of both wild-type and Tβ4-deficient platelets with recombinant Tβ4 at a concentration of 1 µg mL^{-1} and higher rather resulted in faster spreading, which was most striking at 15 minutes after thrombin stimulation, were significantly more wild-type and Tβ4-deficient platelets already reached phase 4 (fully spread platelets) compared to untreated controls (Fig. 44 A, right part and B).

In summary, on the one hand, recombinant Tβ4 does not rescue the impaired integrin inside-out signaling of *Tβ4*$^{-/-}$ platelets to wild-type levels, but further decreases integrin activation. On the other hand, integrin outside-in signaling is enhanced by recombinant Tβ4, which resulted in a significant increase of fully spread platelets already after 15 minutes in both wild-type and *Tβ4*$^{-/-}$ platelets.

4.3.9.3 Enhanced secretion of platelets treated with recombinant Tβ4

Tβ4$^{-/-}$ platelets displayed enhanced granule secretion (Fig. 39). Therefore, it was tested whether pre-incubation with recombinant Tβ4 would normalize granule secretion back to wild-type levels, which was assessed by measurement of agonist-induced ATP release (Fig. 45). In line with its effect on platelet aggregation, recombinant Tβ4 further enhanced the elevated ATP secretion in *Tβ4*$^{-/-}$ platelets, except after stimulation with CRP, where it even further decreased granule release. Tyrosine phosphorylation assays of known hem(ITAM) downstream signaling molecules, such as Syk, LAT and PLC will address the differential effects of CRP vs. collagen stimulation on GPVI signaling in *Tβ4*$^{-/-}$ platelets.

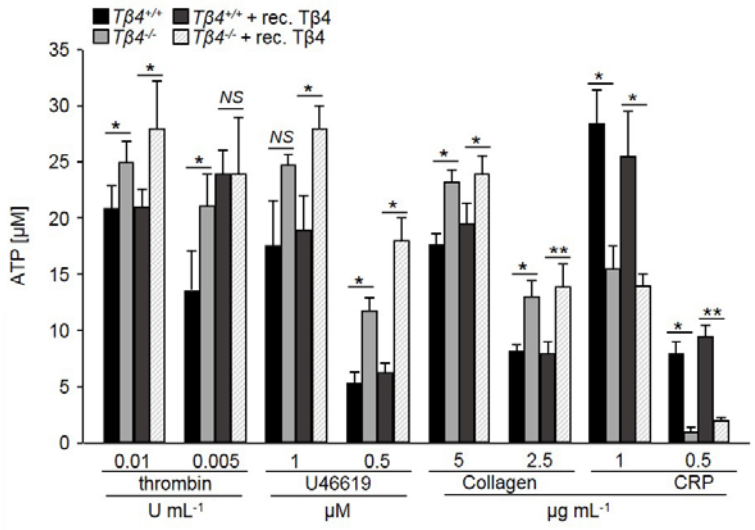

Figure 45. Recombinant Tβ4 enhances ATP release of wild-type and *Tβ4*$^{-/-}$ platelets. Washed platelets were pre-incubated with 5 µg mL^{-1} recombinant Tβ4 or left untreated prior to the stimulation. Luminometric measurement of released ATP of activated wild-type and *Tβ4*$^{-/-}$ platelets. Results are given as mean ATP concentration [µM] ± SD (n= 6 mice per group). Unpaired Student's *t*-test: ***P*< 0.01; **P*< 0.05.

4.3.10 Construct design, expression and purification of recombinant Tβ4

To further elucidate the effects of recombinant Tβ4 and the underlying signaling pathways, large amounts of recombinant protein will be needed, especially for *in vivo* experiments, which would not be feasible with commercial Tβ4. Therefore, the aim was to establish an expression and purification protocol for recombinant Tβ4 from *E. coli*. Successful overexpression of full-length Tβ4 in *E. coli* had previously been described [188]. The herein described strategy was used as starting point and was partially adopted and optimized in the course of this thesis. Li *et al.* showed that expression of recombinant Tβ4 benefited from a DsbA-solubility tag, which is a feature of the pETM-52 vector [149] (see sections 3.1.4 and 8.2). Therefore, full-length Tβ4 was cloned into this vector using restriction endonucleases (described in the methods part in section 3.2.3). Restriction sites were introduced into the insert by PCR (Fig. 46 B), digested vector and insert were ligated and transformed into competent *E. coli* TOP10 cells and successful cloning was verified by Colony-PCR (Fig. 46 C) and sequencing approaches (data not shown).

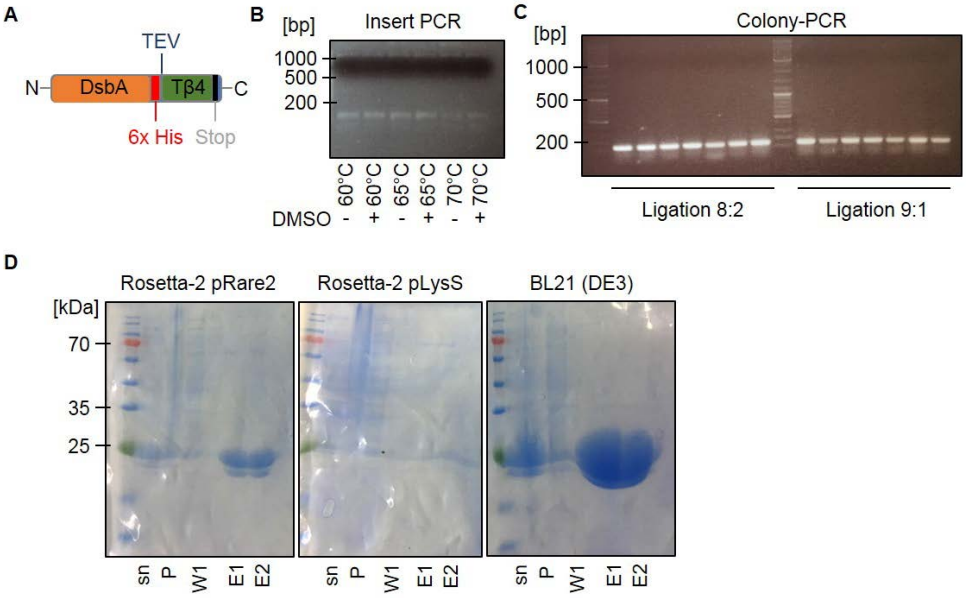

Figure 46. Cloning and expression tests of recombinant Tβ4. (A) Cartoon of the designed construct comprising the N-terminal DsbA-tag, followed by a 6x His-Tag, full-length Tβ4 and a stop codon. N-terminal Tag can be cleaved off by TEV protease. (B) Success of the Insert-PCR adding sites for restriction endonucleases was analyzed by agarose gel electrophoresis. The expected band size of the insert was 180 bp. (C) Successful ligation of the pETM-52 vector with the Tβ4 insert was verified by Colony-PCR of 7 clones per ligation approach (8:2 or 9:1, insert:vector). The expected band size was 180 bp. (D) Expression test of a positive clone using different *E. coli* expression strains (Rosetta-2 pRARE2 and pLysS, BL21 (DE3)). Expression was performed o/N at 20°C, cells were harvested and soluble expression was analyzed by a small-scale expression test where harvested cells were resuspended in lysis buffer, lysed by sonification and centrifuged to separate soluble from insoluble protein. Subsequently, soluble protein was incubated with Ni-NTA and eluted using lysis buffer supplemented with 250 mM imidazole. Sn: supernatant; P: pellet; W1: wash 1; E1, 2: eluate 1, 2.

Expression of the construct was tested by expression tests using different *E. coli* expression strains and two different temperatures (16°C (data not shown), 20°C (Fig. 46 D)). The DsbA-tagged full-length Tβ4 was solubly expressed, with the highest protein yields from *E. coli* BL21 (DE3) expression (Fig. 46 D). The tested temperatures during cultivation did not have a significant effect on protein yield. Therefore, further optimization was not necessary and expression in *E. coli* BL21 (DE3) at 20°C o/N under constant shaking at 200 rpm was applied for all following expressions.

Initial purifications of small-scale expression tests succeeded with a simple Tris buffer at pH 8 supplemented with 150 mM NaCl (Fig. 46 D). Harvested cells were resuspended in this buffer, lysed by sonification and centrifuged to separate soluble from insoluble protein. Subsequently, soluble protein was incubated with Ni-NTA Agarose and eluted using lysis buffer supplemented with 250 mM imidazole. Subsequent analysis of samples taken at every step of the small-scale purification revealed successful purification. Therefore, this protocol was used for upscaling.

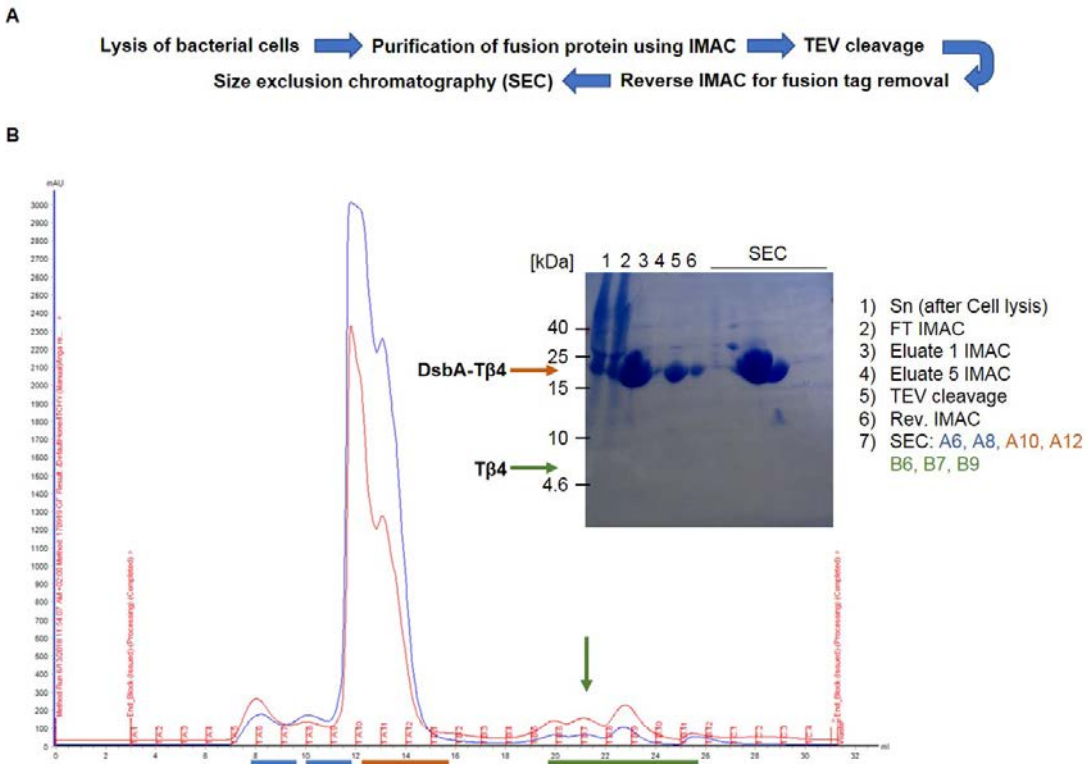

Figure 47. Purification of recombinant Tβ4. (A) Purification protocol including lysis of the cells by sonification, separation of soluble (Sn) and insoluble protein fraction by centrifugation, incubation of the soluble fraction with Ni-NTA Agarose followed by *Immobilized Metal Affinity Chromatography* (IMAC) (fractions FT, E1, E5), a subsequent cleavage of the DsbA-tag using TEV protease (TEV cleavage), a reverse IMAC (rev. IMAC) to separate the cleaved tag from the untagged protein and a final *size exclusion chromatography* (SEC) for improved purity. The arrow indicates the expected elution of untagged Tβ4. (B) Representative size exclusion chromatogram and Coomassie-stained tricine PAGE of a Tβ4 purification. Sn: supernatant; FT: flow-through; E1, 5: eluate 1, 5.

Large-scale purifications were performed in same buffer and comprised the following purification protocol: lysis of the cells by sonification, separation of soluble and insoluble protein fraction by centrifugation, incubation of the soluble fraction with Ni-NTA Agarose followed by a starting *Immobilized Metal Affinity Chromatography* (IMAC), subsequent cleavage of the DsbA-tag using TEV protease, reverse IMAC to separate the cleaved tag from the untagged protein and a final size exclusion chromatography for improved purity. As the size of untagged Tβ4 (5 kDa) was too small to detect it with the usual 15% SDS-PAGE, different gel systems were tested, among these were native PAGE or tricine PAGE. However, it was not possible to detect the untagged recombinant Tβ4. Further optimization is necessary to solve this problem and to successfully purify untagged recombinant Tβ4.

Functionality of the purified protein will be tested using the *in vitro* flow chamber model with a shear flow of 1000 s^{-1}. When an increase of the surface coverage of Tβ4-deficient blood to wild-type levels is detected, the protein will be considered as functional.

5. DISCUSSION

Platelet activation and aggregation at sites of vascular injury is essential to limit blood loss, but under pathological conditions it may lead to complete vessel occlusion resulting in myocardial infarction or stroke. Therefore, platelet signaling has become an important field in clinical research over the last decades and many therapeutical drugs for prevention of cerebro- and cardiovascular diseases, such as aspirin and clopidogrel, act by inhibiting platelet function. However, application of those currently available antithrombotic agents is often associated with an increased bleeding risk; hence, new safe therapeutic options are urgently needed.

Massive reorganization of the actin cytoskeleton is induced upon platelet activation. This enables adhesion and spreading of platelets on ligands immobilized at the injured vessel wall. Likewise, the actin and microtubule cytoskeleton plays a central role in megakaryo- and thrombopoiesis. Thus, cytoskeletal protein aberrations may cause many pathological phenotypes. Although intensive research is carried out to identify the key players, the signaling cascades orchestrating the complex process of cytoskeletal remodeling are still poorly understood. Among the vast number of actin-binding proteins, the ADF-H family members Cof and Twf2a, have been described as critical regulators of cytoskeletal rearrangements required for proper platelet formation and reactivity. However, another protein family member, Cotl1, has not been investigated. Deficiency of the actin-sequestering protein Pfn1 has been described to evoke cytoskeletal instability, which resulted in a partially disrupted cortical actin cytoskeleton. Its impact on platelet reactivity has, however, not been addressed so far. Finally, Tβ4 is a moonlighting protein and its cardioprotective, angiogenic and immunomodulatory effects are intensively studied. However, its function for cytoskeletal dynamics is still poorly understood.

In the current thesis, the actin-binding proteins Cotl1, Pfn1 and Tβ4 have been investigated concerning platelet production and function using transgenic mice. Although effects of a deficiency in one of these proteins are diverse, a common feature is their influence on platelet reactivity. This further emphasizes the importance of a functional actin cytoskeleton for intact platelet function *in vitro* and *in vivo* and shows that actin-binding proteins may serve as new potential targets to treat cerebro- and cardiovascular diseases.

5.1 A complex phenotype dominated by protection from arterial thrombus formation in mice lacking Cotl1

Rearrangements of the actin cytoskeleton play a crucial role for platelet formation and reactivity, which has been demonstrated in several studies on actin-binding proteins, e.g. the ADF-H family members Cof and Twf2a [82, 99]. Therefore, we were interested to investigate

Cotl1, another member of this protein family and its implication in thrombopoiesis and platelet reactivity *in vitro* and *in vivo* using a knock-out approach (PF4-Cre/loxP). A common feature of ADF-H containing proteins is (1) their ability to bind actin and (2) their influence on cytoskeletal dynamics. However, each group of ADF-H family members shows unique actin-binding properties and biological activities, which can be attributed to their differential domain structure. Thus, ADF/cofilins contain one ADF-H domain and can bind both G- and F-actin [69], whereas Twfs consist of two ADF-H domains separated by a short linker region and are only able to bind monomeric actin [38, 66]. Hence, Cof-deficiency decreased stimulus-dependent F-actin assembly, whereas on the contrary, Twf2a-deficient mice displayed enhanced actin dynamics [82, 99]. A study from Kim *et al.* demonstrated that Cotl1 is essential for T cell spreading at the immune synapse by protecting F-actin from Cof-mediated severing [104]. Taken together, it was likely that a deletion of Cotl1 would interfere with cytoskeletal dynamics, too. Surprisingly, however, the results of this study clearly show that Cotl1 is not required for cytoskeletal function *in vitro* (Fig. 12). Moreover, in contrast to Cof and Twf2a, Cotl1 was dispensable for thrombopoiesis (Fig. 11 B) [82, 99]. Thus, *Cotl1*$^{-/-}$ mice represent the first ADF-H KO mouse model with unaltered platelet number and size and cytoskeletal dynamics.

The differential function of Cotl1 compared to other ADF-H family members might in part be explained by the low sequence identity between Cotl1 on the one hand and Twf/Cof on the other hand. Although the actin-binding site is structurally highly conserved, which results in a high structural homology of these proteins and determines their ability to bind to actin, the low sequence identity could result in completely different functions of these proteins. Another hypothesis why Cotl1-deficiency did not affect cytoskeletal dynamics was that other actin-binding proteins compensated for the lack of Cotl1. Strikingly, indeed, a strong increase in Phospho-Cof levels was detected in Cotl1-deficient platelets (Fig. 13 D). The increased phosphorylation of Cof in the absence of Cotl1 may ultimately cause reduced F-actin severing and might thereby act as a compensatory mechanism. This would be in line with findings of Kim *et al.* who showed that Cotl1 and Cof compete with each other for F-actin binding thereby protecting F-actin from Cof-mediated severing [104].

Besides its interaction with F-actin, Cotl1 is known to upregulate *5-lipoxygenase* (5-LO) activity. 5-LO catalyzes the first steps of the conversion of *arachidonic acid* (AA) into *leukotrienes* (LT) [110]. Likewise, cyclooxygenases catalyze the initial step of the conversion of AA into thromboxanes (TxA/B_2), prostacyclin (PGI_2) and prostaglandines (PGE/F_2). Therefore, it was conceivable that Cotl1-deficiency affects AA metabolism. However, TxB_2 levels were not significantly altered in Cotl1-deficient platelets (Fig. 15). Investigation of LT levels did not yield meaningful results, probably due to low amounts of these lipid mediators in

platelets, which were below the detection range of the ELISA kit used here. Further studies are ongoing to determine the exact role of Cotl1 for AA metabolism. Platelet-stored LTs are known to contribute to inflammatory responses, e.g. during acute inflammation [170]. Lack of Cotl1 may lead to downregulation of 5-LO activity and hence reduced LT levels, which might influence *in vivo* platelet function and explain some of the observed *in vivo* defects of Cotl1-deficient platelets.

Cotl1-deficiency resulted in significantly reduced aggregate formation of platelets on collagen *in vitro* under flow (Fig. 16), which translated into defective thrombus formation (Fig. 17 A, B) and prolonged bleeding times *in vivo* (Fig. 17 C). Notably, the reduced aggregate formation on collagen *in vitro* under flow was most striking at high shear rates, thus pointing towards a GPIb-dependent mechanism [8, 172]. Recent studies showed that blockade of the vWF binding site on GPIbα by p0p/B-Fab treatment significantly reduced platelet tethering to the injured carotid artery and thus resulted in abolished aggregate formation at sites of vascular injury [153]. The protection from *in vivo* arterial thrombus formation in Cotl1-deficient mice is in line with these observations. Moreover, adhesion of *Cotl1*$^{-/-}$ platelets to vWF was significantly reduced (Fig. 18). Of note, this defect was not caused by altered GPIb expression levels (Table 1). Altogether, these results suggest defective GPIb-vWF binding in Cotl1-deficient platelets, however, the mechanism how Cotl1 influences this interaction remains elusive. Different hypotheses will be discussed briefly in the following. First, GPIbα is a known target of ADAM family metalloproteases which shed GPIb from the platelet surface [189]. Therefore, enhanced GPIbα shedding could be the reason for the impaired GPIb-vWF interactions in Cotl1-deficient platelets. Shedding of GPIbα from the platelet surface as assessed in a time course experiment by flow cytometry was, however, unaltered in Cotl1-deficient platelets (data not shown). Notably, although vWF is the main ligand of GPIb, other interaction partners are present in the circulating blood, Among these are 14-3-3ζ, Fln A, src family kinases and phosphatidylinositol-3 kinase for GPIbα and calmodulin and 14-3-3ζ for GPIbβ [190]. Further experiments will address whether Cotl1-deficiency also affects the interaction of GPIb with these interaction partners. Fln A expression as assessed by Western blotting was indeed slightly altered in Cotl1-deficient platelets (data not shown), however, this minor decrease cannot account for the observed defects of Cotl1-deficient platelets. Cotl1 might also affect the mechanosensing capability of GPIb. Receptor-mediated cell mechanosensing is a multistep process that is initiated by binding of cell surface receptors to their ligands on the ECM or the surface of adjacent cells. Mechanosensing is per definition the ability of a cell to sense mechanical signals of its microenvironment, including force, stress, and strain but also substrate rigidity, topology, and adhesiveness. This ability is crucial for the cell to respond to the surrounding mechanical

cues and adapt to the changing environment e.g. by (de)activation, proliferation/apoptosis, and (de)differentiation [191].

The release of second wave mediators potentiate thrombus formation at sites of vascular injury. Therefore, impaired release of second wave mediators could be another reason for the reduced aggregate formation of Cotl1-deficient platelets *in vitro* and *in vivo*. Indeed, α-granule release was reduced in Cotl1-deficient platelets (Fig. 19 B). However, contradictory, ATP release from dense granules was significantly enhanced in Cotl1-deficient platelets (Fig. 19 A). Notably, the increased secretion of dense granules of *Cotl1*$^{-/-}$ platelets was not restricted to a specific agonist, but occurred in response to GPCR-, as well as ITAM-coupled agonists. Although the exact role of the actin cytoskeleton in exocytotic events in platelets is controversial, several studies using actin-disrupting agents supported a model, in which the cytoskeleton of resting platelets may act as a barrier for granule release and that platelet activation leads to (partial) rupture of actin filaments, thereby enabling degranulation [192]. Further studies on the secretion of other granule-stored proteins will answer this question. Co-infusion of ADP and the thromboxane analogue U46619 using the *in vitro* flow chamber model largely reverted the defective thrombus formation of Cotl1-deficient platelets; however, it could not be normalized to wild-type levels (Fig. 20). These results suggest that both defective GPIb-vWF interactions and decreased second wave mediator secretion contribute to the reduced aggregate formation in Cotl1-deficient mice. Of note, these results show that the amount of released second wave mediators does not seem to be the major determinant of thrombus growth under the experimental conditions used in this study but that the defective GPIb-vWF interaction predominates the observed protection from arterial thrombus formation in Cotl1-deficient mice.

Taken together, the results presented here revealed multiple and novel roles for Cotl1 during hemostasis and arterial thrombus formation as well as for granule exocytosis, whereas its proposed impact on platelet formation and cytoskeletal remodeling could not be confirmed.

5.2 Profilin 1 regulates integrin function in mouse platelets by mediating cyto-skeletal rearrangements

The MK- and platelet-specific *Pfn1*$^{fl/fl\text{-}Pf4Cre}$ mouse line has previously been investigated by our group [178]. In summary, Pfn1-deficient mice displayed a microthrombocytopenia which was caused by (1) cytoskeletal alterations, (2) an accelerated platelet clearance and 3) premature platelet release into the BM. Pfn1-deficient platelets showed a thicker marginal band and a highly disrupted actin cytoskeleton. However, in this study the impact of Pfn1-deficiency on platelet function has not been addressed.

Due to the highly disrupted actin cytoskeleton in Pfn1-deficient platelets it was conceivable to find impaired αIIbβ3 integrin function as recent studies by Stritt *et al*. showed that the organization of the circumferential actin cytoskeleton modulates calpain-mediated αIIbβ3 integrin closure [99]. Indeed, *Pfn1*$^{fl/fl\text{-}Pf4Cre}$ platelets showed impaired αIIbβ3- and β1-integrin inside-out activation (Fig. 23 A, B). Fibrinogen binding to agonist-stimulated platelets occurs via αIIbβ3 and results in platelet aggregation, presumably by crosslinking adjacent activated platelets, thus contributing to hemostasis and thrombosis [193]. Spontaneous platelet aggregation is, however, prevented by tightly regulating the fibrinogen binding activity of αIIbβ3. Preliminary evidence suggests that the submembranous actin keeps αIIbβ3 in a low affinity state and that relief of this constraint by initiating actin filament turnover enables αIIbβ3 to bind fibrinogen [194]. In line with this, fibrinogen binding to αIIbβ3 integrins was markedly reduced in Pfn1-deficient platelets (Fig. 23 D). As fibrinogen binding to αIIbβ3 integrins is a reversible process, time course experiments were performed, however, reduced fibrinogen binding to αIIbβ3 integrins was observed for all additional time points tested (5 min and 20 min, data not shown) in *Pfn1*$^{fl/fl\text{-}Pf4Cre}$ platelets. Likewise, integrin outside-in signaling in Pfn1-deficient platelets was markedly impaired (Fig. 24 A-C, E). Since integrin outside-in signaling is a process highly dependent on functional cytoskeletal remodeling upon platelet activation [12], it is currently difficult to dissect the contribution of the grossly disrupted actin cytoskeleton and impaired integrin signaling to the defects observed in Pfn1-deficient platelets. Altogether, the observations might point to an impaired linkage of integrins to the submembranous actin cytoskeleton in Pfn1-deficient platelets.

Aggregation responses of *Pfn1*$^{fl/fl\text{-}Pf4Cre}$ platelets were only slightly affected by the impaired integrin activation (Fig. 23 E). In contrast, adhesion and aggregate formation of *Pfn1*$^{fl/fl\text{-}Pf4Cre}$ platelets on collagen under flow were markedly reduced, translating into a profound protection from arterial thrombus formation and prolonged bleeding times *in vivo* (Fig. 25). Thus, the integrin activation defect together with the defective actin cytoskeletal organization in Pfn1-deficient platelets translated into a pronounced *in vivo* phenotype thereby highlighting Pfn1 as a critical factor for platelet function in hemostasis and thrombosis. The discrepancy between aggregation responses *in vitro* versus *in vivo* can be explained by the potentially impaired connection of integrins with the actin cytoskeleton of *Pfn1*$^{fl/fl\text{-}Pf4Cre}$ platelets, which seem to be still sufficient to mediate platelet aggregation in the turbidometric aggregometry assay, but insufficient to resist shear forces generated under flow.

Tln1 recruitment to β-integrin tails represents a key step in integrin activation as lack of Tln1 results in abolished integrin activation [195]. Since we observed defective integrin activation, we speculated that Tln1 recruitment to β-integrin tails is altered in Pfn1-deficient platelets and indeed, an abnormal cytoplasmic localization pattern of Tln1 and β3-integrin could be detected

in *Pfn1*$^{fl/fl\text{-}Pf4Cre}$ platelets (Fig. 26). Moreover, we speculated that the so-called integrin closure, the switch of β3-integrins from high- to low-affinity state, could be affected by lack of Pfn1. Strikingly, a significantly increased percentage of PS-positive *Pfn1*$^{fl/fl\text{-}Pf4Cre}$ platelets with inactivated integrins could be identified upon agonist stimulation (Fig. 27). As described by Stritt *et al*. accelerated integrin closure could be caused by increased calpain-mediated cleavage of αIIbβ3 integrins in Pfn1-deficient platelets [99]. Strikingly, cleavage of β3-integrin tails and hence dissociation of the integrin-cytoskeleton linkage was increased in stimulated *Pfn1*$^{fl/fl\text{-}Pf4Cre}$ platelets, which was reverted by chemical inhibition of calpain (Fig. 28). Similarly, calpain inhibition improved spreading of *Pfn1*$^{fl/fl\text{-}Pf4Cre}$ platelets on fibrinogen and restored Tln1 and β3-integrin localization (Fig. 29). These results support the previously described mechanism of calpain-mediated integrin closure and show that accelerated integrin closure caused by enhanced calpain activity, is the underlying reason for the impaired integrin activation in Pfn1-deficient platelets.

The full reversion of the accelerated loss of β3-integrin in stimulated *Pfn1*$^{fl/fl\text{-}Pf4Cre}$ platelets to wild-type levels by inhibition of actin assembly using the F-actin polymerization inhibitor Latrunculin A (Fig. 30), supports the hypothesis that both enhanced calpain-mediated integrin closure as well as the defective organization of the cortical actin cytoskeleton contribute to the defects observed in of *Pfn1*$^{fl/fl\text{-}Pf4Cre}$ platelets. Therefore, Pfn1 might act as an organizer of the circumferential actin network, thereby linking integrins to the underlying cytoskeleton and limiting calpain-mediated integrin closure. In support of this, an increased Pfn1 activity could be detected in *Twf2a*$^{-/-}$ platelets, which resulted in a thickened cortical cytoskeleton and sustained integrin activation due to limited calpain-mediated inactivation [99]. In summary, these findings highlight a central role of Pfn1-mediated actin rearrangements for platelet integrin function with implications for hemostasis and thrombosis.

5.3 Thymosin β4 regulates reactivity and procoagulant activity of platelets

Tβ4 is a moonlighting protein and hence it exerts intra- and extracellular functions. The multiple biological functions of extracellular Tβ4 are intensively studied: for example, Tβ4 administration promotes EC migration, tubule formation and angiogenesis *in vitro* [143] and promotes angiogenesis and wound repair *in vivo* [144, 145]. Direct administration of Tβ4 following a myocardial infarction in mice protected heart tissue from cell death and enabled heart myocytes to survive after hypoxia [144]. All these observations make Tβ4 a potential therapeutic treatment, although the underlying mechanisms remain largely unknown [129]. Moreover, its function for cytoskeletal dynamics is still poorly studied. Therefore, the aim of this thesis was to investigate the effect of a constitutive Tβ4 KO on platelet formation and

function and to shed light on the underlying signaling network by analyzing the effect of recombinant Tβ4.

The deletion of Tβ4 resulted in a moderate thrombocytopenia, but largely normally sized platelets. The reduced platelet counts were not accompanied by elevated MK numbers in BM and spleen. Further studies will be required to address the reason for the thrombocytopenia in *Tβ4*$^{-/-}$ platelets. Possible mechanisms are defective proplatelet formation as seen for Pfn1-deficient animals or an accelerated clearance from the circulation, e.g. by macrophages as shown for Twf2-deficient platelets [99] [129]. Since Tβ4 is one of the major actin-sequestering molecules in cells, it was likely that lack of Tβ4 affects the platelet cytoskeleton. Indeed, *Tβ4*$^{-/-}$ platelets displayed an increased F-actin content in the resting state and significantly reduced agonist-induced F-actin assembly, which could be rescued by pre-incubation with the F-actin polymerization inhibitor Latrunculin A (Fig. 32 A, B). This suggested that either a diminished G-actin pool or a defective actin polymerization was the reason for the reduced agonist-induced F-actin assembly of Tβ4-deficient platelets. Sedimentation of the actin cytoskeleton of Tβ4-deficient platelets revealed a marked reduction in the content of G-actin (Fig. 32 C, D), which is in line with studies suggesting that Tβ4 complexes about half of the monomeric actin in resting cells [184]. The robust reduction of their G-actin pool might be a reason for the reduced F-actin assembly in *Tβ4*$^{-/-}$ platelets. Investigation of the tubulin cytoskeleton of Tβ4-deficient platelets revealed increased levels of microtubules. Interestingly, a significant increase in the number of microtubules per platelet has been described for Pfn1-deficient platelets suggesting that both actin-sequestering proteins exert additional (indirect) effects on the microtubule cytoskeleton [129]. In Pfn1-deficient platelets, an increased microtubule stability could be observed. However, Tβ4-deficient platelets showed no alteration in microtubule stability. This suggested a minor influence of Tβ4 on microtubule functionality. The increased number of microtubules might rather act as a compensatory mechanism to guarantee a grossly normal platelet structure and shape.

As altered cytoskeletal dynamics were shown to influence platelet reactivity [99], we speculated that lack of Tβ4 may affect integrin activation. *Tβ4*$^{-/-}$ platelets showed significantly impaired αIIbβ3 integrin activation, whereas β1-integrin activation and degranulation were only moderately altered (Fig. 35 A, B). Tβ4-deficient platelets displayed a profound aggregation defect upon stimulation with thrombin, CRP and CVX; however, aggregation was increased upon collagen stimulation (Fig. 35 D). The hyperresponsiveness towards collagen stimulation was caused neither by altered $\alpha_2\beta1$ activity nor by increased second wave mediator release (data not shown). In summary, ITAM-coupled agonists induced a variable platelet activation response, which might be the reason of a differential GPVI signaling. Integrin outside-in

signaling was, on the contrary, significantly enhanced in *Tβ4*$^{-/-}$ platelets (Fig. 36 A, C), which could not be reverted by second wave mediator blockade (data not shown). This discrepancy between decreased integrin inside-out and accelerated outside-in signaling may in part be explained by increased F-actin levels in Tβ4-deficient platelets as integrin outside-in signaling is highly dependent on actin dynamics [12].

The altered platelet reactivity under static conditions translated into defective aggregate formation under flow (Fig. 37) and into a profound protection from arterial thrombus formation *in vivo* (Fig. 38). So far, it remains unclear whether the altered cytoskeletal dynamics or the lack of exogenous Tβ4 in *Tβ4*$^{-/-}$ mice caused the observed thrombus formation defect. Studies on KO mouse models of other actin-binding proteins with impaired actin dynamics such as Pfn1 or Cof revealed a similar protection from thrombus formation under flow ([129] and unpublished observations). However, the use of a constitutive KO mouse model in this study makes it difficult to distinguish between effects of Tβ4-deficiency in platelets or other cell types. In assays were not only washed platelet are investigated, effects of other cell types may be important as Tβ4 is highly abundant in many different cell types. For example, high concentrations of Tβ4 are stored in PMNs, which are among the first cells to enter a wound site and release factors, which then recruit additional cells to the injured site [143]. Taken together, the observed *in vivo* defects are influenced by many factors and further studies will address whether the defective thrombus formation in Tβ4-deficient mice is caused by altered actin dynamics or the lack of exogenous Tβ4. To differentiate between the role of endo- and exogenous protein function in *in vivo* assays, it might be helpful to generate bone marrow chimeras or to transfer Tβ4-deficient platelets into wild-type animals.

As thrombus formation is potentiated by the release of second wave mediators, we assessed agonist-induced dense granule ATP release, which was overall increased in Tβ4-deficient platelets, except a profound decrease upon CRP stimulation (Fig. 39 A). In line with this, α-granule release was significantly decreased upon CRP stimulation (Fig. 35 C). The number of granules seems, however, unaffected in Tβ4-deficient platelets as assessed by TEM of washed platelets (data not shown) and thus cannot account for the observed altered granule release. To assess this further, it will be interesting to determine the total content of P-selectin and ATP as well as the agonist-induced release of other granule-stored proteins, such as Serotonin in Tβ4-deficient platelets.

Procoagulant activity under flow and thrombin generation was increased in *Tβ4*$^{-/-}$ platelets (Fig. 40, 41 A-C). In line with this, an enhanced intrinsic coagulation (Fig. 41 D-E) could be observed in *Tβ4*$^{-/-}$ mice. Notably, these assays are carried out in plasma or whole blood, hence platelet-unspecific factors must be considered in interpretation of this results. To shed light on the

question, which of the observed effects are caused by endogenous (the actin-sequestering function) or exogenous Tβ4 protein functions (Tβ4 release by platelets and other blood cells), a set of experiments was repeated where platelets were pre-incubated with recombinant protein. As the described Tβ4 concentration in human plasma was estimated to 0.03-0.4 µg mL^{-1} [139], a concentration range of 0.1 to 10 µg mL^{-1} was chosen for the *in vitro* pre-incubation of platelets. Notably, the concentration of recombinant Tβ4 used for *in vivo* assays is much higher- 6 mg kg^{-1} [196]. Whereas aggregate formation under flow was reverted to wild-type levels by addition of recombinant Tβ4 (pre-incubation or co-infusion; Fig. 42 and preliminary observations), the defective αIIbβ3 integrin inside-out activation of *Tβ4*$^{-/-}$ platelets was even more pronounced. Interestingly, pre-incubation with recombinant Tβ4 further enhanced aggregation of both wild-type and *Tβ4*$^{-/-}$ platelets in comparison to the untreated controls upon collagen stimulation (Fig. 43 B). In line with this, recombinant Tβ4 increased the spreading rate and elevated ATP secretion (except for CRP stimulation) of both wild-type and *Tβ4*$^{-/-}$ platelets (Fig. 44, 45). These diverse results need further investigation to better understand the mode of action of Tβ4. Therefore, another aim of the thesis was to establish an expression and purification protocol for recombinant Tβ4, which was adopted from Li *et al.* [188]. Successful expression and purification of recombinant DsbA-tagged Tβ4 could be achieved using *E. coli* expression strain BL21 (DE3) (Fig. 46, 47). The production of untagged protein, however, requires further optimization. Experiments with the recombinant protein will focus especially on its *in vivo* effects, release and uptake in platelets, its half-life and its effects on major platelet signaling pathways. Due to the current lack of knowledge about all these aspects, these experiments are of high clinical relevance.

5.4 Concluding remarks and future perspectives

The findings presented in this thesis provide new insights into the regulation of cytoskeletal dynamics and the role of several actin-binding proteins for platelet production and function. Although the ADF-H protein family member Cotl1 is dispensable for platelet production and actin dynamics, this thesis shows for the first time that Cotl1 is a major regulator of hemostasis and thrombosis in mice. This might be a result of defective GPIb-vWF signaling or a reduced release or dampened sensitivity towards second wave mediators. Moreover, altered 5-LO activity might account for the observed defects in Cotl1-deficient mice, which is under current investigation. To this end, it is planned to assess levels of AA metabolites by mass spectrometry with the help of our collaboration partners. Furthermore, biomechanical properties of the KO platelets will be assessed to check whether altered stability and thus a stronger deformation of the platelets might be a reason for the observed defects of Cotl1-deficient platelets *in vitro* under flow and *in vivo*. The findings presented here underline the

diversity of actin-binding proteins, which share some common features but their differential sequence and structure often results in complete distinct biological functions. The protection from *in vivo* thrombus formation in Cotl1-deficient mice highlight Cotl1 as potential novel target for anti-thrombotic drug development. However, although bleeding times were not strikingly higher, an increased bleeding risk must be considered.

The importance of Pfn1 for thrombopoiesis has been elucidated in earlier studies. The work presented here focused on its role for platelet function and established Pfn1 as a central regulator of platelet integrin activation. The suggested underlying mechanisms of the observed defects of *Pfn1*$^{fl/fl\text{-}Pf4Cre}$ platelets are an enhanced calpain-mediated integrin closure together with a defective organization of the cortical actin cytoskeleton. The results described in this thesis further stress the importance of a functional actin cytoskeleton for proper platelet function *in vitro* and *in vivo* highlighting the outstanding role of Pfn1 as a master regulator of platelet integrin function and of the organization of the actin cytoskeleton.

Tβ4 has previously been described as a miracle cure, exerting various beneficial functions in a large variety of disease models. Moreover, it fulfils an important intracellular function, since it is one of the major G-actin-sequestering proteins. In this thesis, the expected role of Tβ4 in cytoskeletal dynamics could be confirmed. Accordingly, the G-actin pool of Tβ4-deficient platelets was largely diminished concomitant with an increase in F-actin levels. This had divergent effects on platelet reactivity, since spreading, clot retraction as well as granule release were markedly enhanced in KO platelets, whereas signaling events upon CRP stimulation were significantly diminished *in vitro*. Additionally, aggregation defects on collagen *in vitro* under flow and a protection from arterial thrombus formation *in vivo* could be detected. In contrast, Tβ4-deficiency caused enhanced thrombin generation, procoagulant activity and coagulation, which was a result of increased levels of FVIII, IX and XI. Together, these results establish Tβ4 as a critical regulator of thrombosis, platelet reactivity and coagulation. In addition to its intracellular role, pre-incubation of platelets and blood with recombinant Tβ4 revealed an overall stimulatory role of exogenous Tβ4. However, the underlying mechanisms or signaling pathways remain elusive and are under current investigation. To this end, further experiments with the recombinant protein (commercial and self-made) are planned. These will address its effect in *in vivo* models of arterial thrombosis or thrombo-inflammatory brain infarction. In additional experiments, the underlying signaling pathways by which Tβ4 exerts its effects will be investigated. Here, the Akt-ILK-PINCH pathway will be of major interest, since Tβ4 was already shown to upregulate Akt phosphorylation. The protection from *in vivo* thrombus formation in Tβ4-deficient mice highlight Tβ4 as potential novel target for anti-thrombotic drug development. However, Tβ4 is expressed in many different cell types and

hence interfering with Tβ4 expression or release might have severe side effects. Nevertheless, elucidation of the role of exogenous Tβ4 is of high clinical relevance as its status as miracle cure highlights it as novel drug for anti-inflammatory and pro-angiogenic treatment.

In summary, the work presented in this thesis will ultimately help to understand the diverse regulatory machinery guaranteeing actin polymerization and sequestering in platelets.

6. REFERENCES

1. Italiano, J.E., Jr., S. Patel-Hett, and J.H. Hartwig, *Mechanics of proplatelet elaboration.* J Thromb Haemost, 2007. **5 Suppl 1**: p. 18-23.
2. Ruggeri, Z.M., *Platelets in atherothrombosis.* Nat Med, 2002. **8**(11): p. 1227-34.
3. Caro, J.J., K.F. Huybrechts, and I. Duchesne, *Management Patterns and Costs of Acute Ischemic Stroke.* An International Study, 2000. **31**(3): p. 582-590.
4. Lopez, A.D., et al., *Global and regional burden of disease and risk factors, 2001: systematic analysis of population health data.* The Lancet, 2006. **367**(9524): p. 1747-1757.
5. Sachs, U.J. and B. Nieswandt, *In vivo thrombus formation in murine models.* Circ Res, 2007. **100**(7): p. 979-91.
6. Varga-Szabo, D., I. Pleines, and B. Nieswandt, *Cell Adhesion Mechanisms in Platelets.* Arteriosclerosis, Thrombosis, and Vascular Biology, 2008. **28**(3): p. 403-412.
7. Elvers, M., et al., *Impaired α(IIb)β(3) integrin activation and shear-dependent thrombus formation in mice lacking phospholipase D1.* Science signaling, 2010. **3**(103): p. ra1-ra1.
8. Turitto, V.T., H.J. Weiss, and H.R. Baumgartner, *The effect of shear rate on platelet interaction with subendothelium exposed to citrated human blood.* Microvascular Research, 1980. **19**(3): p. 352-365.
9. Nieswandt, B. and S.P. Watson, *Platelet-collagen interaction: is GPVI the central receptor?* Blood, 2003. **102**(2): p. 449-461.
10. Suzuki-Inoue, K., et al., *Involvement of the Snake Toxin Receptor CLEC-2, in Podoplanin-mediated Platelet Activation, by Cancer Cells.* Journal of Biological Chemistry, 2007. **282**(36): p. 25993-26001.
11. WATSON, S.P., et al., *GPVI and integrin αIIbβ3 signaling in platelets.* Journal of Thrombosis and Haemostasis, 2005. **3**(8): p. 1752-1762.
12. Varga-Szabo, D., A. Braun, and B. Nieswandt, *Calcium signaling in platelets.* J Thromb Haemost, 2009. **7**(7): p. 1057-66.
13. HARPER, M.T. and A.W. POOLE, *Diverse functions of protein kinase C isoforms in platelet activation and thrombus formation.* Journal of Thrombosis and Haemostasis, 2010. **8**(3): p. 454-462.
14. Ren, Q., S. Ye, and S.W. Whiteheart, *The platelet release reaction: just when you thought platelet secretion was simple.* Curr Opin Hematol, 2008. **15**(5): p. 537-41.
15. Krishnaswamy, S., et al., *[15] Assembly of prothrombinase complex*, in *Methods in Enzymology*. 1993, Academic Press. p. 260-280.
16. Maas, C., C. Oschatz, and T. Renne, *The plasma contact system 2.0.* Semin Thromb Hemost, 2011. **37**(4): p. 375-81.
17. Offermanns, S., *Activation of platelet function through G protein-coupled receptors.* Circ Res, 2006. **99**(12): p. 1293-304.
18. Offermanns, S., et al., *Defective platelet activation in Gαq-deficient mice.* Nature, 1997. **389**: p. 183.
19. Stegner, D. and B. Nieswandt, *Platelet receptor signaling in thrombus formation.* J Mol Med (Berl), 2011. **89**(2): p. 109-21.
20. Badolia, R., et al., *G_q-mediated Akt translocation to the membrane: a novel PIP₃-independent mechanism in platelets.* Blood, 2015. **125**(1): p. 175-184.
21. Hart, M.J., et al., *Direct Stimulation of the Guanine Nucleotide Exchange Activity of p115 RhoGEF by Gα₁₃.* Science, 1998. **280**(5372): p. 2112-2114.
22. Cantley, L.C., *The Phosphoinositide 3-Kinase Pathway.* Science, 2002. **296**(5573): p. 1655-1657.
23. Clapham, D.E. and E.J. Neer, *G PROTEIN βγ SUBUNITS.* Annual Review of Pharmacology and Toxicology, 1997. **37**(1): p. 167-203.
24. Fox, J.E., *The platelet cytoskeleton.* Thromb Haemost, 1993. **70**(6): p. 884-93.

25. Weisenberg, R.C., *Microtubule Formation in vitro in Solutions Containing Low Calcium Concentrations.* Science, 1972. **177**(4054): p. 1104-1105.
26. Chrétien, D., et al., *Lattice defects in microtubules: protofilament numbers vary within individual microtubules.* The Journal of Cell Biology, 1992. **117**(5): p. 1031-1040.
27. Walker, R.A., et al., *Dynamic instability of individual microtubules analyzed by video light microscopy: rate constants and transition frequencies.* The Journal of Cell Biology, 1988. **107**(4): p. 1437-1448.
28. Mitchison, T. and M. Kirschner, *Dynamic instability of microtubule growth.* Nature, 1984. **312**: p. 237.
29. Song, Y. and S.T. Brady, *Post-translational modifications of tubulin: pathways to functional diversity of microtubules.* Trends in Cell Biology, 2015. **25**(3): p. 125-136.
30. Kalebic, N., et al., *αTAT1 is the major α-tubulin acetyltransferase in mice.* Nature Communications, 2013. **4**: p. 1962.
31. Perdiz, D., et al., *The ins and outs of tubulin acetylation: More than just a post-translational modification?* Cellular Signalling, 2011. **23**(5): p. 763-771.
32. Witt, O., et al., *HDAC family: What are the cancer relevant targets?* Cancer Letters. **277**(1): p. 8-21.
33. Yang, P., et al., *HDAC6: Physiological function and its selective inhibitors for cancer treatment.* Drug Discoveries & Therapeutics, 2013. **7**(6): p. 233-242.
34. Vale, R.D., *The Molecular Motor Toolbox for Intracellular Transport.* Cell, 2003. **112**(4): p. 467-480.
35. White, J.G., *Effects of colchicine and Vinca alkaloids on human platelets. I. Influence on platelet microtubules and contractile function.* The American Journal of Pathology, 1968. **53**(2): p. 281-291.
36. Schwer, H.D., et al., *A lineage-restricted and divergent β-tubulin isoform is essential for the biogenesis, structure and function of blood platelets.* Current Biology, 2001. **11**(8): p. 579-586.
37. Tondeleir, D., et al., *Actin isoform expression patterns during mammalian development and in pathology: Insights from mouse models.* Cell Motility, 2009. **66**(10): p. 798-815.
38. Hartwig, J.H. and M. DeSisto, *The cytoskeleton of the resting human blood platelet: structure of the membrane skeleton and its attachment to actin filaments.* The Journal of Cell Biology, 1991. **112**(3): p. 407-425.
39. Tablin, F., M. Castro, and R.M. Leven, *Blood platelet formation in vitro. The role of the cytoskeleton in megakaryocyte fragmentation.* Journal of Cell Science, 1990. **97**(1): p. 59-70.
40. Hartwig, J.H., *Mechanisms of actin rearrangements mediating platelet activation.* The Journal of Cell Biology, 1992. **118**(6): p. 1421-1442.
41. Jennings, L.K., et al., *Changes in the cytoskeletal structure of human platelets following thrombin activation.* Journal of Biological Chemistry, 1981. **256**(13): p. 6927-6932.
42. Paavilainen, V.O., et al., *Regulation of cytoskeletal dynamics by actin-monomer-binding proteins.* Trends in Cell Biology, 2004. **14**(7): p. 386-394.
43. Rosenberg, S., A. Stracher, and R.C. Lucas, *Isolation and characterization of actin and actin-binding protein from human platelets.* The Journal of Cell Biology, 1981. **91**(1): p. 201-211.
44. Falet, H., et al., *A novel interaction between FlnA and Syk regulates platelet ITAM-mediated receptor signaling and function.* The Journal of Experimental Medicine, 2010.
45. Wegner, A., *Head to tail polymerization of actin.* Journal of Molecular Biology, 1976. **108**(1): p. 139-150.
46. Pollard, T.D. and G.G. Borisy, *Cellular Motility Driven by Assembly and Disassembly of Actin Filaments.* Cell, 2003. **112**(4): p. 453-465.

47. Goode, B.L., D.G. Drubin, and P. Lappalainen, *Regulation of the Cortical Actin Cytoskeleton in Budding Yeast by Twinfilin, a Ubiquitous Actin Monomer-sequestering Protein.* The Journal of Cell Biology, 1998. **142**(3): p. 723-733.
48. Helfer, E., et al., *Mammalian twinfilin sequesters ADP-G-actin and caps filament barbed ends: implications in motility.* The EMBO Journal, 2006. **25**(6): p. 1184-1195.
49. Lassing, I. and U. Lindberg, *Specific interaction between phosphatidylinositol 4,5-bisphosphate and profilactin.* Nature, 1985. **314**: p. 472.
50. Palmgren, S., et al., *Interactions with PIP₂, ADP-actin monomers, and capping protein regulate the activity and localization of yeast twinfilin.* The Journal of Cell Biology, 2001. **155**(2): p. 251-260.
51. Bamburg, J.R., *Proteins of the ADF/Cofilin Family: Essential Regulators of Actin Dynamics.* Annual Review of Cell and Developmental Biology, 1999. **15**(1): p. 185-230.
52. Carlier, M.-F., et al., *Actin Depolymerizing Factor (ADF/Cofilin) Enhances the Rate of Filament Turnover: Implication in Actin-based Motility.* The Journal of Cell Biology, 1997. **136**(6): p. 1307-1322.
53. Maciver, S.K., *How ADF/cofilin depolymerizes actin filaments.* Current Opinion in Cell Biology, 1998. **10**(1): p. 140-144.
54. McGough, A., et al., *Cofilin Changes the Twist of F-Actin: Implications for Actin Filament Dynamics and Cellular Function.* The Journal of Cell Biology, 1997. **138**(4): p. 771-781.
55. HUBBERSTEY, A.V. and E.P. MOTTILLO, *Cyclase-associated proteins: CAPacity for linking signal transduction and actin polymerization.* The FASEB Journal, 2002. **16**(6): p. 487-499.
56. Fedor-Chaiken, M., R.J. Deschenes, and J.R. Broach, *SRV2, a gene required for RAS activation of adenylate cyclase in yeast.* Cell, 1990. **61**(2): p. 329-340.
57. Field, J., et al., *Cloning and characterization of CAP, the S. cerevisiae gene encoding the 70 kd adenylyl cyclase-associated protein.* Cell, 1990. **61**(2): p. 319-327.
58. Lila, T. and D.G. Drubin, *Evidence for physical and functional interactions among two Saccharomyces cerevisiae SH3 domain proteins, an adenylyl cyclase-associated protein and the actin cytoskeleton.* Molecular Biology of the Cell, 1997. **8**(2): p. 367-385.
59. Balcer, H.I., et al., *Coordinated Regulation of Actin Filament Turnover by a High-Molecular-Weight Srv2/CAP Complex, Cofilin, Profilin, and Aip1.* Current Biology, 2003. **13**(24): p. 2159-2169.
60. Moriyama, K. and I. Yahara, *Human CAP1 is a key factor in the recycling of cofilin and actin for rapid actin turnover.* Journal of Cell Science, 2002. **115**(8): p. 1591-1601.
61. Johnston, A.B., A. Collins, and B.L. Goode, *High-speed depolymerization at actin filament ends jointly catalysed by Twinfilin and Srv2/CAP.* Nature Cell Biology, 2015. **17**: p. 1504.
62. Thrasher, A.J. and S.O. Burns, *WASP: a key immunological multitasker.* Nature Reviews Immunology, 2010. **10**: p. 182.
63. Villa, A., et al., *X–linked thrombocytopenia and Wiskott–Aldrich syndrome are allelic diseases with mutations in the WASP gene.* Nature Genetics, 1995. **9**: p. 414.
64. Symons, M., et al., *Wiskott–Aldrich Syndrome Protein, a Novel Effector for the GTPase CDC42Hs, Is Implicated in Actin Polymerization.* Cell, 1996. **84**(5): p. 723-734.
65. de la Fuente, M.A., et al., *WIP is a chaperone for Wiskott–Aldrich syndrome protein (WASP).* Proceedings of the National Academy of Sciences, 2007. **104**(3): p. 926-931.
66. Falet, H., et al., *Platelet-associated IgAs and impaired GPVI responses in platelets lacking WIP.* Blood, 2009. **114**(21): p. 4729-4737.

67. Ramaekers, F.C. and F.T. Bosman, *The cytoskeleton and disease.* The Journal of Pathology, 2004. **204**(4): p. 351-354.
68. Lappalainen, P., et al., *The ADF Homology (ADF-H) Domain: A Highly Exploited Actin-binding Module.* Molecular Biology of the Cell, 1998. **9**(8): p. 1951-1959.
69. Bamburg, J.R., A. McGough, and S. Ono, *Putting a new twist on actin: ADF/cofilins modulate actin dynamics.* Trends in Cell Biology, 1999. **9**(9): p. 364-370.
70. Goode, B.L., et al., *Activation of the Arp2/3 Complex by the Actin Filament Binding Protein Abp1p.* The Journal of Cell Biology, 2001. **153**(3): p. 627-634.
71. Maciver, S.K. and P.J. Hussey, *The ADF/cofilin family: actin-remodeling proteins.* Genome Biology, 2002. **3**(5): p. reviews3007.1.
72. Vartiainen, M.K., et al., *The Three Mouse Actin-depolymerizing Factor/Cofilins Evolved to Fulfill Cell-Type–specific Requirements for Actin Dynamics.* Molecular Biology of the Cell, 2002. **13**(1): p. 183-194.
73. Bamburg, J.R. and D. Bray, *Distribution and cellular localization of actin depolymerizing factor.* The Journal of Cell Biology, 1987. **105**(6): p. 2817-2825.
74. Ono, S., *Mechanism of Depolymerization and Severing of Actin Filaments and Its Significance in Cytoskeletal Dynamics*, in *International Review of Cytology*. 2007, Academic Press. p. 1-82.
75. Maciver, S.K., H.G. Zot, and T.D. Pollard, *Characterization of actin filament severing by actophorin from Acanthamoeba castellanii.* The Journal of Cell Biology, 1991. **115**(6): p. 1611-1620.
76. Abe, H., et al., *Xenopus laevis actin-depolymerizing factor/cofilin: a phosphorylation-regulated protein essential for development.* The Journal of Cell Biology, 1996. **132**(5): p. 871-885.
77. Arber, S., et al., *Regulation of actin dynamics through phosphorylation of cofilin by LIM-kinase.* Nature, 1998. **393**: p. 805.
78. Maekawa, M., et al., *Signaling from Rho to the Actin Cytoskeleton Through Protein Kinases ROCK and LIM-kinase.* Science, 1999. **285**(5429): p. 895-898.
79. Toshima, J., et al., *Cofilin Phosphorylation by Protein Kinase Testicular Protein Kinase 1 and Its Role in Integrin-mediated Actin Reorganization and Focal Adhesion Formation.* Molecular Biology of the Cell, 2001. **12**(4): p. 1131-1145.
80. Niwa, R., et al., *Control of Actin Reorganization by Slingshot, a Family of Phosphatases that Dephosphorylate ADF/Cofilin.* Cell, 2002. **108**(2): p. 233-246.
81. Gohla, A., J. Birkenfeld, and G.M. Bokoch, *Chronophin, a novel HAD-type serine protein phosphatase, regulates cofilin-dependent actin dynamics.* Nature Cell Biology, 2004. **7**: p. 21.
82. Falet, H., et al., *Integrin alpha(IIb)beta3 signals lead cofilin to accelerate platelet actin dynamics.* Am J Physiol Cell Physiol, 2005. **289**(4): p. C819-25.
83. Gunsalus, K.C., et al., *Mutations in twinstar, a Drosophila gene encoding a cofilin/ADF homologue, result in defects in centrosome migration and cytokinesis.* The Journal of Cell Biology, 1995. **131**(5): p. 1243.
84. Kazuko, I., et al., *Isolation of a yeast essential gene, COF1, that encodes a homologue of mammalian cofilin, a low-Mr actin-binding and depolymerizing protein.* Gene, 1993. **124**(1): p. 115-120.
85. Ono, S., D.L. Baillie, and G.M. Benian, *UNC-60B, an ADF/Cofilin Family Protein, Is Required for Proper Assembly of Actin into Myofibrils in Caenorhabditis elegans Body Wall Muscle.* The Journal of Cell Biology, 1999. **145**(3): p. 491-502.
86. McKim, K.S., et al., *The Caenorhabditis elegans unc-60 gene encodes proteins homologous to a family of actin-binding proteins.* Molecular and General Genetics MGG, 1994. **242**(3): p. 346-357.
87. Gurniak, C.B., E. Perlas, and W. Witke, *The actin depolymerizing factor n-cofilin is essential for neural tube morphogenesis and neural crest cell migration.* Developmental Biology, 2005. **278**(1): p. 231-241.

88. Bellenchi, G.C., et al., *N-cofilin is associated with neuronal migration disorders and cell cycle control in the cerebral cortex.* Genes & Development, 2007. **21**(18): p. 2347-2357.
89. Li, W., et al., *Stimulation of the platelet-derived growth factor beta receptor signaling pathway activates protein kinase C-delta.* Molecular and Cellular Biology, 1994. **14**(10): p. 6727-6735.
90. Beeler, J.F., et al., *Cloning and characterization of the mouse homolog of the human A6 gene.* Gene, 1997. **193**(1): p. 31-37.
91. Rohwer, A., et al., *Cloning, expression and characterization of an A6-related protein.* European Journal of Biochemistry, 1999. **263**(2): p. 518-525.
92. Paavilainen, V.O., et al., *Structural Conservation between the Actin Monomer-binding Sites of Twinfilin and Actin-depolymerizing Factor (ADF)/Cofilin.* Journal of Biological Chemistry, 2002. **277**(45): p. 43089-43095.
93. Vartiainen, M.K., et al., *Mammals Have Two Twinfilin Isoforms Whose Subcellular Localizations and Tissue Distributions Are Differentially Regulated.* Journal of Biological Chemistry, 2003. **278**(36): p. 34347-34355.
94. Nevalainen, Elisa M., et al., *Two biochemically distinct and tissue-specific twinfilin isoforms are generated from the mouse Twf2 gene by alternative promoter usage.* Biochemical Journal, 2009. **417**(2): p. 593-600.
95. Ojala, P.J., et al., *The Two ADF-H Domains of Twinfilin Play Functionally Distinct Roles in Interactions with Actin Monomers.* Molecular Biology of the Cell, 2002. **13**(11): p. 3811-3821.
96. Falck, S., et al., *Biological role and structural mechanism of twinfilin–capping protein interaction.* The EMBO Journal, 2004. **23**(15): p. 3010-3019.
97. Moseley, J.B. and B.L. Goode, *The Yeast Actin Cytoskeleton: from Cellular Function to Biochemical Mechanism.* Microbiology and Molecular Biology Reviews, 2006. **70**(3): p. 605-645.
98. Wahlström, G., et al., *Twinfilin is required for actin-dependent developmental processes in Drosophila.* The Journal of Cell Biology, 2001. **155**(5): p. 787-796.
99. Stritt, S., et al., *Twinfilin 2a regulates platelet reactivity and turnover in mice.* Blood, 2017. **130**(15): p. 1746-1756.
100. Hostos, E.L.d., et al., *Coactosin, a 17 kDA F-actin binding protein from Dictyostelium discoideum.* Cell Motility, 1993. **26**(3): p. 181-191.
101. Provost, P., et al., *Coactosin-like protein, a human F-actin-binding protein: critical role of lysine-75.* Biochem J, 2001. **359**(Pt 2): p. 255-63.
102. Hellman, M., et al., *Solution structure of coactosin reveals structural homology to ADF/cofilin family proteins.* FEBS Letters, 2004. **576**(1-2): p. 91-96.
103. Röhrig, U., et al., *Coactosin interferes with the capping of actin filaments.* FEBS Letters, 1995. **374**(2): p. 284-286.
104. Kim, J., et al., *Coactosin-Like 1 Antagonizes Cofilin to Promote Lamellipodial Protrusion at the Immune Synapse.* PLoS ONE, 2014. **9**(1): p. e85090.
105. Provost, P., et al., *5-Lipoxygenase Interacts with Coactosin-like Protein.* Journal of Biological Chemistry, 2001. **276**(19): p. 16520-16527.
106. Samuelsson, B., *Leukotrienes: mediators of immediate hypersensitivity reactions and inflammation.* Science, 1983. **220**(4597): p. 568-575.
107. Peters-Golden , M. and W.R.J. Henderson *Leukotrienes.* New England Journal of Medicine, 2007. **357**(18): p. 1841-1854.
108. Werz, O. and D. Steinhilber, *Therapeutic options for 5-lipoxygenase inhibitors.* Pharmacology & Therapeutics, 2006. **112**(3): p. 701-718.
109. Chen, Y., et al., *Loss of the Alox5 gene impairs leukemia stem cells and prevents chronic myeloid leukemia.* Nature Genetics, 2009. **41**: p. 783.

110. Basavarajappa, D., et al., *Roles of coactosin-like protein (CLP) and 5-lipoxygenase-activating protein (FLAP) in cellular leukotriene biosynthesis.* Proceedings of the National Academy of Sciences, 2014. **111**(31): p. 11371-11376.
111. Esser, J., et al., *Coactosin-like protein functions as a stabilizing chaperone for 5-lipoxygenase: role of tryptophan 102.* Biochemical Journal, 2010. **425**(1): p. 265-274.
112. Carlsson, L., et al., *Actin polymerizability is influenced by profilin, a low molecular weight protein in non-muscle cells.* Journal of Molecular Biology, 1977. **115**(3): p. 465-483.
113. Honoré, B., et al., *Cloning and expression of a novel human profilin variant, profilin II.* FEBS Letters, 1993. **330**(2): p. 151-155.
114. Hu, E., et al., *Molecular Cloning and Characterization of Profilin-3: A Novel Cytoskeleton-Associated Gene Expressed in Rat Kidney and Testes.* Nephron Experimental Nephrology, 2001. **9**(4): p. 265-274.
115. Obermann, H., et al., *Novel testis-expressed profilin IV associated with acrosome biogenesis and spermatid elongation.* MHR: Basic science of reproductive medicine, 2005. **11**(1): p. 53-64.
116. Lambrechts, A., et al., *Profilin II Is Alternatively Spliced, Resulting in Profilin Isoforms That Are Differentially Expressed and Have Distinct Biochemical Properties.* Molecular and Cellular Biology, 2000. **20**(21): p. 8209-8219.
117. Lassing, I. and U. Lindberg, *Specificity of the interaction between phosphatidylinositol 4,5-bisphosphate and the profilin:actin complex.* Journal of Cellular Biochemistry, 1988. **37**(3): p. 255-267.
118. Witke, W., *The role of profilin complexes in cell motility and other cellular processes.* Trends in Cell Biology, 2004. **14**(8): p. 461-469.
119. Lambrechts, A., et al., *Profilin-I-ligand interactions influence various aspects of neuronal differentiation.* Journal of Cell Science, 2006. **119**(8): p. 1570-1578.
120. Böttcher, R.T., et al., *Profilin 1 is required for abscission during late cytokinesis of chondrocytes.* The EMBO Journal, 2009. **28**(8): p. 1157-1169.
121. Stritt, S., *The role of the cytoskeleton in platelet production and the pathogenesis of platelet disorders in humans and mice* 2015.
122. Goldschmidt-Clermont, P.J., et al., *Mechanism of the interaction of human platelet profilin with actin.* The Journal of Cell Biology, 1991. **113**(5): p. 1081-1089.
123. Pring, M., A. Weber, and M.R. Bubb, *Profilin-actin complexes directly elongate actin filaments at the barbed end.* Biochemistry, 1992. **31**(6): p. 1827-1836.
124. Pantaloni, D. and M.-F. Carlier, *How profilin promotes actin filament assembly in the presence of thymosin β4.* Cell, 1993. **75**(5): p. 1007-1014.
125. Witke, W., et al., *In mouse brain profilin I and profilin II associate with regulators of the endocytic pathway and actin assembly.* The EMBO Journal, 1998. **17**(4): p. 967-976.
126. Auerbuch, V., et al., *Ena/VASP proteins contribute to Listeria monocytogenes pathogenesis by controlling temporal and spatial persistence of bacterial actin-based motility.* Molecular Microbiology, 2003. **49**(5): p. 1361-1375.
127. Verheyen, E.M. and L. Cooley, *Profilin mutations disrupt multiple actin-dependent processes during Drosophila development.* Development, 1994. **120**(4): p. 717-728.
128. Witke, W., et al., *Profilin I is essential for cell survival and cell division in early mouse development.* Proceedings of the National Academy of Sciences, 2001. **98**(7): p. 3832-3836.
129. Goldstein, A.L., E. Hannappel, and H.K. Kleinman, *Thymosin beta4: actin-sequestering protein moonlights to repair injured tissues.* Trends Mol Med, 2005. **11**(9): p. 421-9.
130. Low, T.L., S.K. Hu, and A.L. Goldstein, *Complete amino acid sequence of bovine thymosin beta 4: a thymic hormone that induces terminal deoxynucleotidyl transferase activity in thymocyte populations.* Proceedings of the National Academy of Sciences of the United States of America, 1981. **78**(2): p. 1162-1166.

131. Freire, M., et al., *Purification of thymus mRNA coding for a 16,000-dalton polypeptide containing the thymosin alpha 1 sequence.* Proceedings of the National Academy of Sciences of the United States of America, 1981. **78**(1): p. 192-195.
132. Mannherz, H.G. and E. Hannappel, *The β-thymosins: Intracellular and extracellular activities of a versatile actin binding protein family.* Cell Motility, 2009. **66**(10): p. 839-851.
133. HUFF, T., et al., *Thymosin β4 is released from human blood platelets and attached by factor XIIIa (transglutaminase) to fibrin and collagen.* The FASEB Journal, 2002. **16**(7): p. 691-696.
134. Xue, B., et al., *Structural basis of thymosin-β4/profilin exchange leading to actin filament polymerization.* Proceedings of the National Academy of Sciences, 2014. **111**(43): p. E4596-E4605.
135. Paunola, E., P.K. Mattila, and P. Lappalainen, *WH2 domain: a small, versatile adapter for actin monomers.* FEBS Letters, 2002. **513**(1): p. 92-97.
136. Aguda, A.H., et al., *The Structural Basis of Actin Interaction with Multiple WH2/β-Thymosin Motif-Containing Proteins.* Structure, 2006. **14**(3): p. 469-476.
137. Haj, A.A., et al., *Thymosin beta4 inhibits ADF/cofilin stimulated F-actin cycling and hela cell migration: Reversal by active Arp2/3 complex.* Cytoskeleton, 2014. **71**(2): p. 95-107.
138. Huff, T., et al., *Nuclear localisation of the G-actin sequestering peptide thymosin β₄.* Journal of Cell Science, 2004. **117**(22): p. 5333-5341.
139. Hannapel, E. and M. van Kampen, *Determination of thymosin β4 in human blood cells and serum.* Journal of Chromatography A, 1987. **397**: p. 279-285.
140. BODENDORF, S., G. BORN, and E. HANNAPPEL, *Determination of Thymosin β4 and Protein in Human Wound Fluid after Abdominal Surgery.* Annals of the New York Academy of Sciences, 2007. **1112**(1): p. 418-424.
141. BADAMCHIAN, M., et al., *Identification and Quantification of Thymosin β4 in Human Saliva and Tears.* Annals of the New York Academy of Sciences, 2007. **1112**(1): p. 458-465.
142. Nemolato, S., et al., *Thymosin β4 and β10 Levels in Pre-Term Newborn Oral Cavity and Foetal Salivary Glands Evidence a Switch of Secretion during Foetal Development.* PLOS ONE, 2009. **4**(4): p. e5109.
143. Shrivastava, S., et al., *Thymosin beta4 and cardiac repair.* Ann N Y Acad Sci, 2010. **1194**: p. 87-96.
144. Srivastava, D., et al., *Thymosin beta4 is cardioprotective after myocardial infarction.* Ann N Y Acad Sci, 2007. **1112**: p. 161-70.
145. Bock-Marquette, I., et al., *Thymosin β4 activates integrin-linked kinase and promotes cardiac cell migration, survival and cardiac repair.* Nature, 2004. **432**: p. 466.
146. Young, J.D., et al., *Thymosin β 4 sulfoxide is an anti-inflammatory agent generated by monocytes in the presence of glucocorticoids.* Nature Medicine, 1999. **5**: p. 1424.
147. Sosne, G., et al., *Thymosin Beta 4 Promotes Corneal Wound Healing and Modulates Inflammatory Mediators in vivo.* Experimental Eye Research, 2001. **72**(5): p. 605-608.
148. Badamchian, M., et al., *Thymosin β4 reduces lethality and down-regulates inflammatory mediators in endotoxin-induced septic shock.* International Immunopharmacology, 2003. **3**(8): p. 1225-1233.
149. Dümmler, A., A.-M. Lawrence, and A. de Marco, *Simplified screening for the detection of soluble fusion constructs expressed in E. coli using a modular set of vectors.* Microbial Cell Factories, 2005. **4**(1): p. 34.
150. Nieswandt, B., et al., *Acute Systemic Reaction and Lung Alterations Induced by an Antiplatelet Integrin gpIIb/IIIa Antibody in Mice.* Blood, 1999. **94**(2): p. 684-693.
151. Nieswandt, B., et al., *Identification of critical antigen-specific mechanisms in the development of immune thrombocytopenic purpura in mice.* Blood, 2000. **96**(7): p. 2520-2527.

152. Bergmeier, W., et al., *Flow cytometric detection of activated mouse integrin αIIbβ3 with a novel monoclonal antibody.* Cytometry, 2002. **48**(2): p. 80-86.
153. Massberg, S., et al., *A Crucial Role of Glycoprotein VI for Platelet Recruitment to the Injured Arterial Wall In Vivo.* The Journal of Experimental Medicine, 2003. **197**(1): p. 41-49.
154. Nieswandt, B., et al., *Long-Term Antithrombotic Protection by in Vivo Depletion of Platelet Glycoprotein VI in Mice.* The Journal of Experimental Medicine, 2001. **193**(4): p. 459-470.
155. May, F., et al., *CLEC-2 is an essential platelet-activating receptor in hemostasis and thrombosis.* Blood, 2009. **114**(16): p. 3464-3472.
156. HOFMANN, S., et al., *The SLAM family member CD84 is regulated by ADAM10 and calpain in platelets.* Journal of Thrombosis and Haemostasis, 2012. **10**(12): p. 2581-2592.
157. Stritt, S., et al., *Rap1-GTP-interacting adaptor molecule (RIAM) is dispensable for platelet integrin activation and function in mice.* Blood, 2015. **125**(2): p. 219-22.
158. *Characterization of a monoclonal antibody directed against mouse macrophage and lymphocyte Fc receptors.* The Journal of Experimental Medicine, 1979. **150**(3): p. 580-596.
159. Tiedt, R., et al., *Pf4-Cre transgenic mice allow the generation of lineage-restricted gene knockouts for studying megakaryocyte and platelet function in vivo.* Blood, 2007. **109**(4): p. 1503-1506.
160. Laemmli, U.K., *Cleavage of Structural Proteins during the Assembly of the Head of Bacteriophage T4.* Nature, 1970. **227**: p. 680.
161. Hemker, H.C., et al., *The Calibrated Automated Thrombogram (CAT): a universal routine test for hyper- and hypocoagulability.* Pathophysiology of Haemostasis and Thrombosis, 2002. **32**(5-6): p. 249-253.
162. Kleinschnitz, C., et al., *Targeting Platelets in Acute Experimental Stroke.* Impact of Glycoprotein Ib, VI, and IIb/IIIa Blockade on Infarct Size, Functional Outcome, and Intracranial Bleeding, 2007. **115**(17): p. 2323-2330.
163. Bederson, J.B., et al., *Rat middle cerebral artery occlusion: evaluation of the model and development of a neurologic examination.* Stroke, 1986. **17**(3): p. 472-476.
164. Moran, P.M., et al., *Age-related learning deficits in transgenic mice expressing the 751-amino acid isoform of human beta-amyloid precursor protein.* Proceedings of the National Academy of Sciences of the United States of America, 1995. **92**(12): p. 5341-5345.
165. Swanson, R.A., et al., *A Semiautomated Method for Measuring Brain Infarct Volume.* Journal of Cerebral Blood Flow & Metabolism, 1990. **10**(2): p. 290-293.
166. Dirnagl, U., *Bench to Bedside: The Quest for Quality in Experimental Stroke Research.* Journal of Cerebral Blood Flow & Metabolism, 2006. **26**(12): p. 1465-1478.
167. Samuelsson, B., et al., *Leukotrienes and lipoxins: structures, biosynthesis, and biological effects.* Science, 1987. **237**(4819): p. 1171-1176.
168. Hamberg, M. and B. Samuelsson, *Detection and Isolation of an Endoperoxide Intermediate in Prostaglandin Biosynthesis.* Proceedings of the National Academy of Sciences of the United States of America, 1973. **70**(3): p. 899-903.
169. Nugteren, D.H. and E. Hazelhof, *Isolation and properties of intermediates in prostaglandin biosynthesis.* Biochimica et Biophysica Acta (BBA) - Lipids and Lipid Metabolism, 1973. **326**(3): p. 448-461.
170. Evangelista, V., et al., *Platelet contribution to leukotriene production in inflammation: in vivo evidence in the rabbit.* Thromb Haemost, 1999. **81**(3): p. 442-8.
171. M., B., H. I., and N. B., *Genetic and antibody-induced glycoprotein VI deficiency equally protects mice from mechanically and FeCl3-induced thrombosis.* Journal of Thrombosis and Haemostasis, 2011. **9**(7): p. 1423-1426.

172. Turitto, V.T. and H.R. Baumgartner, *Effect of Temperature on Platelet Interaction with Subendothelium Exposed to Flowing Blood.* Pathophysiology of Haemostasis and Thrombosis, 1974. **3**(4): p. 224-236.
173. Kleinschnitz, C., et al., *Deficiency of von Willebrand factor protects mice from ischemic stroke.* Blood, 2009. **113**(15): p. 3600-3603.
174. Gruner, S., et al., *Anti-glycoprotein VI treatment severely compromises hemostasis in mice with reduced alpha2beta1 levels or concomitant aspirin therapy.* Circulation, 2004. **110**(18): p. 2946-51.
175. Nieswandt, B., I. Pleines, and M. Bender, *Platelet adhesion and activation mechanisms in arterial thrombosis and ischaemic stroke.* J Thromb Haemost, 2011. **9 Suppl 1**: p. 92-104.
176. Dutting, S., M. Bender, and B. Nieswandt, *Platelet GPVI: a target for antithrombotic therapy?!* Trends Pharmacol Sci, 2012. **33**(11): p. 583-90.
177. Heemskerk, J.W.M., E.M. Bevers, and T. Lindhout, *Platelet Activation and Blood Coagulation.* Thrombosis and Haemostasis, 2002. **88**(2): p. 186-193.
178. Bender, M., et al., *Megakaryocyte-specific Profilin1-deficiency alters microtubule stability and causes a Wiskott-Aldrich syndrome-like platelet defect.* Nat Commun, 2014. **5**: p. 4746.
179. Stritt, S., et al., *Profilin 1–mediated cytoskeletal rearrangements regulate integrin function in mouse platelets.* Blood Advances, 2018. **2**(9): p. 1040-1045.
180. Munnix, I.C.A., et al., *Segregation of Platelet Aggregatory and Procoagulant Microdomains in Thrombus Formation.* Regulation by Transient Integrin Activation, 2007. **27**(11): p. 2484-2490.
181. M., C.J.M.E., et al., *Multiple ways to switch platelet integrins on and off.* Journal of Thrombosis and Haemostasis, 2008. **6**(8): p. 1253-1261.
182. Mattheij, N.J., et al., *Dual mechanism of integrin alphaIIbbeta3 closure in procoagulant platelets.* J Biol Chem, 2013. **288**(19): p. 13325-36.
183. Rossdeutsch, A., et al., *Essential role for thymosin beta4 in regulating vascular smooth muscle cell development and vessel wall stability.* Circ Res, 2012. **111**(4): p. e89-102.
184. Mannherz, H.G. and E. Hannappel, *The beta-thymosins: intracellular and extracellular activities of a versatile actin binding protein family.* Cell Motil Cytoskeleton, 2009. **66**(10): p. 839-51.
185. P., C.L., B.L. J., and D.H. R., *Use of fluorescently labelled deoxyribonuclease I to spatially measure G-actin levels in migrating and non-migrating cells.* Cell Motility, 2002. **51**(1): p. 27-38.
186. M., H.J.W., M.N.J. A., and C.J.M.E. M., *Platelet-based coagulation: different populations, different functions.* Journal of Thrombosis and Haemostasis, 2013. **11**(1): p. 2-16.
187. Zwaal, R.F.A. and A.J. Schroit, *Pathophysiologic Implications of Membrane Phospholipid Asymmetry in Blood Cells.* Blood, 1997. **89**(4): p. 1121-1132.
188. Li, T., et al., *Production and characterization of highly purified recombinant thymosin beta 4 in Escherichia coli.* Protein Expr Purif, 2013. **90**(2): p. 90-5.
189. E., G.E., et al., *Controlled shedding of platelet glycoprotein (GP)VI and GPIb–IX–V by ADAM family metalloproteinases.* Journal of Thrombosis and Haemostasis, 2007. **5**(7): p. 1530-1537.
190. E., G.E., *A GPIb-IX-V complex signaling environment.* Journal of Thrombosis and Haemostasis, 2010. **8**(5): p. 1075-1076.
191. Chen, Y., et al., *Receptor-mediated cell mechanosensing.* Molecular Biology of the Cell, 2017. **28**(23): p. 3134-3155.
192. Flaumenhaft, R., et al., *The actin cytoskeleton differentially regulates platelet α-granule and dense-granule secretion.* Blood, 2005. **105**(10): p. 3879-3887.
193. Peerschke, E.I.B., *Reversible and irreversible binding of fibrinogen to platelets.* Platelets, 1997. **8**(5): p. 311-318.

194. S., B.J., *Platelet-Fibrinogen Interactions.* Annals of the New York Academy of Sciences, 2001. **936**(1): p. 340-354.
195. Nieswandt, B., et al., *Loss of talin1 in platelets abrogates integrin activation, platelet aggregation, and thrombus formation in vitro and in vivo.* The Journal of Experimental Medicine, 2007. **204**(13): p. 3113-3118.
196. Brady, R.D., et al., *Thymosin beta4 administration enhances fracture healing in mice.* J Orthop Res, 2014. **32**(10): p. 1277-82.

7. APPENDIX

7.1 Abbreviations

AA	Arachidonic acid
AC	adenylyl cyclase
ACD	Acid citrate dextrose
Abp1	Actin-binding protein 1
ADF	Actin depolymerizing factor
ADF-H	ADF-homology domain
ADP	Adenosine diphosphate
α-TAT1	α-tubulin N-acetyltransferase 1
Akt	Protein kinase B
Anxa5	Annexin V
APC	Adenomatous polyposis coli
APS	Ammonium persulfate
Arp2/3	Actin-related proteins 2/3
ATP	Adenosine triphosphate
BM	Bone marrow
bp	Base pairs
βT	β-thymosin
BSA	Bovine serum albumin
C. elegans	*Caenorhabditis elegans*
Ca^{2+}	Calcium cation
CA	Central/acidic domain
CalDAG-GEFI	Ca^{2+}-dependent DAG-regulated guanine nucleotide exchange factor
cAMP	Cyclic adenosine diphosphate
CAP	Cyclase-associated protein
Cdc42	Cell division control protein 42
CLEC-2	C-type lectin-like type II transmembrane receptor
Cof	Cofilin
Coll	Collagen
COTL1	Coactosin-like protein 1
CRP	Collagen-related peptide
CP	Capping protein
CVX	Convulxin
D. melanogaster	*Drosophila melanogaster*
D. discoideum	*Dictyostelium discoideum*
DAG	Diacylglycerol
DAPI	4'-6-Diamidino-2-phenylindole
°C	Degree Celsius
Da	Dalton
DIAPH	Mammalian Diaphanous
DIC	Differential interference contrast
DNA	Deoxyribonucleic acid
dNTP	Deoxynucleotide triphosphates
DMSO	Dimethylsulfoxide
DTT	1,4-Dithiothreitol

E. coli	*Escherichia coli*
EC	Endothelial cell
ECL	Enhanced chemiluminescence
ECM	Extracellular matrix
EDTA	Ethylenediaminetetraacetic acid
e.g.	Exempli gratia
EGTA	Ethylene glycol tetraacetic acid
ELISA	Enzyme-linked immunosorbent assay
et al.	Et alii
ETP	Endogenous thrombin potential
F-actin	Filamentous actin
FACS	Fluorescence-activated cell sorting
f.c.	Final concentration
FCS	Fetal calf serum
FcR	Fc receptor
Fig.	Figure
FITC	Fluorescein-isothiocyanate
FLAP	5-lipoxygenase-activating protein
FlnA	FilaminA
FSC	Forward scatter
g	Gravitation force
G-actin	Globular actin
γ-TuRC	γ-tubulin-ring complex
GAPDH	Glycerinaldehyd-3-phosphat-Dehydrogenase
GEF	Guanine nucleotide-exchange factor
GP	Glycoprotein
GPCR	G-protein coupled receptors
Grb2	Growth factor receptor-bound protein2
GTP	Guanosine triphosphate
h	Hours
HDAC	Histone deacetylase
HE	Hematoxylin and eosin
Hem	Hematopoietic protein
HEPES	N-2-Hydroxyethylpiperazine-N'-2-ethanesulfonic acid
5-HETE	5-Hydroxyeicosatetraenoic acid
5-HPETE	Arachidonic acid 5-hydroperoxide
HRP	Horseradish peroxidase
Ig	Immunoglobulin
IHC	Immunohistochemistry
ILK	Integrin-linked kinase
IMAC	Immobilized metal-ion affinity chromatography
IP	Immunoprecipitation
IP_3	Inositol-1,4,5-triphosphate
IPTG	Isopropyl β-D-1-thiogalactopyranoside
ITAM	Immunoreceptor tyrosine-based activation motif
i.v.	Intravenously
k	Kilo

K_D	Dissociation constant
KO	Knockout
LAT	Linker of activated T-cells
LatA	Latrunculin A
LB	Luria-Bertani
LIMK	LIM domain kinase
5-LO	5-lipoxygenase
LT	Leukotriene
M	Molar
mDia	Mammalian Diaphanous
Mena	Mammalian Ena orthologue
MFI	Mean fluorescence intensity
min	Minute
MK	Megakaryocyte
MLC	Myosin light chain
MMP	Matrix metalloproteases
MPV	Mean platelet volume
MT	Microtubule
MTOC	Microtubule-organizing center
NAD	Nicotinamide adenine dinucleotide
NMMIIA	Non-muscle myosin IIA
NP-40	Nonidet P-40
NS	Non-significant
O.D.	Optical density
o/N	Over night
Orai1	Ca^{2+} release-activated calcium channel protein 1
5-oxo-ETE	5-oxo-eicosatetraenoic acid
P	Phosphorylation/ Pellet
P. pastoris	*Pichia pastoris*
PAA	Polyacrylamide
PAGE	Polyacrylamide gel electrophoresis
PAK	p21/Cdc42/Rac1-activated kinase
PAR	Protease activated receptors
PBMC	Peripheral blood mononuclear cells
PBS	Phosphate buffered saline
PC	Phosphatidylcholine
PCR	Polymerase chain reaction
PE	R-phycoerythrin
PF4	Platelet factor 4
PFA	Paraformaldehyde
Pfn	Profilin
PGE	Prostaglandin
PGI_2	Prostacyclin
PH	Pleckstrin homology domain
Pi	Inorganic phosphate
PI	Propidium iodide/ protease inhibitors
PI3K	Phosphoinositide 3-kinase

PIP_2	Phosphatidylinositol 4,5-bisphosphate
PIP_3	Phosphatidylinositol-3,4,5-trisphosphate
PIPES	Piperazine-N,N′-bis(2-ethanesulfonic acid)
PK	Proteinkinase
PL	Phospholipase
PLP	Poly-L-proline
PMN	Polymorphonuclear cell
PMSF	Phenylmethylsulphonylfluorid
PRP	Platelet rich plasma
PVDF	Polyvinylidene difluoride
PS	Phosphatidylserine
PTT	Partial thromboplastin time
Rac1	Ras-related C3 botulinum toxin substrate 1
RBC	Red blood cell
Rest	Resting
Rhd	Rhodocytin
RhoA	Ras homolog gene family, member A
Rho-GEF	Rho-specific guanine nucleotide exchange factor
Rho-GTPase	Ras-homologue-guanine triphosphatase
RNA	Ribonucleic acid
ROCE	Receptor-operated Ca2+ entry
ROCK	*Rho associated coiled-coil containing protein kinase*
rpm	Rotation per minute
RT	Room temperature
RT-PCR	Reverse transcription polymerase chain reaction
s	Second(s)
S	Soluble
S. cerevisiae	*Saccharomyces cerevisiae*
SD	standard deviation
SDS-PAGE	Sodium dodecyl sulfate polyacrylamide gel electrophoresis
SH2	Src-homology 2
SIRT2	NAD-dependent deacetylase sirtuin-2
SLP-76	SH2 domain-containing leukocyte protein of 76 kDa
SN	Supernatant
SOCE	Store-operated Ca2+ entry
SSC	Side scatter
STED	Stimulated emission depletion
STIM	Stromal interaction molecule
Syk	Spleen tyrosine kinase
t	Time
T	Total
TAE	TRIS acetate EDTA
TBS	TRIS buffered saline
TEM	Transmission electron microscopy
TEMED	Tetramethylethylenediamine
TESK	TES kinase
TF	Tissue factor

TGF-β1	Transforming growth factor-β1
Thr	Thrombin
Tln-1	Talin-1
TMB	3,3,5,5-tetramethylbenzidine
tMCAO	Transient middle cerebral artery occlusion
Tβ4	β4-thymosin
TP	TxA_2 receptor
TRIS	Tris(hydroxymethyl)aminomethane
TTC	2,3,5-triphenyltetrazolium chloride
TTL	Tubulin-tyrosine kinase
TLLL	TTL-like family member
TRPM7	Transient receptor potential melastatin-like 7
Twf	Twinfilin
TxA_2	Thromboxane A_2
U	Units
U46	U46619
UV	Ultraviolet
V	Verproline homology motif
VASP	Vasodilator-stimulated phosphoprotein
vWF	Von Willebrand factor
WAS	Wiskott-Aldrich syndrome
WASp	Wiskott-Aldrich syndrome protein
WAVE	WASp family verprolin-homologous protein
WIP	WASp-interacting protein
WT	Wild-type
X. laevis	*Xenopus laevis*

7.2 Vectors

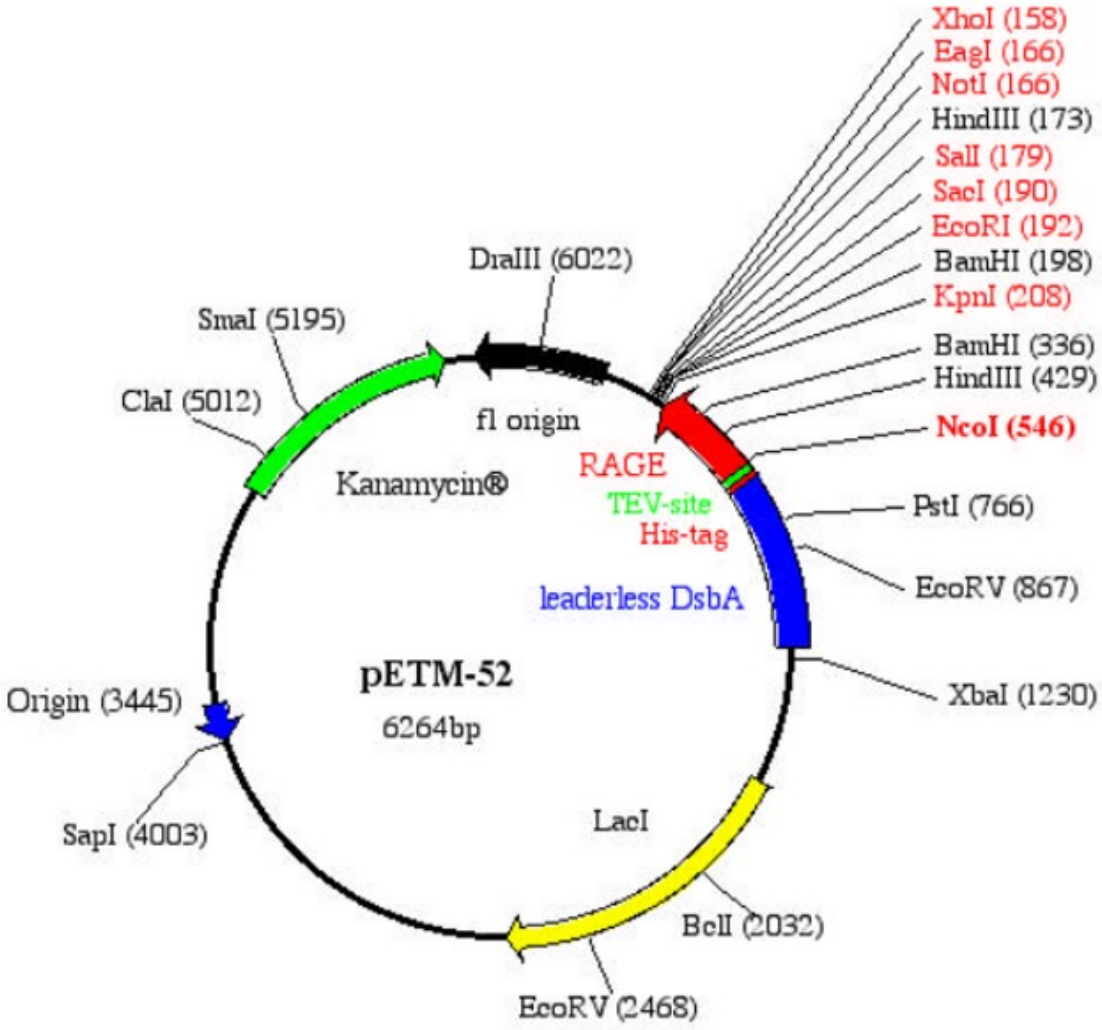
XhoI (158)
EagI (166)
NotI (166)
HindIII (173)
SalI (179)
SacI (190)
EcoRI (192)
BamHI (198)
KpnI (208)
BamHI (336)
HindIII (429)
NcoI (546)
PstI (766)
EcoRV (867)
XbaI (1230)
BclI (2032)
EcoRV (2468)
LacI
SapI (4003)
Origin (3445)
pETM-52
6264bp
leaderless DsbA
His-tag
TEV-site
RAGE
Kanamycin®
f1 origin
ClaI (5012)
SmaI (5195)
DraIII (6022)

pETM-52

```
     T7 promoter  -->            Lac operator     XbaI
GAAATTAATACGACTCACTATAGGGGAATTGTGAGCGGATAACAATTCCCCTCTAGAAATAAT
CTTTAATTATGCTGAGTGATATCCCCTTAACACTCGCCTATTGTTAAGGGGAGATCTTTATTA

                rbs
TTTGTTTAACTTTAAGAAGGAGATATACCATGAAAGCGCAGTATGAAGAT...534bp..TAC
AAACAAATTGAAATTCTTCCTCTATATGGTACTTTTTCTAAACCGACCTA..LL-DsbA.ATG
                           METLysAlaGlnTyrGluAsp...178aa..Tyr

                                                His-tag
TTAAGCGAGAAAAAAGGATCAACTAGTGGTTCTGGTCATCACCATCACCATCACTCCGCGGGT
AATTCGCTCTTTTTTCCTAGTTGATCACCAAGACCAGTAGTGGTAGTGGTAGTGAGGCGCCCA
LeuSerGluLysLysGlySerThrSerGlySerGlyHisHisHisHisHisHisSerAlaGly

          TEV-site      NcoI
GAGAATCTTTATTTTCAG GGCGCCATGGGTGCTCAAAACATC...300bp...GTAGATTCT
CTCTTAGAAATAAAAGTC CCGCGGTACCCACGAGTTTTGTAG...RAGE....CATCTAAGA
GluAsnLeuTyrPheGln|GlyAlaMETGlyAlaGlnAsnIle...100aa...ValAspSer

                                  SacI                  NotI
              KpnI        EcoRI       SalI          EagI     XhoI
GCCTCTGAATAAGGTACCGGATCCGAATTCGAGCTCCGTCGACAAGCTTGCGGCCGCACTCGA
CGGAGACTTATTCCATGGCCTAGGCTTAAGCTCGAGGCAGCTGTTCGAACGCCGGCGTGAGCT
AlaSerGlu***

GCACCACCACCACCACCACTGAGATCCG
CGTGGTGGTGGTGGTGGTGACACTAGGC
 HisHisHisHisHisHis***
```

Single Cutters Listed by Site Order

158	XhoI	204	Asp718I	766	PstI	3082	BglI
160	SciI	204	Acc65I	850	BspMI	3100	MstI
166	XmaIII	208	KpnI	1131	AscI	4003	SapI
166	NotI	289	Eco31I	1142	AgeI	4978	NruI
166	Eco52I	546	NcoI	1142	PinAI	4978	SpoI
166	EagI	577	Mlu113I	1230	XbaI	5012	ClaI
179	SalI	579	SstII	1337	SgrAI	5193	XmaI
188	EcoICRI	579	SacII	1493	SphI	5195	SmaI
188	Ecl136II	610	SpeI	1702	ApaBI	5321	PvuI
190	SstI	632	AflII	2018	MluI	5321	XorII
190	SacI	748	MfeI	2032	BclI	6022	DraIII
192	EcoRI						

Non Cutting Enzymes

AatII	AhaIII	AsuII	AvrII	BalI	Bsp1407I
Bsu36I	Csp45I	CspI	CvnI	DraI	Eam1105I
Eco72I	FseI	I-PpoI	MscI	MstII	NdeI

7.3 Acknowledgements

The work presented here was accomplished in the group of Prof. Dr. Bernhard Nieswandt at the Institute of Experimental Biomedicine, University Hospital and the Rudolf Virchow Center, University of Würzburg. During the period of my PhD studies, many people supported and accompanied me on my way to whom I would like to express my sincere gratitude:

My supervisor, Prof. Dr. Bernhard Nieswandt, for giving me the opportunity to pursue my PhD projects in his group, for his mentorship, scientific input as well as financial support. Especially, I would like to thank him for allowing me to present my work at an international conference, which enabled me getting to know many people in the scientific community and gather experience for my future professional life.

The members of my thesis committee, Prof. Dr. Antje Gohla and PD Dr. Heike Hermanns for the fruitful scientific discussions and reviewing my thesis.

Dr. Irina Pleines, Dr. David Stegner, Dr. Attila Braun, Dr. Markus Bender, *Dr. Julia Preu* and *Dr. Martha-Lena Müller* for many valuable discussions, critical input and support on my projects.

Dr. Simon Stritt for handing over many interesting projects and for his constant support, scientific discussions and sharing his knowledge with me.

Dr. Dr Katharina Remer and all animal care takers for their excellent work concerning mouse business.

Birgit, Sylvie, Juliana, Steffi and Ewa for their support and chats during the daily lab work and the efforts to keep the lab running.

The Bioimaging Centre for providing technical infrastructure and support.

The team of the Graduate School of Life Sciences for providing fellowships that allowed me to attend interesting courses and conferences, for their great scientific course program, the Mentoring program and for their constant support especially during my work as member of the Eureka Organizing Committee and the DRC.

The MK and platelet seminar members for constant encouragement, support and fruitful discussion- without you some of these studies would have get lost over time!

All colleagues in the two PhD offices, especially Max, Carina, Julia, Yvonne and Vanessa for critical discussions, support in good and bad times, and many fun moments.

Sarah and Isabelle for their collaboration, constant support and fruitful discussions.

Sarah, Carina, Isabelle, Katja, Markus S., Vanessa and Max for carefully proof-reading this thesis.

All present and former members of the Institute, who have not been mentioned here by name, but spent their time and knowledge with me and for the great and supporting working atmosphere.

My dear friend Dr. Carolyn Delto (Structural Biology, Rudolf Virchow Center), who encouraged me to start a new PhD project and gave me constant trust and support during a very bad time. Moreover, I am grateful for all her help concerning scientific problems, such as Cloning, Protein expression and Purification.

My close friends and family for their constant encouragement, everlasting support and patience.

My parents, who were very supportive, understanding and patient with me and my commitment to work.

Julian, who believed in me and stood by my side against all odds.

7.5 Publications

7.5.1 Original articles

Stritt, S.*, **Birkholz, I.***, Beck, S., Sorrentino, S., Sapra, K.T., Viaud, J., Heck, J., Gaits-Iacovoni, F., Schulze, H., Du, X., Hartwig, J.H., Braun, A., Bender, M., Medalia, O., Nieswandt, B. Profilin 1–mediated cytoskeletal rearrangements regulate integrin function in mouse platelets. Blood Advances, 2018. **2**(9): p. 1040-1045.

* these authors contributed equally

7.5.2 Oral presentations

XXVI International Society on Thrombosis and Haemostasis (ISTH) congress, Berlin, Germany, July 2017, ‘Coactosin-like 1 is a novel regulator of arterial thrombosis and hemostasis in mice’ (oral presentation)

7.5.3 Poster presentations

10/2017	International Symposium of the Graduate School of Life Sciences Würzburg ‘Coactosin-like 1 is a novel regulator of arterial thrombosis and hemostasis in mice’
10/2016	International Symposium of the Graduate School of Life Sciences Würzburg ‘Coactosin-like 1 regulates thrombosis and hemostasis in mice’
10/2015	International Symposium of the Graduate School of Life Sciences Würzburg ‘Megakaryocyte *in vitro* culture put to the test’

7.6 Affidavit

I hereby confirm that my thesis entitled “Studies on the role of actin-binding proteins in platelet production and function in mice” is the result of my own work. I did not receive any help or support from commercial consultants. All sources and/or materials applied are listed and specified in the thesis.

Furthermore, I confirm that this thesis has not yet been submitted as part of another examination process neither in identical nor in similar form.

Würzburg, July 2018 _____

Inga Birkholz

7.7 Eidesstattliche Erklärung

Hiermit erkläre ich an Eides statt, die Dissertation „Zur Rolle von Aktin-bindenden Protein in der Bildung und der Funktion von Thrombozyten in der Maus“ eigenständig, d.h. insbesondere selbständig und ohne Hilfe eines kommerziellen Promotionsberaters, angefertigt und keine anderen als die von mir angegebenen Quellen und Hilfsmittel verwendet zu haben.

Ich erkläre außerdem, dass die Dissertation weder in gleicher noch in ähnlicher Form bereits in einem anderen Prüfungsverfahren vorgelegen hat.

Würzburg, Juli 2018 _____

Inga Birkholz